CHARACTERIZATION OF VEGETATION PROPERTIES: CANOPY MODELING OF PINYON-JUNIPER AND PONDEROSA PINE WOODLANDS

final report to the Los Alamos National Laboratory

Environmental Science Group EES-15

for Subcontract 9-XA1-X3682-1, Period 7/1/91-9/30/94

Principal Investigator

Paul M. Rich
Biological Sciences
University of Kansas
Lawrence, KS 66045-2106
telephone: (913)864-7769
FAX: (913)864-7789
e-mail: prich@oz.kbs.ukans.edu

1 September 1994

ABSTRACT

Studies of plant canopies in pinyon-juniper woodland, ponderosa pine woodland, and waste sites at Los Alamos National Laboratory involved five basic areas of research: 1) application of hemispherical photography and other gap fraction techniques to study solar radiation regimes and canopy architecture, coupled with application of time-domain reflectometry to study soil moisture; 2) detailed characterization of canopy architecture using stand mapping and allometry; 3) development of an integrated geographical information system (GIS) database for relating canopy architecture with ecological, hydrological, and system modeling approaches; 4) development of geometric models that simulate complex sky obstruction, incoming solar radiation for complex topographic surfaces, and the coupling of incoming solar radiation with energy and water balance, with simulations of incoming solar radiation for selected native vegetation and experimental waste cover design sites; and 5) evaluation of the strengths and limitations of the various field sampling techniques. Studies to date have provided 1) sampling methods for measuring such fundamental canopy properties as stand geometry, expected light penetration, expected incoming solar radiation at soil level, productive and non-productive biomass, leaf area index, and leaf inclination; 2) baseline data concerning these canopy properties for representative native vegetation and waste sites; 3) the geometric models CANOPY and SOLARFLUX for describing incoming solar radiation; and 4) recommendations on how to conduct detailed future studies of canopy properties and processes. This work serves as a pilot project for future projects that study the role of vegetation in energy, carbon, and water balances using remote sensing, GIS, and three-dimensional models that relate canopy architecture and turbulent exchange.

DISCLAIMER

Portions of this document may be illegible in electronic image products. Images are produced from the best available original document.

1.0. INTRODUCTION

1.1. Background

Herein we describe a pilot project to use advanced instrumentation and sampling techniques to characterize fundamental plant canopy properties, to understand basic ecological processes in semiarid woodlands, and to examine the role of vegetation in waste site design and remediation at Los Alamos National Laboratory (LANL).

1.1.1. The role of vegetation: In order evaluate the role of vegetation in local, regional, and global ecosystem processes, it is essential to understand energy and gas-exchange properties of plant canopies (Houghton and Woodwell 1989). We are faced with major challenges to characterize the geometry of plant canopies and relate this canopy architecture to processes of energy, water, and carbon flux. Further challenges involve relating more-easily-quantified local processes at the microsite and organism levels to whole-canopy flux, and beyond to the regional and global levels. To meet these challenges, we require new tools, new conceptual frameworks, and solid data.

1.1.2. Relevance for waste site design and remediation: Predicting the long-term integrity of waste sites and remediated sites at Los Alamos National Laboratory depends largely on the ability to predict the stability of the surface soils and vegetation at a site. Prediction of site stability require developing models of site closure, and parameterizing these models so that both the short-term and long-term vegetation structure and function are appropriately represented. Very little data exists on the structure and function of vegetation at Los Alamos, either on disturbed sites (such as a recently remediated area) or in areas with native vegetation, such as might exist on a waste site after hundreds to thousands of years.

1.1.3. Study Site: The Los Alamos National Environmental Research Park (NERP) in northern New Mexico, established in 1976 for study of technological impacts on nature, is the site of long-term studies of ecology, hydrology, and meteorology. The NERP comprises 111 km^2 of natural lands across a 1200 m elevational gradient (1645-2864 m), encompassing six major vegetation types: 1) juniper-grassland, 2) pinyon-juniper (PJ) woodland, 3) ponderosa pine (PP) woodland, 4) mixed conifer forests, 5) spruce-fir forests, and 6) subalpine grassland. Mixed stands of one-seeded juniper (*Juniperus monosperma*), a shrub, and pinyon pine (*Pinus edulis*), a small tree, grow in an elevational belt from roughly 1600 to 2200 m. Junipers dominate in the lower, dryer sites and pinyons in the higher, more mesic sites. These stands are characterized by heterogeneous spatial patterns, with clumps of the shrubs and small trees surrounded by openings. With increasing elevation, clump size and individual heights increase, while spaces between clumps decrease. Ponderosa pine (*Pinus ponderosa*), a tall tree, dominates at elevations from roughly 2200 to 2700 m.

1.2. Relations Between Climate and Vegetation

1.2.1 Importance of Climate in Semiarid Woodlands: Climate is a primary determinant of the distribution of pinyon-juniper (PJ) and ponderosa pine (PP) woodlands and influences such fundamental characteristics as 1) species composition, in particular the relative dominance of pinyons, junipers, and ponderosa pines; 2) canopy architecture, the size, form, and spacing of individual plants; 3) energy balance; 4) water balance; and 5) carbon balance. PJ and PP woodlands occur in semiarid regions. In these semiarid regions, droughts are common, and the infrequent rainfall can be intense with rapid runoff. Typically PJ woodland occurs at mid-elevations in the mountains of southwestern North America, along an inversion zone where average temperatures tend to be higher and somewhat less extreme relative to locations at higher and lower elevations, while PP woodland occurs at slightly higher elevations (Billings 1954, West et al. 1978).

1.2.2. Study of Elevational Gradients to Understand the Ecology of Semiarid Woodlands: The major influences of climate on PJ and PP woodlands are readily observable along elevation gradients. Increase in precipitation and decrease in temperature is associated with increase in elevation. These climatic effects directly and indirectly influence three basic properties of PJ woodlands with increase in elevation: 1) water stress on vegetation decreases; 2) juniper decreases in relative abundance, while pinyon increases; and 3) pinyon and juniper size and cover increases, while spacing between individuals decreases. With still higher elevation, under conditions of greater precipitation and lower temperature, PP woodland dominates. Because elevation gradients correspond to primary gradients of temperature and precipitation, they can be viewed as a surrogate for investigating influence of climate change. For example, with climate change involving increased temperature and/or decreased rainfall, we would expect location along an elevational gradient to take on characteristics of lower elevations, including a decrease in cover and increased dominance of juniper. However, even under a sustained change in climate, these change involve significant time lags that depend upon population processes of growth, death, and recruitment. Historical effects, such as the establishment of stands under driver or wetter climatic conditions, may have an effect that lingers for many decades and even for hundreds of years. Similarly, soil erosion due to overgrazing or local nutrient enrichment from cultivation may also influence ecological characteristics for long periods of time. This is further complicated because temperature and precipitation are not the only factors that vary with elevation; also associated with differences in elevation are such physical factors such as levels of ultraviolet radiation and biological factors such as differences in native grazer and browser populations. These considerations not withstanding, careful study of elevation patterns serves as an essential tool for understanding influences of climate, in particular with three major foci: 1) study of changes in composition, architecture, and associated flux (water, carbon, and nutrients) within PJ and PP woodlands; 2) study of the nature and stability of the PJ/grassland ecotone at the lowermost elevational limits of PJ woodlands; and 3) study of the nature and stability of the PJ/ponderosa pine woodland ecotone at the uppermost elevation limits PJ woodland.

1.2.3. Influences of Topography and Vegetation on Microclimate: At a local scale, prevailing climate is dramatically modified by topography and vegetation (Geiger 1965). The resulting microclimate involves energy and water balances that vary markedly across the landscape. The major patterns of microclimate variation are readily modelled based upon topography and canopy architecture. Herein we use the term canopy architecture to refer to the geometric or spatial organization of aboveground plant parts. There are three major effects of topography and canopy architecture: 1) obstruction or impedance of flows, such as blockage of solar radiation from certain sky directions; 2) channelization of flows, as cold air drainage along canyon bottoms; and 3) modification of the geometry of interception, such as differences in energy balance for north- vs. south-facing slopes. For a given general elevation, patterns of microclimate change predictably between north vs. south-facing slopes, between east vs. west-facing slopes, and between mesa tops canyon bottoms. Topographic features can result in strong local gradients on scales ranging from centimeters to kilometers, and to patchiness of locations with similar physical conditions. At the scale of centimeters to meters, canopy architecture can similarly generate strong local gradients and patchiness that may be key to understanding the basic functioning of PJ woodlands. For example, energy and water balances beneath clumps of pinyons and junipers is often very different from balances in intercanopy patches (Rich et al. 1993a, Breshears 1993).

1.2.4. The Central Role of Canopy Architecture: Canopy architecture, the three-dimensional arrangement of aboveground vegetation elements (leaves, stems, and reproductive structures), plays a central role in models of atmosphere-ecosystem fluxes and couples micrometeorology to the disciplines of remote sensing and terrestrial ecology. With respect to remote sensing, a canopy is a complex surface that determines measurable patterns of reflected radiation (Goel 1988, Hall et al. 1991, Strahler and Jupp 1990). With respect to ecology, canopy architecture regulates physiological processes that determine exchanges of heat, water, and carbon (Baldocchi et al. 1988, McNaughton 1989, Mooney et al. 1987). These physiological responses, in turn, are expressed in terms of growth, survival, and reproduction of plants that

comprise the canopy. The complexity of canopy architecture and geometry makes it difficult to quantify and translate into effects on ecophysiology, population dynamics, and plant community composition.

2.0. APPLICATION OF HEMISPHERICAL PHOTOGRAPHY, OTHER GAP FRACTION TECHNIQUES, AND TIME-DOMAIN REFLECTOMETRY

We used four new technologies in our studies of canopy architecture and its importance in energy and water balances: 1) hemispherical photography; 2) the Licor LAI-2000 Canopy Analyzer; 3) the Decagon Sunfleck Ceptometer; and 4) time-domain reflectometry (TDR). The first three techniques provide gap fraction data, which can be used to calculate solar radiation penetration through canopies, and to estimate leaf area index (LAI) and leaf inclination (Welles 1990, Martens *et al.* 1991) using either a one-dimensional inversion model (Norman and Campbell 1989) or the Beer-Lambert Law (Pierce and Running 1988). TDR provides measurements of soil moisture.

2.1. Techniques Employed

2.1.1. Hemispherical Photography: We used hemispherical photography to calculate expected incoming solar radiation at ground level and to measure gap fraction. Hemispherical (fisheye) canopy photography is a technique for characterizing plant canopies using photographs through an extreme wide-angle lens looking upward from within a plant canopy (Anderson 1964, Rich 1990). The resulting photographs serve as permanent records of the geometry of canopy openings. The geometric distribution of openings can be measured precisely and used to estimate potential solar radiation penetration through openings. Rich (1988, 1989, 1990) has recently developed video image analysis techniques at Los Alamos National Laboratory to allow efficient analysis of large numbers of photographs. The program CANOPY allows rapid calculation of direct and indirect site factors (indices of direct and indirect light penetration) and gap fraction as a function of sky direction. Photographs can be taken along transects or in horizontal or vertical grid patterns to sample spatial heterogeneity within canopies. Applications of the technique range from assessment of local microenvironments to ecosystem level characterization of canopy architecture.

2.1.2. Licor LAI-2000 Canopy Analyzer and Decagon Sunfleck Ceptometer: The LAI-2000 Canopy Analyzer has five concentric silicon ring detectors that measure the gap fraction in each of five ranges of zenith angle. An onboard microprocessor inverts data taken from above and below the canopy to calculate LAI and leaf inclination.

2.1.3. Decagon Sunfleck Ceptometer: The Decagon Sunfleck Ceptometer has 80 adjacent 1 cm^2 photosynthetically active radiation (PAR) sensors along an 80 cm bar. The instrument can be used to examine canopy architecture either by measuring sunflecks and estimating gap fraction or by examining the transmittance of radiation through the canopy, determined by measurements taken above and below the canopy.

2.1.4. Associated measurements of soil moisture: Time-domain reflectometry (TDR) offers a rapid, effective, and low-cost means for monitoring soil moisture (Topp *et al.* 1980, 1982a, 1982b, Topp and Davis 1985). TDR is the process of sending an electronic pulse through a coaxial cable and a substance of unknown water content and observing the reflected waveform. Because the dielectric constant of water is high, a signal propagates more slowly in a relatively moist medium than in a drier one. Thus, if the length and conductivity of the probe are held constant, the variation in the waveforms represents variation in water content. We used TDR to measure soil moisture at the one-meter sample stations along each transect. PB30 30cm soil probes were implanted at each sample station, with the two rods attached to a twin lead 50 ohm coaxial cable. A PS1502B Power Control Module was used for signal generation, read with a

Tektronix 1502B TDR Cable Tester, and digitized with a Campbell Scientific SDM1502 Communications interface attached to an IBM AT laptop computer. Initial complete data set was collected on 8 August 1991 for the PJ site and 9 August 1991 for the PP site, after a series of storms that left soils near saturation. Soil probes and cables were left in place at 5 m intervals along all three transects. Subsequent measurements have been continued by LANL personnel and have employed multiplexer systems to allow collection of soil moisture throughout the year.

2.2. Data Sets Collected

2.2.1. Pinyon-juniper transect characterization: A 100 m linear transect was established to characterize PJ woodland at LANL Technical Area 51, with a bearing of approximately 33^{o}, and with sample stations marked each meter with flags. Eleven neutron access tubes, spaced approximately 10 m apart, were placed along this transect in 1988 and soil moisture data are available from 1988 through the present. Appendices 1-2 summarize results of hemispherical photograph analyses, Appendix 7 summarizes sunfleck ceptometer measurements, and Appendix 9 summarizes TDR measurements taken at each station along the PJ transect in 1991. Additional hemispherical analyses at monthly intervals, for this and other sites, are available in computer data files supplied to LANL.

2.2.2. Ponderosa Pine transects characterization: PP woodland was sampled along two 50 m linear transects located at LANL Technical Area 6 at 2310 m (7580ft) elevation. The transects were situated at the center of sites for future soil runoff collection stations. One transect, bearing 133^{o}, was in a dense, closed-canopy stand that was harvested approximately forty years ago. The other transect, bearing 97^{o}, was located in an open-canopy stand with much older trees. *Pinus ponderosa* (ponderosa pine) was the dominant overstory species. As for the PJ site, sample stations were marked with flags at one-meter intervals along the transect lines. Appendices 3-6 summarize results of hemispherical photograph analyses, Appendices 8 summarizes sunfleck ceptometer measurements, and Appendix 10 summarizes TDR measurements taken at each station along the PP transects in 1991.

2.2.3. Lower elevation Pinyon-Juniper site characterization: A series of 35 hemispherical photographs were taken in 1992 at selected locations at the Tsierge PJ woodland stand at lower elevations of the NERP. Appendix 11 summarizes results of hemispherical photograph analyses for the Tsierge PJ site.

2.2.4. Protective barrier inclined plot site characterization: Arrays of hemispherical photographs were taken in 1992 at a series of inclined plots, established to examine impacts of slope on water balance and erosion on sites with different waste cover designs. Appendices 12-13 summarize results of hemispherical photograph analyses for the inclined plot sites. Appendix 14 gives monthly direct calculations of incoming solar radiation for the inclined slopes. Calculations for daily and instantaneous direct radiation are available in computer data files supplied to LANL.

2.2.5. TDR plot site characterization: Appendix 15 summarizes results of hemispherical photograph analyses conducted in 1994 for a series of TDR study sites in PJ woodland at LANL Technical Area 51.

2.2.6. Ponderosa Pine hydrology plot characterization: Appendix 16 sumarizes results of hemispherical photograph analyses conducted in 1994 for the PP woodland hydrology study site at LANL Technical Area 6.

3.0. DETAILED CHARACTERIZATION OF STAND CANOPY ARCHITECTURE

Characterization of canopy architecture requires detailed knowledge of the distribution of individual plant parts in space, including measures of location, area, inclination, and azimuth.

Detailed description of canopy geometry is especially difficult in non-homogeneous systems as they occur in nature. We employed basic stand mapping techniques to characterize canopy overstory geometry (*e.g.*, location, stem diameter (DBH), height, and crown radius dimensions. More detailed measurement of canopy geometry can be made using stratified sampling methods similar to those used by Martens (pers. comm.). This involves sampling spatial locations of canopy elements (leaves, branches) as a function of position within individual trees of different heights and computer reconstruction of detailed geometry.

3.1. Pilot Studies of PJ Woodland

3.1.1. Methodologies: Pilot studies for a three-hectare PJ woodland study site at the Los Alamos NERP employed three basic methodologies (Rich et al. 1993a): 1) mapping and automation of georeferenced locations, stem diameters, and heights of all pinyons and junipers in a three-hectare stand using GIS (ARC/INFO and GRID); 2) using GIS to construct a canopy digital elevation model (CDEM) based on the allometry of crown radius to stem diameter and the assumption that tree crown form can be approximated as the upper half of an ellipsoid; and 3) simulation of intercepted solar radiation using the insolation model SOLARFLUX (see Section 4.2).

3.2. Construction of Canopy Digital Elevation Models and Integrated Geographical Information System

3.2.1. Overview of Approach: Our approach for constructing spatially explicit models of semiarid woodland canopies combines traditional ground-based stand measures (e.g., individual location, stem diameter, height), remote sensing (e.g., high resolution aerial photography), and a GIS for data management and modelling. Canopy surface topography is characterized by producing a canopy digital elevation model (CDEM) in which an array, or grid, describes elevation values for each canopy location. CDEMs can be derived in three basic ways: 1) from individual location and crown dimensions based on ground measurements alone; 2) from a combination of ground measurements and measurements of crown dimensions from orthoimagery; or 3) from photogrammetric analysis of stereoimagery, much in the same way that terrain maps are produced.

3.2.2. Focus of work: Work has focused primarily at the same intensively studied PJ woodland site as described in Section 3.1.1. Data already collected include basic physiography (topography, watershed delineation, geologic and soil formations), meteorology (precipitation, temperature, humidity), stand characteristics (mapped locations of individuals, stem diameter, height, crown dimensions), hydrology (interception, runoff, evapotranspiration, soil moisture, groundwater flow), and ecophysiology (photosynthesis, transpiration, nutrient cycling). In addition a growing catalog of remotely sensed imagery has been collected for the area, ranging from satellite imagery to low altitude overflights and ground-based measurements from an extendable boom. These diverse, geographically referenced data sets are being brought together in a GIS database to facilitate access, allow for efficient ongoing data collection, enable spatial analysis, and serve as a modeling platform.

3.3.3. Work completed: Strict quality control was performed on all georeferenced data collected for mapping the PJ woodland at LANL Technical Area 51. The ARC/INFO GIS database includes the following information for each tree and shrub: individual number, species, x,y location, diameter at base, height, and crown radius. Digital elevation models employing GRID have been built of the underlying terrain and of the envelope of the canopy surface (a CDEM). The CDEM was constructed based on individual locations and crown dimensions derived from individual height and stem diameter, in particular assuming that crown shape can be approximated as the upper half of an ellipse. Thus the CDEM represents an approximation of the envelope that bounds the topmost portion of the canopy.

3.3.4. PJ Stand Characteristics: The PJ study site has a distribution of trees and shrubs typical of mid-elevation sites at the Los Alamos NERP. The overall stand density was about 500 ind/ha, with near equal densities of pinyons and junipers, and with a total crown coverage of near 50%. Pinyons had a mean crown height of about 6.0 m and mean crown radius (C) of about 2.4 m, whereas junipers had a mean of about 2.6 m and mean C of about 1.25 m. The surface topography of the PJ site is highly heterogeneous, with distinct clumps and open areas between clumps.

4.0. GEOMETRIC MODELS FOR SOLAR RADIATION

4.1. Solar Radiation as Modified by Complex Sky Obstruction (CANOPY software)

4.2.1. Enhancements to CANOPY: Two major enhancements were developed for CANOPY hemispherical image analysis system: 1) a batch program called FASTCAN was developed to allow automated analysis of list of digitized hemispherical images; and 2) a utility program called COSCOR was developed to allow calculation of cosine correction coefficient to enable analysis of solar radiation regimes for any specified plane.

4.2.2. Work enabled by enhancements to CANOPY: The batch program FASTCAN enables us to reanalyze digitized hemispherical photographs under different sets of assumptions, for example applying different distribution of incoming diffuse radiation, and after editing, as has been required for many of the LANL images analyzed to date. The utility program COSCOR enabled us to analyze the influences of slope using hemispherical photographs for the protective barrier inclined plots.

4.2. Solar Radiation Flux on Complex Surfaces (SOLARFLUX)

4.2.1. Development of SOLARFLUX: SOLARFLUX is a GIS-based software program that we developed for this project to predict incoming solar radiation based on surface orientation, solar angle, topographic shading, and atmospheric conditions (Hetrick *et al.* 1993a, 1993b, Dubayah and Rich in press, Rich et al. in press). SOLARFLUX was implemented in Arc Macro Language (AML) using the ARC/INFO and GRID GIS platforms. The menu system allows the user to define all program parameters including global location of the surface (latitude and longitude) and time interval for calculation. Surface topography is defined by an array (GRID) of elevation data. Solar radiation flux, the energy intercepted per unit area, is comprised of direct, diffuse, and reflected insolation components (Monteith and Unsworth 1990). Direct radiation is generally the largest component of total radiation, ranging from about 85% direct and 15% diffuse radiation under clear sky conditions to no direct and near 100% diffuse under overcast conditions. Reflected radiation, by contrast, in which direct and diffuse components are reflected to a location from surrounding topographic features, generally accounts for a small proportion of total incident radiation (Gates 1980). Calculations for each surface location are integrated for a specified time interval by summing insolation components over a series of discrete time increments. A graphical display shows a hemispherical projection of the solar track for each incremental time of simulation. The current version of SOLARFLUX calculates total direct radiation, duration of direct sunlight, total diffuse radiation, skyview factor (proportion of unobscured sky), and fisheye projections of sky obstructions for specified surface locations. SOLARFLUX is in the public domain and is made available by anonymous FTP. A manual has been produced that fully describes the theory and operation of SOLARFLUX (Rich et al. in press).

4.2.2. Simulations of incoming solar radiation using SOLARFLUX: SOLARFLUX was been used to simulate heterogeneity of solar radiation regimes for the PJ woodland study site at LANL Technical Area 51. Overall, the estimated daily insolation was highest at the summer solstice, and lowest at the winter solstice. As would be expected based on the shadow patterns, the south side of clumps tended to receive more insolation in the winter. Heterogeneity

of insolation was important during all times of year, but most pronounced during the winter solstice.

4.2.3. Inferences from geometrical models: For the relatively open, heterogeneous canopies of semiarid woodlands, interactions between canopy architecture and solar radiation lead to heterogeneous and changeable microclimates. There is strong differentiation between microsites on different sides of clumps; and sharp microclimate gradients extend from the center of clumps to the center of openings. Thus modelling the explicit geometry of the canopy architecture as it interacts with solar angle permits prediction of the distribution of microclimates as they shift during the day and through the seasons. Detailed studies are required to validate the predictions of our solar radiation flux models and to understand the consequences for processes such as heat flux, water flux, and productivity. Validation at a local level can be accomplished using hemispherical photography or light sensors (Rich 1990, Rich et al. 1993).

5.0. EVALUATION OF FIELD TECHNIQUES

5.1. Hemispherical Photography

5.1.1. Advantages of hemispherical photography: Of the three gap fraction methods used for analysis of light environment and characterization of canopy architecture, hemispherical photography is the only one that provides a permanent record of canopy geometry. This allows repeated analyses using different assumptions, for example different assumption about the indirect radiation originating from different sky directions. The technique also allows for future analysis as new theory is developed and more sophisticated techniques become available. The fundamental difference between hemispherical photography and the other techniques is that it is a direct measure of geometry, not of radiation. With canopy photography, it is possible to make calculations of radiation penetration for times of day and year other than the time of photograph acquisition. It is also possible to integrate these measure over time, as is done in calculating yearly ISF and DSF values. However, in order to extrapolate to future or past times, one must assume that canopy geometry does not change.

5.1.2. Limitations of hemispherical photography: As with any field technique, errors can occur at each stage of data acquisition and processing (Rich 1989). The subjectivity of setting the threshold introduces systematic error and is among the greatest problems with the technique. Inadequate quality control at any stage of the process will reduce data quality--especially during photo acquisition, screening of negative quality, and registration during video input to the digitizer. A further major limitation of the technique results because uneven skylight leads to uninterpretable photographs. For this reason it is advisable to take photographs under uniform overcast skies at twilight. Because of the prevailing sky conditions at our New Mexico study sites, we limited our photo sessions to one-half hour before sunrise, which ensured proper light conditions. Sky conditions during the day tended to either be sunny or had uneven cloud cover. It was also not possible to obtain good photographs after sunset because of cloudy conditions. To extend the period of available field time we pushed the 400 ASA T-Max film to 800 ASA with no detectable degradation of quality.

5.1.3. Calibration of hemispherical photography measurements: Need for Hemispherical photographs have been successfully used to predict photon flux density (PFD) (Rich 1992). To obtain good estimates of PFD from hemispherical photographs, it is desirable to establish facilities for long-term monitoring of solar radiation above the canopy. Both direct and indirect solar radiation should be measured for the particular site being studied.

5.1.4. Summary evaluation of hemispherical photography: Hemispherical photography is the most effective technique for predicting solar radiation penetration in forest canopies. Other techniques require ongoing measurement through time, whereas hemispherical photography predicts radiation penetration from canopy geometry.

5.2. Decagon Sunfleck Ceptometer

5.2.1. Advantages of Sunfleck Ceptometer: The sunfleck ceptometer provides an easy, one-step method for measuring PAR and percent sunflecks. Though it does not create an image of the canopy geometry, the ceptometer offers immediate feedback about canopy openness. Downloading of the data directly into a personal computer is also efficient.

5.2.2. Limitations of Sunfleck Ceptometer: The Sunfleck Ceptometer samples of PAR at a point in time, and is therefore subject to problems of changes in solar angle and atmospheric conditions. The ceptometer spatially resolves the PAR measurements along its 0.8 m length, allowing for calculation of percent sunflecks. Measurement with linear sensor array also eliminates very small scale spatial heterogeneity (on the scale of cm) by averaging along the length of the array. The instrument can theoretically be used either to measure immediate radiation conditions or to infer canopy structure. As with the other devices for evaluation of light environment, we found use of the Sunfleck Ceptometer to be limited by the weather conditions. Patchy clouds affected light measurements when they moved between the sun and the sensors. We found, however, that restricting our field session to mid and late morning permitted meaningful data collection. However, restricting data collection only to a given time of day also restricted incident solar radiation to a narrow range of solar angles. As such, it only allows us to infer a limited amount of information about the interaction between solar radiation and canopy geometry. Further study is needed to determine how solar angle interacts with canopy geometry to give different reading of PAR and percent sunflecks. Also, study is required to determine whether percent sunfleck data can be used as input for gap fraction models to predict canopy structure.

5.2.3. Summary evaluation of sunfleck ceptometer: The Sunfleck Ceptometer is easy to use and allows rapid collection of point-in-time PAR and percent sunfleck data sampled along an 80 cm sensor array.

5.3. Licor LAI-2000 Canopy Analyzer

5.3.1. Advantages for the Canopy Analyzer: The Canopy Analyzer was also relatively easily used and understood. It does require approximately twice as much time to gather the field measurements as the Sunfleck Ceptometer. The instrument offers the advantage of automated data logging. The Canopy Analyzer, if used properly, provides a rapid and efficient means for gap fraction analysis of canopy geometry.

5.3.2. Limitations of the Canopy Analyzer: A central limitation of this instrument is the need for above canopy readings. This is not a problem in the crop canopies for which this instrument was designed. For study of taller canopies, such as forest canopies, towers or access to nearby large clearings are required for above-canopy readings. We were unable to obtain valid readings because of the inability to obtain above-canopy readings. Under ideal circumstances, two Canopy Analyzers would be employed to take simultaneous measurements above and below the canopy. Another limitation is the effect of sky conditions. Because overcast and cloudy sky conditions tend to change rapidly, it is probably best to acquire data under evenly overcast skies or in the early morning, as for hemispherical photography. This is especially important if simultaneous above and below-canopy readings are not possible. Calculations of canopy structure from gap fraction generally assume random distributions of canopy elements, an assumption which is not met for forest canopies. One can partially compensate for this by using a narrow view restrictor and by taking a series of readings in different view directions. This can be accomplished by sustaining the sensor head (in the shade cast by the operator) and rotating the view restrictor through a series of directions. Ideally, the above-canopy readings would also be taken in the same series of view directions. More study is required to determine the utility of the Canopy Analyzer in canopies with non-random

distribution of canopy elements. It is also desirable to determine how close in time above and below-canopy readings must be taken.

5.3.3. Summary evaluation of the Canopy Analyzer: The LAI-2000 Canopy Analyzer is the best instrument for obtaining rapid calculations of LAI and leaf inclination, but is only effective if nearly simultaneous above and below-canopy readings are obtained.

5.4. Stand Mapping and Measurement of Allometry

5.4.1. Advantages of stand mapping and measurment of allometry: Basic measurements of species identity, location, stem diameter, tree height, and crown dimensions have high utility for any ecological study at a site. Surveying and placement of grid markers facilitate mapping of stem locations and crown dimensions. For canopies up to 15 m tall, tree-measuring poles are the easiest and most accurate means to measure heights.

5.4.2. Limitations of mapping and allometry techniques: Mapping and measurement of stand allometry was the most labor intensive segment of our field studies. Of the basic stand characteristics, measurement of crown dimensions is the most difficult. Even more difficult is faithfully representing the distribution of canopy elements (and by complement, the openings). There is a need for better means for detailed characterization of canopy geometry. The most promising approaches involve remote sensing. In particular, stereo imagery can be used to 1) map the surface topography of the canopy, 2) map locations and species identity of individual crowns, and 3) estimate productive biomass.

5.4.3. Summary evaluation of mapping and allometry techniques: Basic mapping of stand structure is the most direct means for representing canopy geometry and essential for stand characterization in all ecological studies.

5.5. Time-Domain Reflectometry

5.5.1. Advantages of time-domain reflectometry (TDR): TDR can be an efficient means for monitoring changes in soil moisture with minimal disturbance of soil structure. If probes are left in place, they can be readily accessed and read. Multiplexers can further increase the efficiency of the process by sequentially reading an array of soil probes. Soil moisture as a function of depth can be monitored by using probes of different lengths. In comparison with soil core techniques, TDR is easier and less disruptive in the long term because soil probes can be left in the soil for ongoing data collection. In comparison with neutron access tube techniques, TDR is also easier and does not require the labor and resources for implantation of sampling tubes. TDR eliminates the need for a radioactive neutron source and is, in that respect, safer for the user.

5.5.2. Limitations of time-domain reflectometry: The initial setup of a TDR sample array is complicated and labor intensive. A permanently implanted array is desirable. Movement of TDR soil probes between sample locations is impractical because the equipment is easily damaged.

5.5.3. Summary evaluation of time-domain reflectometry: TDR is an excellent means for non-disruptive monitoring of soil moisture.

6.0. RECOMMENDATIONS FOR FUTURE WORK

The complex vegetation patterns of the LANL NERP result from numerous environmental factors, both biotic and abiotic. Long-term detailed studies of the

interrelationships of both physical parameters (water balance, solar radiation balance, carbon flux, nutrient cycling; microclimate, geology, and micrometeorology), and the biotic parameters (ecology of both flora and fauna) are essential for understanding the complex relationships that affect the ecology of native communities and succession that is likely to occur on remediated sites. Such long-term studies require use of advanced non-invasive instrumentation, and must be coupled with detailed ecological models. The following is a set of recommendations that will assist in planning future ecological studies in the NERP.

6.1. Basic Research Needs

Four basic hypotheses need to be addressed concerning effects of canopy architecture on microclimate, coupling to ecological processes, and relevance for predicting effects of climate change at local and regional scales:

6.1.1. Hypothesis One: Ecologically significant differences in near-ground microclimate (heat and water balance) are most pronounced in open canopies and result in strong differentiation between microsites; based on canopy geometry, microsite differences are expected a) to be greatest beneath canopy openings that have a diameter on the same order of magnitude as the canopy height, b) to show strong diurnal differences along east-west axes, and c) to show strong seasonal differences along north-south axes.

6.1.2. Hypothesis Two: Spatial patterns in arid woodlands, with clumped patches of shrubs and trees, result because seedlings are only able to germinate and survive in safe microsites beneath or on the edges of existing clumps and because water limitations require extensive root growth in spaces between clumps; from the perspective of a seedling, establishment requires both the moderated microclimate at a clump edge and release of water and nutrients as the result of disturbance or senescence of larger individuals; seedlings will tend to become established in safe microsites on the north edges of clumps, while older individuals will tend to die on the south edges.

6.1.3. Hypothesis Three: Short-term response to changes in climatic conditions will be predictable as changes in carbon and water flux within existing canopies; in particular, the microclimate model will enable a) prediction of water balance for any location in a given woodland; and b) local differences in water balance will be measurable as differences in soil moisture.

6.1.4. Hypothesis Four: Longer-term responses to climate change will result in changes in associated flux properties, and community composition that will be predictable as habitat shifts along existing environmental gradients, and measurable as changes in canopy architecture; warmer or drier conditions will lead to lower rates of recruitment, greater spacing between clumps of trees and shrubs, and greater prevalence of junipers; whereas cooler and wetter (cloudier) conditions will result in higher rates of recruitment, and greater prevalence of pinyons. This pattern is readily observable along existing elevational gradients.

6.2. Development of Coupled GIS-Based Microclimate and Ecological Models

6.2.1. Development of GIS databases: Basic GIS databases need to be expanded for the NERP. Baseline maps required for the overall NERP should include topography, facilities, geology, soils, and vegetation. More detailed maps are required for the long-term study areas. These should include more detailed maps of surveyed microtopography, individual tree and shrub distributions, and canopy geometry. The GIS will be especially valuable for development of spatially explicit microclimate and ecological models.

6.2.2. Microclimate model: The microclimate model needs to couple two submodels: one to calculate energy balance and a second to calculate water balance. In essence, the

microclimate model would calculate energy balance as a function of solar radiation input, ambient air temperature, relative humidity, and latent energy flux (based on measures of evapotranspiration). Effects of air turbulence should be incorporated as needed. Such a microclimate model would predict changes local in temperature, humidity, and availability of PAR, as well as indices of water stress. Solar radiation calculations could be based on a modified version of SOLARFLUX (Hetrick et al. 1993a, 1993b, Dubayah and Rich in press), in which empirical values of solar radiation (changes in transmittivity) are be incorporated in calculations. The model calculates incoming solar radiation based upon surface orientation and sky obstruction (shading) by topographic features (trees, shrubs, terrain...). The water balance submodel could be based on models developed at LANL (E. Springer pers. comm., J. Nyhan pers. comm., D. Breshears pers. comm.) that examine the timing and duration of precipitation events, canopy interception, detailed knowledge of runoff and infiltration, and evapotranspiration coupled to basic climatic conditions.

6.2.3. Safe microsite model: Recent work in ecological modeling have focused on integrating of patch dynamics approaches (Holt 1993), with mechanistically richer models, such as SORTIE (Pacala et al. in press) and ZELIG (Smith and Urban 1988), which include species-specific submodels of growth, mortality, fecundity, dispersal, and establishment as affected by local resource abundance. A "safe microsite model" of community dynamics in arid woodlands that would provide a synthesis of the known physiology, demography, water relations, productivity, and nutrient dynamics for PJ woodlands. Such a model would couple canopy architecture, microclimate, and population submodels (figure 4A). We expect that recruitment patterns will be severely limited by the availability of microsites where water stress does not lead to low growth rates or high mortality (figure 4B). From the perspective of a seedling, establishment requires a safe microsite, the distribution and extent of which vary in predictable spatial patterns with climatic fluctuations.

6.3. Field Research Needs

6.3.1. Establishment of additional mapped forest plots: additional mapped forest plots need to be established for long-term study at a full range of elevations at the Los Alamos NERP.

6.3.2. Micrometeorology measurements: measurements of temperature, humidity, total solar radiation, PAR, and air turbulence are needed as a function of canopy position. Temperature measurements should include soil, leaf surface, and air measurements using thermocouples and an infrared thermometer. Such measurements should be carefully stratified by position relative to PJ clumps (i.e., beneath, between, and on N, S, E, or W edge), and by height.

6.3.3. Geometrical Reconstruction of Plant Canopy Architecture: Work needs to continue on developing techniques for reconstruction of canopy architecture to produce canopy digital elevation models (CDEMs) of the upper canopy surface by two independent means: 1) using allometric reconstruction, based upon measurements of individual location, stem diameter, height, and crown dimensions, in conjunction with high resolution orthoimagery to better define irregularities in crown shape (Rich et al. 1993a); and 2) using stereoimagery and recently developed software (e.g., ERDAS Digital Orthomax). If successful, this latter approach could be used to determine canopy surface topography of any canopy based on high resolution stereoimagery, with only minimal need for field verification. The ultimate goal is to construct more detailed 3-dimensional reconstructions of canopy elements within individual trees and shrubs, following approaches such as those developed by Scott Martens (LANL) and Richard Fournier (Canada Centre for Remote Sensing).

6.3.4. Measurement of soil moisture using neutron scattering and TDR: Extensive long-term data are available for the PJ study site, based upon ongoing monitoring using in situ neutron scattering (approximately 10 years data) and time-domain reflectometry (TDR)

techniques (approximately 3 years data) (Lin et al. 1992). These measurements should be continued and expanded in scope.

6.3.5. Ecophysiology measurements: While extensive publish transpiration and photosynthesis measurements have been made in PJ at the LANL NERP (e.g., Lajtha and Barnes 1991) further measurements are need with careful stratification by canopy position and micrometeorology measurements.

6.3.6. Tagged seedling studies: Ongoing population studies are needed of natural populations to better understand relations between microclimate and population processes in PJ woodlands. This approach involves monitoring of tagged populations of pinyon and juniper seedlings within mapped study sites to determine recruitment, growth, and survivorship as a function of microsite.

6.3.7. Soil moisture using multifrequency radar: Over the last two decades several investigators have studied the utility of microwave sensors for determining soil moisture content of bare and vegetation-covered soils (Schmugge et al. 1974, Njoku and Kong 1977, Wang et al. 1987, 1992, Newton and Rouse 1980, Ulaby 1974, Ulaby et al. 1978, 1979, 1982, Jackson et al. 1981, 1987, Dobson and Ulaby, 1986). Studies are needed to 1) evaluate the utility of multifrequency radars in estimating the moisture profile as a function of depth; 2) investigate the effect of surface roughness and vegetation on the backscattered signal, particularly at frequencies between 300 MHz and 2000 MHz; and 3) develop an algorithm for obtaining volumetric soil moisture content directly from the measured data. By extending the radar frequency into the lower part of the microwave spectrum we can obtain greater penetration into soil. By using a wide range of microwave frequencies we may be able to determine soil moisture content as a function of depth.

6.3.8. Greenhouse amd Field Experiments Concerning Water Stress in Seedlings: Greenhouse and field experiments are required to investigate seedling responses to different levels of water stress in pinyons and junipers. For example, a factoral design of the greenhouse experiment could involve the growing seedlings of the dominant species under different solar radiation, water, and temperature regimes, all with appropriate replication. Likewise, a factoral design of a field experiment could involve planting seedlings of the dominant species in a variety of microclimates as determined by spatial location (e.g., under clumps; at N, S, E, and W edges; and between clumps), again with appropriate replication.

7.0. CONCLUSIONS

7.1. Need for Integrative Approaches and New Technologies for Study of Canopy Architecture and Function: An important objective of modern ecology is integration across traditional disciplines, levels of organization, and methodologies. The complexity of ecological systems demands rigorous new approaches and new technology for data acquisition and analysis. Our approach to development of spatially explicit models that examine influence of canopy architecture on microclimate in semiarid woodlands can be used to predict distributions of key factors limiting ecological processes, and thus provides the means for integrating local effects to stand and landscape scales. This approach is provides the following benefits for waste site design and remediation: 1) improved methodology for monitoring the post-closure status of sites at Los Alamos; 2) improved ability to parameterize hydrologic models for predicting the stability of site closure designs; 3) improved ability to predict the long-term consequences of closure designs of remediation efforts at LANL.

7.2. Remote Sensing for Characterization of Canopy Architecture: New remote sensing techniques promise to provide rich array of new tools for characterizing canopy architecture and soil moisture. Automated reconstruction of canopy surface topography from stereoimagery may

provide key input to coupled microclimate and ecological models. Multispectral radar technique may revolutionize our ability to construct soil moisture profiles, validate the microclimate model, and integrate to a regional scale.

7.3. Microclimate Modeling Approaches to Link Architecture to Ecological Processes: Microclimate heterogeneity, resulting from canopy heterogeneity, is expected to have a strong influence on heat balance, water balance, and conditions that affect rates of transpiration and photosynthesis. The diversity of microsites is likely to have profound effects at the community level, since hotter, drier microsites may be unsuitable for seedling growth and survival. At the same time, microsites beneath and at the edges of clumps may be limited by light during much of the year. Thus, climatic changes will be translated into differences in the distribution and extent of "safe microsites" for establishment growth of a particular species.

7.4. Issues of Scale and Prediction of Responses to Climate Change: Whether applied locally (Rich 1990, Rich et al. 1993b, Galo et al. 1992, Rich and Weiss 1991) or at broader spatial scales (Rich et al. 1992, Saving et al. 1993), microclimate models can provide a mechanistic understanding of the fundamental biophysical factors that govern ecological systems, and provide a powerful means for evaluating potential ecological impacts of global climate change.

8.0. LITERATURE CITED

Anderson, M. C. 1964. Studies of the woodland light climate I. The photographic computation of light condition. Journal of Ecology 52:27-41.

Baldocchi, D.D., B.B. Hicks, and T.P. Meyers. 1988. Measuring biosphere-atmosphere exchanges of biologically related gases with micrometeorological methods. Ecology 69:1331-1340.

Billings, W.D. 1954. Temperature inversion in the pinyon-juniper zone of a Nevada mountain range. Butler University Botanical Studies 11:112-117.

Breshears, D.D. 1993. Spatial partitioning of water use by herbaceous and woody lifeforms in semiarid woodlands. Ph.D. Dissertation. Colorado State University. Fort Collins, CO.

Dobson, M.C., and F.T. Ulaby. 1986. Preliminary evaluation of the SIR-B response to soil moisture, surface roughness and crop canopy cover. IEEE Transactions on Geoscience and Remote Sensing, GE24: 517-526.

Dubayah, R. and P.M. Rich. 1994. GIS-based solar radiation modeling. Proceedings of the Second International Conference on Integrating Geographical Information Systems and Environmental Modeling. In Press.

Galo, A.T., P.M. Rich, and J.J. Ewel. 1992. Effects of forest edges on the solar radiation regime in a series of reconstructed tropical ecosystems. American Society for Photogrammetry and Remote Sensing Technical Papers. pp 98-108.

Geiger, R. 1965. The climate near the ground. Harvard University Press, Cambridge, MA.

Hall, F.G., D. Botkin, D.E. Strebel, K.D. Woods and S.J. Goetz. 1991. Large-scale patterns of forest succession as determined by remote sensing. Ecology 72(2):628-640.

Hetrick, W.A., P.M. Rich, and F.J. Barnes, and S.B. Weiss. 1993. GIS-based solar radiation flux models. American Society for Photogrammetry and Remote Sensing Technical Papers, Vol 3 GIS Photogrammetry and Modeling. pp 132-143.

Hetrick, W.A., P.M. Rich, and S.B. Weiss. 1993. Modeling insolation on complex surfaces. Thirteenth Annual ESRI User Conference, Volume 2. pp 447-458.

Holt, R.D. 1993. Ecology at the mesoscale: the influence of regional processes on local communities. In: R. Ricklefs and D. Schluter (eds.) Species diversity in ecological communities. University of Chicago Press.

Houghton, R. A. and G. A. Woodwell. 1989. Global climate change. Scientific American 260:18-16.

Jackson, T.J., A. Chang, and T.J. Schmugge. 1981. Active microwave measurements for estimating soil moisture in Oklahoma. Photogrammetric Engineering and Remote Sensing 47: 801-805.

Jackson, T.J., M.E. Hawley, and P.E. O'Neill. 1987. Preplanting soil moisture using passive microwave sensors. Water Resources Bulletin 23: 11-19.

Lajtha, K. and F.J. Barnes. 1991. Carbon gain and water use in pinyon-juniper woodlands of northern New Mexico: field versus phytotron chamber measurements. Tree Physiology 9:59-67.

Lin, T., P.M. Rich, D.A. Heisler, and F.J. Barnes. 1992. Influences of canopy geometry on near-ground solar radiation and water balances of pinyon-juniper and ponderosa pine woodlands. American Society for Photogrammetry and Remote Sensing Technical Papers. pp 285-294.

Martens, S. N., S. L. Ustin, and J. M. Norman. 1991. Measurement of tree canopy architecture. International Journal of Remote Sensing.

Martens, S. N., S. L. Ustin, and R. A. Rousseau. 1991. Estimation of tree canopy leaf area index by gap fraction analysis.

McNaughton, K.G. 1989. Regional interactions between canopies and the atmosphere. in: Russell, G., B. Marshall, and P.G. Jarvis. Plant canopies: their growth, form and function. Cambridge University Press, New York. 178 p.

Mooney, H.A., P.M. Vitousek, and P.A. Matson. 1987. Exchange of materials between terrestrial ecosystems and the atmosphere. Science 238:926-932.

Newton, R.W., and J.W. Rouse. 1980. Microwave radiometer measurements of soil moisture content. IEEE Transactions on Antennas and Propagation AP28: 680-686.

Njoku, E.G., and J.A. Kong. 1977. Theory of passive microwave remote sensing of near-surface soil moisture. J. Geophysical Research 82: 3108-3118.

Norman, J. M. and G. S. Campbell. 1989. Canopy structure. pp. 301-235 In: Pearcy, R. W., J. Ehleringer, H. A. Mooney, and P. W. Rundel. Plant Physiological Ecology: Field Methods and Instrumentation. Chapman and Hall. New York.

Pacala, S.W., C.D. Canham, and J.A. Silander, Jr. In Press. Forst models defined by field measurements: I. the design of a northeastern forest simulator. Canadian Journal of Forestry Research.

Rich, P. M, D. M. Ranken, and J. S. George. 1989. A manual for microcomputer image analysis. Los Alamos National Laboratory Report LA-11732-M.

Rich, P. M. 1988. Video image analysis of hemispherical canopy photography. pp. 84-95 In: P. W. Mausel (ed). First Special Workshop on Videography. Terre Haute, Indiana. May 19-20, 1988. American Society for Photogrammetry and Remote Sensing.

Rich, P. M. 1989. A manual for analysis of hemispherical canopy photography. Los Alamos National Laboratory Report LA-11733-M.

Rich, P. M., D. B. Clark, D. A. Clark, and S. F. Oberbauer. 1992. Long-term study of light environments in tropical wet forest using quantum sensors and hemispherical photography. Agricultural and Forest Meteorology. In Press.

Rich, P.M. 1990. Characterizing plant canopies with hemispherical photography. In: N.S. Goel and J.M. Norman (eds). Instrumentation for studying vegetation canopies for remote sensing in optical and thermal infrared regions. Remote Sensing Reviews 5:13-29.

Rich, P.M. and S.B. Weiss. 1991. Spatial models of microclimate and habitat suitability: lessons from threatened species. Proceedings of the Eleventh Annual ESRI User Conference. pp 95-99.

Rich, P.M., G.S. Hughes, and F.J. Barnes. 1993a. Using GIS to reconstruct canopy architecture and model ecological processes in pinyon-juniper woodlands. Thirteenth Annual ESRI User Conference, Volume 2. pp 435-445.

Rich, P.M., D.A. Clark, D.B. Clark, and S.F. Oberbauer. 1993b. Long-term study of solar radiation regimes in a tropical wet forest using quantum sensors and hemispherical photography. Agricultural and Forest Meteorology 65:107-127.

Rich, P.M., W.A. Hetrick, and S.C. Saving. in press. A manual for analyzing topographic effects on solar radiation: the SOLARFLUX software program. Los Alamos National Laboratory Report.

Saving, S.C., P.M. Rich, and J.T. Smiley. 1993. GIS-based microclimate models for assessment of habitat quality in natural reserves. American Society for Photogrammetry and Remote Sensing Technical Papers, Vol 3 GIS Photogrammetry and Modeling. pp 319-330.

Schmugge, T.J., P. Gloersen, T. Wilheit, and F. Geiger. 1974. Remote Sensing of Soil Moisture with Microwave Radiometers. J. Geophysical Research 79: 317-323.

Smith, T.M. and D.L. Urban. 1988. Scale and resolution of forest structural patterns. Vegetation 4: 143-150.

Strahler, A.H. and D.L.B. Jupp. 1990. Modelling bidirectional reflectance of forests and woodlands using boolean models and geometric optics. Remote Sens Environ 34:153-166.

Topp, G. C. and J. L. Davis. 1985. Measurement of soil water content using time-domain reflectrometry (TDR):a field evaluation. Soil Science Society of America Journal 49:19-24.

Topp, G. C., J. L. Davis, and A. P. Annan. 1980. Electromagnetic determination of soil water content: measurement in coaxial transmission lines. Water Res. Res. 16:574-582.

Topp, G. C., J. L. Davis, and A. P. Annan. 1982a. Electromagnetic determination of soil water content using TDR: I. Applications to wetting fronts and steep gradients. Soil Science Society of America Journal 46:672-677.

Topp, G. C., J. L. Davis, and A. P. Annan. 1982b. Electromagnetic determination of soil water content using TDR: II. Evaluation of installation and configuration of parallel transmission lines. Soil Science Society of America Journal 46:678-684.

Ulaby, F.T. 1974. Radar measurement of soil moisture content. IEEE Transactions on Antennas and Propagation AP22: 257-265.

Ulaby, F.T., A. Aflam, and M.C. Dobson. 1982. Effect of vegetation cover on radar sensitivity to soil moisture. IEEE Transactions on Geoscience and Remote Sensing GE-20: 476-481.

Ulaby, F.T., G.A. Bradley, and M.C. Dobson. 1979. Microwave backscatter dependence on surface roughness, soil moisture, and soil texture: (2) vegetation-covered soil. IEEE Transactions on Geoscience and Electronics GE17: 33-40.

Ulaby, F.T., P.P. Batlivala, and M.C. Dobson. 1978. Microwave backscatter dependence on surface roughness, soil moisture, and soil texture: (1) bare soil. IEEE Transactions on Geoscience and Electronics GE16: 476-481.

Wang, J.R., E.T. Engman, T.J. Schmugge, T. Mo, and J.C. Shiue. 1987. The effects of soil moisture, surface roughness, and vegetation on L-Band emission and backscatter. IEEE Transactions on Geoscience and Remote Sensing GE25: 825-833.

Wang, J.R., S. Gogineni, and J. Ampe. 1992. Active and passive microwave measurements of soil moisture in FIFE. Journal of Geophysical Research 97: 18,979-18,985.

Welles, Jon M. 1990. Some indirect methods of estimating canopy structure. Remote Sensing Reviews 5:31-43.

West, N.E., R.J. Tausch, K.H. Rea, and P.T. Tueller. 1978. Phytogeographical variation within pinyon-juniper woodlands of the Great Basin. pp. 119-136 In: K.T. Harper and J.L. Reveal (editors) Intermountain biogeography: a symposium. Great Basin Naturalist Memoirs 2. Brigham Young University. Provo, UT.

9.0. PROJECT PUBLICATIONS AND PRESENTATIONS

9.1. PUBLICATIONS

Rich, P.M., R. Dubayah, W.A. Hetrick, and S.C. Saving. 1994. Using viewshed models to calculate intercepted solar radiation: applications in ecology. American Society for Photogrammetry and Remote Sensing Technical Papers. pp 524-529.

Dubayah, R. and P.M. Rich. 1994. Topographic solar radiation models for GIS. International Journal of Geographic Information and Analysis. In Press.

Dubayah, R. and P.M. Rich. 1994. GIS-based solar radiation modeling. Proceedings of the Second International Conference on Integrating Geographical Information Systems and Environmental Modeling. In Press.

Saving, S.C., W.A. Hetrick, P.M. Rich, A.D. Weiss, S.B. Weiss. 1994. Physiographic inventory methodology. Proceedings of the Fourteenth Annual ESRI User Conference.

Rich, P.M., D.A. Clark, D.B. Clark, and S.F. Oberbauer. 1993. Long-term study of solar radiation regimes in a tropical wet forest using quantum sensors and hemispherical photography. Agricultural and Forest Meteorology 65:107-127.

Rich, P.M., G.S. Hughes, and F.J. Barnes. 1993. Using GIS to reconstruct canopy architecture and model ecological processes in pinyon-juniper woodlands. Thirteenth Annual ESRI User Conference, Volume 2. pp 435-445.

Hetrick, W.A., P.M. Rich, and S.B. Weiss. 1993. Modelling insolation on complex surfaces. Thirteenth Annual ESRI User Conference, Volume 2. pp 447-458.

Hetrick, W.A., P.M. Rich, and F.J. Barnes, and S.B. Weiss. 1993. GIS-based solar radiation flux models. American Society for Photogrammetry and Remote Sensing Technical Papers, Vol 3 GIS Photogrammetry and Modeling. pp 132-143.

Saving, S.C., P.M. Rich, S.B. Weiss, and J.T. Smiley. 1993. GIS-based microclimate models for assessment of habitat quality in natural reserves. American Society for Photogrammetry and Remote Sensing Technical Papers, Vol 3 GIS Photogrammetry and Modeling. pp 319-330.

Lin, T., P.M. Rich, D.A. Heisler, and F.J. Barnes. 1992. Influences of canopy geometry on near-ground solar radiation and water balances of pinyon-juniper and ponderosa pine woodlands. American Society for Photogrammetry and Remote Sensing Technical Papers. pp 285-294.

9.2. PRESENTATIONS

Rich, P.M., R.L. Chazdon, and J.S. Denslow. 1994. Spatial and temporal variation of solar radiation regimes in plant canopy gaps. Annual Meeting of the Ecological Society of America.

Rich, P.M., W.A. Hetrick, S. C. Saving, and R. Dubayah. 1994. Using viewshed models to calculate intercepted solar radiation: applications in ecology. Annual Meeting of the American Society for Photogrammetry and Remote Sensing.

Rich, P.M. and R. Dubayah. 1994. Spatial and temporal patterns of solar radiation along topographic surfaces: coupling with energy balance models. Ninth Annual U.S. Landscape Ecology Symposium.

Rich, P.M. 1994. Biophysical factors in the ecology of pinyon-juniper woodlands. Workshop on Integrative Modeling of Pinyon-Juniper Woodland Ecology, Santa Fe, NM. Co-organized by Paul M. Rich and Scott Martens.

Price, K.P. and P.M. Rich. 1994. Development of digital canopy model using digital stereopairs. Annual Meeting of the American Association of Geographers.

Price, K.P., P.M. Rich, and R. O'Neal. 1994. Measurement and three-dimensional modeling of plant canopies using remotely sensed data. 126th Kansas Academy of Science Meeting, Washburn University.

Saving, S.C., W.A. Hetrick, P.M. Rich, A.D. Weiss, S.B. Weiss. 1994. Physiographic inventory methodology. Fourteenth Annual ESRI User Conference.

Dubayah, R. and P.M. Rich. 1993. GIS-based solar radiation modeling. Second International Conference on Integrating Geographical Information Systems and Environmental Modeling.

Rich, P.M., K.P. Price, R.D. Holt, and F.J. Barnes. 1993. Spatially explicit models of microclimate and ecophysiology within pinyon-juniper woodland canopies: a GIS and remote sensing approach. Annual Meeting of the Ecological Society of America.

Rich, P.M., F.J. Barnes, and K.P. Price. 1993. Spatial patterns of canopy architecture in pinyon-juniper woodlands: inferences from stand allometry and remote sensing. Eighth Annual U.S. Landscape Ecology Symposium.

Hetrick, W.A., P.M. Rich, and S.B. Weiss. 1993. Modelling insolation on complex surfaces. Thirteenth Annual ESRI User Conference.

Hughes, G.S. P.M. Rich, and F.J. Barnes. 1993. Using GIS to reconstruct canopy architecture and model ecological processes in pinyon-juniper woodlands. Thirteenth Annual ESRI User Conference.

Hetrick, W.A., P.M. Rich, and F.J. Barnes, and S.B. Weiss. 1993. GIS-based solar radiation flux models. Annual Meeting of the American Society for Photogrammetry and Remote Sensing.

Saving, S.C., P.M. Rich, and J.T. Smiley. 1993. GIS-based microclimate models for assessment of habitat quality in natural reserves. Annual Meeting of the American Society for Photogrammetry and Remote Sensing.

Barnes, F.J., P.M. Rich, C. Lin, B. Wilcox, J. Nyhan, D. Breshears, and S. Tarbox. 1992. Spatial and temporal variability in water balance components in pinyon-juniper and ponderosa pine communities along an elevational gradient. Annual Meeting of the Society of Landscape Ecologists.

Lin, T., D.A. Heisler, P.M. Rich, and F.J. Barnes. 1992. Influences of canopy geometry on near-ground solar radiation and water balances of pinyon-juniper and ponderosa pine woodlands. Annual Meeting of the American Society for Photogrammetry and Remote Sensing.

Appendix 1. Indirect Site Factor without and with cosine correction (ISFU and ISFC, respectively), Direct Site Factor without with cosine correction (DSFU and DSFC, respectively) calculated from hemispherical photographs at the 1.75 m level for the PJ Woodland Transect. locations are designated by the label of a neutron access tube, followed by a decimal point and the distance from that neutron access tube along the transect line toward the next neutron access tube. Full data sets for this and other appendices have been provided to LANL on computer disk. The hemispherical photograph analyses include gap fraction tables and monthly values.

LOCATION	POSITION (m)	ISFU	ISFC	DSFU	DSFC
1401.0	0	0.46197	0.57335	0.41381	0.41143
1401.1	1	0.47346	0.60665	0.43756	0.43281
1401.2	2	0.53288	0.69061	0.56961	0.57415
1401.3	3	0.53533	0.71548	0.66963	0.70904
1401.4	4	0.49950	0.68830	0.66191	0.70451
1401.5	5	0.51030	0.69551	0.69398	0.74017
1401.6	6	0.47844	0.64745	0.64194	0.68541
1401.7	7	0.44859	0.59685	0.62148	0.64983
1401.8	8	0.43144	0.56141	0.58849	0.60194
1401.9	9	0.37790	0.46788	0.51938	0.50900
1402.0	10	0.37277	0.45229	0.58567	0.60890
1402.1	11	0.34709	0.37927	0.54095	0.52277
1402.2	12	0.27887	0.28261	0.31476	0.28253
1402.3	13	0.22589	0.22639	0.17573	0.14840
1402.4	14	0.37459	0.37938	0.33158	0.30522
1402.5	15	0.46755	0.55558	0.44524	0.44074
1402.6	16	0.52903	0.67407	0.57422	0.58087
1402.7	17	0.55400	0.71845	0.66968	0.68474
1402.8	18	0.57547	0.76113	0.75113	0.78859
1402.9	19	0.61352	0.79996	0.80516	0.84348
1403.0	20	0.62317	0.80980	0.80119	0.84170
1403.1	21	0.61253	0.80460	0.82907	0.86845
1403.2	22	0.60888	0.79500	0.85314	0.88896
1403.3	23	0.59910	0.77719	0.84246	0.88476
1403.4	24	0.57507	0.73625	0.79071	0.83461
1403.5	25	0.51922	0.64149	0.70037	0.73760
1403.6	26	0.39391	0.44606	0.47452	0.46401
1403.7	27	0.33249	0.36111	0.30506	0.27146
1403.8	28	0.34929	0.37029	0.32625	0.28884
1403.9	29	0.33356	0.34437	0.28071	0.24497
1404.0	30	0.38243	0.41204	0.26603	0.22254
1404.1	31	0.50331	0.59872	0.46989	0.45086
1404.2	32	0.51270	0.65765	0.51224	0.52907
1404.3	33	0.54355	0.72532	0.60573	0.65841
1404.4	34	0.56009	0.75240	0.66839	0.73075
1404.5	35	0.56071	0.75727	0.68515	0.74756
1404.6	36	0.57784	0.77558	0.70613	0.76934
1404.7	37	0.59025	0.79779	0.77388	0.82959
1404.8	38	0.59756	0.80320	0.84682	0.88701
1404.9	39	0.59566	0.79118	0.89025	0.91895
1405.0	40	0.57587	0.75266	0.88418	0.91542
1405.1	41	0.50992	0.65373	0.81423	0.85371
1405.2	42	0.41450	0.47884	0.67223	0.68171
1405.3	43	0.30286	0.32344	0.42030	0.37686
1405.4	44	0.24974	0.26527	0.33186	0.29157
1405.5	45	0.21980	0.24382	0.19749	0.16783
1405.6	46	0.28309	0.31203	0.22593	0.19547

1405.7	47	0.23623	0.26451	0.17825	0.16931
1405.8	48	0.38384	0.46742	0.27232	0.25182
1406.0	49	0.43229	0.54893	0.32429	0.30853
1406.1	50	0.37810	0.48148	0.27907	0.28311
1406.2	51	0.36312	0.51825	0.39652	0.43075
1406.3	52	0.34986	0.45312	0.46433	0.48223
1406.4	53	0.29098	0.38613	0.60099	0.65791
1406.5	54	0.21597	0.24223	0.31483	0.32188
1406.6	55	0.20603	0.24663	0.27842	0.29605
1406.7	56	0.17061	0.20818	0.24443	0.24207
1406.8	57	0.23006	0.25527	0.23093	0.23061
1406.9	58	0.31590	0.38129	0.28414	0.27425
1406.10	59	0.43941	0.55601	0.41538	0.43084
1406.11	60	0.49596	0.64879	0.52341	0.57385
1407.0	61	0.48807	0.63684	0.50417	0.55163
1407.1	62	0.46554	0.60744	0.45844	0.48637
1407.2	63	0.40871	0.53665	0.41870	0.45750
1407.3	64	0.37195	0.44375	0.21485	0.19602
1407.4	65	0.60916	0.81218	0.74947	0.79460
1407.5	66	0.61893	0.82870	0.80662	0.85006
1407.6	67	0.54856	0.74844	0.84156	0.88072
1407.7	68	0.39405	0.49601	0.63150	0.61219
1407.8	69	0.42919	0.58933	0.59573	0.65180
1408.0	70	0.53880	0.73046	0.69758	0.74703
1408.1	71	0.56445	0.76238	0.77326	0.82626
1408.2	72	0.55695	0.74050	0.77268	0.81368
1408.3	73	0.53149	0.70015	0.73302	0.77417
1408.4	74	0.51861	0.68008	0.63890	0.68552
1408.5	75	0.52243	0.69139	0.56383	0.60818
1408.6	76	0.55689	0.73122	0.59520	0.64120
1408.7	77	0.58043	0.75907	0.62997	0.67953
1408.8	78	0.55628	0.74581	0.62991	0.68226
1408.9	79	0.51122	0.70984	0.66255	0.71666
1408.10	80	0.30628	0.45189	0.43445	0.49491
1408.11	81	0.26902	0.35548	0.31845	0.33613
1409.0	82	0.52039	0.72839	0.57479	0.66251
1409.1	83	0.58410	0.80050	0.71412	0.79003
1409.2	84	0.60446	0.82049	0.77396	0.83281
1409.3	85	0.61116	0.82850	0.80818	0.85629
1409.4	86	0.60764	0.82391	0.83459	0.87597
1409.5	87	0.59505	0.80620	0.84626	0.88529
1409.6	88	0.56464	0.76934	0.84831	0.88569
1409.7	89	0.52605	0.73185	0.77770	0.82919
1409.8	90	0.49367	0.70481	0.72566	0.78366
1409.9	91	0.48917	0.69852	0.70959	0.76810
1409.10	92	0.48568	0.68920	0.70900	0.76321
1410.0	93	0.45517	0.62509	0.62654	0.66181
1410.1	94	0.43591	0.58728	0.61882	0.64407
1410.2	95	0.39623	0.53756	0.63274	0.66934
1410.3	96	0.36611	0.47732	0.60607	0.64307
1410.4	97	0.32031	0.41558	0.52793	0.56128
1410.5	98	0.25429	0.31935	0.40245	0.41575
1410.6	99	0.23819	0.28856	0.29447	0.28970
1410.7	100	0.24310	0.30217	0.30039	0.27538
1410.8	101	0.29862	0.38798	0.36452	0.35850
1411.0	102	0.30706	0.39914	0.40484	0.40678

Appendix 2. ISFU, ISFC, DSFU, and DSFC at the 1.0 m level for the PJ Woodland Transect. Note: locations are designated by the label of a neutron access tube, followed by a decimal point and the distance from that neutron access tube along the transect line toward the next neutron access tube.

LOCATION	POSITION (m)	ISFU	ISFC	DSFU	DSFC
1401.0	0	0.38937	0.51485	0.39483	0.39728
1401.1	1	0.42598	0.57200	0.44715	0.45214
1401.2	2	0.44488	0.60883	0.49235	0.51571
1401.3	3	0.43610	0.60638	0.57770	0.62607
1401.4	4	0.43301	0.61762	0.58960	0.64800
1401.5	5	0.41857	0.59579	0.59762	0.65659
1401.6	6	0.41093	0.57091	0.58636	0.63256
1401.7	7	0.36005	0.48954	0.53920	0.57722
1401.8	8	0.31861	0.43184	0.48841	0.51756
1401.9	9	0.30551	0.39872	0.44207	0.45352
1402.0	10	0.29540	0.35836	0.47637	0.50396
1402.1	11	0.27461	0.31311	0.43326	0.44118
1402.2	12	0.23367	0.23625	0.27598	0.24001
1402.3	13	0.23799	0.24777	0.19730	0.17361
1402.4	14	0.36417	0.40772	0.27151	0.22992
1402.5	15	0.39700	0.50010	0.36708	0.36877
1402.6	16	0.42615	0.57257	0.43864	0.46479
1402.7	17	0.48654	0.65201	0.59039	0.61651
1402.8	18	0.53632	0.71618	0.71882	0.75887
1402.9	19	0.56894	0.75676	0.77792	0.82076
1403.0	20	0.58165	0.76481	0.79654	0.83635
1403.1	21	0.56467	0.74925	0.80158	0.84420
1403.2	22	0.55407	0.73862	0.81663	0.86282
1403.3	23	0.53786	0.71130	0.79685	0.84796
1403.4	24	0.52492	0.68156	0.72930	0.77537
1403.5	25	0.48283	0.60589	0.64907	0.68290
1403.6	26	0.41653	0.49716	0.49130	0.49850
1403.7	27	0.35629	0.41051	0.36270	0.34670
1403.8	28	0.30962	0.33762	0.30558	0.27461
1403.9	29	0.32554	0.34946	0.29316	0.25944
1404.0	30	0.36147	0.42193	0.27576	0.24207
1404.1	31	0.41649	0.52333	0.35455	0.35274
1404.2	32	0.43712	0.58687	0.42768	0.45493
1404.3	33	0.47618	0.64678	0.51851	0.56488
1404.4	34	0.46836	0.65066	0.53623	0.60117
1404.5	35	0.47821	0.66011	0.56476	0.61942
1404.6	36	0.49370	0.68191	0.59381	0.65416
1404.7	37	0.51772	0.72233	0.65593	0.72747
1404.8	38	0.52637	0.73513	0.72192	0.79134
1404.9	39	0.52080	0.72249	0.78164	0.84162
1405.0	40	0.50329	0.68582	0.79914	0.85592
1405.1	41	0.47353	0.61731	0.78661	0.83797
1405.2	42	0.39199	0.47678	0.65013	0.66962
1405.3	43	0.30288	0.33437	0.47390	0.44371
1405.4	44	0.20433	0.20211	0.24976	0.21448
1405.5	45	0.17897	0.18876	0.12999	0.11093
1405.6	46	0.20643	0.21018	0.11265	0.09183
1405.7	47	0.20237	0.23540	0.17156	0.14774
1405.8	48	0.27973	0.37226	0.17063	0.17022
1406.0	49	0.34382	0.46555	0.26503	0.26791

1406.1	50	0.29607	0.41466	0.28046	0.28840
1406.2	51	0.18993	0.25301	0.15676	0.15749
1406.3	52	0.29521	0.41489	0.41118	0.46457
1406.4	53	0.17503	0.20139	0.33425	0.34455
1406.5	54	0.15489	0.17397	0.21457	0.20901
1406.6	55	0.17541	0.21300	0.22345	0.23595
1406.7	56	0.19425	0.22387	0.21031	0.20946
1406.8	57	0.14870	0.17281	0.18529	0.18751
1406.9	58	0.20938	0.23373	0.13418	0.12866
1406.10	59	0.33036	0.43057	0.27479	0.29839
1406.11	60	0.41881	0.56066	0.42750	0.48778
1407.0	61	0.42831	0.56826	0.43177	0.48826
1407.1	62	0.41201	0.53788	0.39280	0.41653
1407.2	63	0.39778	0.51157	0.38670	0.41236
1407.3	64	0.42690	0.54372	0.34143	0.33044
1407.4	65	0.52433	0.71944	0.60822	0.65942
1407.5	66	0.52084	0.73453	0.71385	0.77730
1407.6	67	0.43641	0.60685	0.76027	0.81690
1407.7	68	0.29469	0.38453	0.47135	0.50591
1407.8	69	0.34275	0.46590	0.40278	0.42913
1408.0	70	0.43850	0.60520	0.54578	0.59448
1408.1	71	0.40771	0.54766	0.62930	0.64704
1408.2	72	0.47763	0.65772	0.70298	0.75905
1408.3	73	0.46923	0.63747	0.70283	0.74866
1408.4	74	0.47400	0.63920	0.64420	0.68987
1408.5	75	0.49219	0.66672	0.57303	0.61506
1408.6	76	0.51174	0.69577	0.57467	0.61885
1408.7	77	0.51269	0.70492	0.58353	0.63217
1408.8	78	0.48534	0.68298	0.59421	0.64805
1408.9	79	0.39473	0.55845	0.52254	0.56648
1408.10	80	0.22811	0.31411	0.30847	0.32595
1408.11	81	0.18064	0.23889	0.19643	0.20570
1409.0	82	0.40333	0.57869	0.39414	0.47027
1409.1	83	0.50034	0.71556	0.57315	0.66608
1409.2	84	0.53300	0.75575	0.66514	0.74563
1409.3	85	0.54653	0.77112	0.72091	0.79061
1409.4	86	0.53772	0.75884	0.73824	0.80281
1409.5	87	0.52734	0.74480	0.76441	0.82495
1409.6	88	0.49283	0.70461	0.79249	0.84742
1409.7	89	0.43665	0.63243	0.63804	0.69664
1409.8	90	0.39616	0.59625	0.57227	0.63972
1409.9	91	0.39606	0.59747	0.57543	0.64578
1409.10	92	0.25063	0.34849	0.32685	0.32111
1410.0	93	0.30042	0.44395	0.30764	0.34532
1410.1	94	0.34475	0.49860	0.48169	0.52297
1410.2	95	0.34031	0.47552	0.53414	0.57822
1410.3	96	0.32174	0.43941	0.55901	0.60008
1410.4	97	0.27233	0.36976	0.49510	0.53696
1410.5	98	0.25844	0.34946	0.43300	0.46325
1410.6	99	0.23048	0.30191	0.30494	0.30425
1410.7	100	0.17952	0.23431	0.22852	0.22190
1410.8	101	0.25956	0.34882	0.30377	0.32211
1411.0	102	0.27747	0.36724	0.36162	0.37512

Appendix 3. IFSU, ISFC, DSFU, and DSFC at the 1.75 m level for the open-canopy PP Woodland Transect.

POSITION (m)	ISFU	ISFC	DSFU	DSFC
0	0.30573	0.40712	0.33656	0.34478
1	0.31213	0.41449	0.34524	0.34776
2	0.31995	0.42586	0.34014	0.33399
3	0.34968	0.46352	0.38874	0.38010
4	0.36228	0.48310	0.42443	0.41480
5	0.37165	0.49609	0.44888	0.44042
6	0.37090	0.49869	0.46022	0.45711
7	0.37524	0.50847	0.48850	0.49625
8	0.38608	0.52390	0.51319	0.52286
9	0.39708	0.53783	0.54704	0.56212
10	0.38928	0.52922	0.54961	0.56923
11	0.39619	0.53118	0.55575	0.57522
12	0.39977	0.53434	0.56406	0.58430
13	0.40207	0.53458	0.56633	0.57892
14	0.40723	0.53478	0.55530	0.57188
15	0.39980	0.52501	0.56272	0.57036
16	0.39251	0.51459	0.55562	0.56154
17	0.39776	0.52027	0.56547	0.56681
18	0.39707	0.52149	0.55922	0.56020
19	0.39258	0.51679	0.55449	0.55673
20	0.39008	0.51387	0.54474	0.54623
21	0.38498	0.51039	0.53944	0.54026
22	0.41311	0.54219	0.56757	0.56416
23	0.42429	0.55138	0.57987	0.57690
24	0.39280	0.51704	0.54947	0.54854
25	0.39446	0.51574	0.56718	0.56018
26	0.40668	0.52623	0.58616	0.57909
27	0.40469	0.52380	0.58520	0.58214
28	0.40881	0.52487	0.59450	0.59928
29	0.42111	0.53763	0.61238	0.62219
30	0.41302	0.52941	0.62251	0.64041
31	0.41624	0.54096	0.63756	0.66842
32	0.42774	0.56884	0.64393	0.68411
33	0.43562	0.58884	0.65181	0.70063
34	0.46981	0.62781	0.66779	0.71130
35	0.48715	0.65240	0.68835	0.73702
36	0.48229	0.65484	0.67691	0.72990
37	0.48113	0.65828	0.66715	0.72575
38	0.47086	0.64996	0.65289	0.71442
39	0.46208	0.64286	0.64152	0.70594
40	0.46743	0.64508	0.64012	0.70716
41	0.47501	0.64786	0.65990	0.72425
42	0.45369	0.61912	0.64255	0.70907
43	0.45042	0.60562	0.64643	0.71131
44	0.42829	0.57097	0.63486	0.69903
45	0.39745	0.52111	0.59777	0.65513
46	0.37527	0.46967	0.58050	0.62140
47	0.34338	0.42119	0.51344	0.53157
48	0.33411	0.40507	0.48643	0.49336
49	0.38929	0.49197	0.53282	0.55073
50	0.44379	0.58382	0.57364	0.61261

Appendix 4. ISFU, ISFC, DSFU, and DSFC at the 1.75 m level for the closed-canopy PP Woodland Transect.

POSITION (m)	ISFU	ISFC	DSFU	DSFC
0	0.26936	0.35476	0.40677	0.42746
1	0.24617	0.33399	0.37731	0.40633
2	0.24671	0.32765	0.35086	0.37274
3	0.25888	0.35009	0.30787	0.31830
4	0.25511	0.35109	0.31386	0.33256
5	0.24611	0.34311	0.28893	0.30709
6	0.29441	0.40737	0.36320	0.38632
7	0.29875	0.41685	0.36280	0.39082
8	0.30903	0.43128	0.35273	0.38208
9	0.32260	0.45524	0.37496	0.41247
10	0.34090	0.47739	0.41461	0.45365
11	0.29507	0.42030	0.35502	0.39008
12	0.30138	0.42899	0.36048	0.39129
13	0.30532	0.43196	0.39629	0.43569
14	0.29314	0.41621	0.41700	0.47078
15	0.30979	0.43514	0.47573	0.53340
16	0.27200	0.38839	0.41487	0.46821
17	0.26977	0.38423	0.37166	0.41426
18	0.25646	0.35957	0.34530	0.37877
19	0.27524	0.39005	0.38491	0.42578
20	0.28348	0.39362	0.38941	0.42612
21	0.29091	0.40247	0.42879	0.46599
22	0.24651	0.34161	0.36134	0.39857
23	0.25343	0.34220	0.36187	0.39351
24	0.25771	0.35116	0.33783	0.36415
25	0.27488	0.37517	0.34929	0.37522
26	0.28291	0.38653	0.36923	0.39572
27	0.26254	0.35749	0.31028	0.33502
28	0.26324	0.35867	0.30972	0.33780
29	0.27857	0.38625	0.35549	0.39041
30	0.27404	0.38246	0.34637	0.37861
31	0.27969	0.38893	0.36961	0.39659
32	0.26895	0.37394	0.38149	0.41805
33	0.25795	0.35563	0.35694	0.39553
34	0.23741	0.32429	0.31740	0.35057
35	0.22887	0.31414	0.33274	0.36408
36	0.22895	0.31613	0.31049	0.33241
37	0.21474	0.30549	0.29294	0.32140
38	0.25375	0.36252	0.33301	0.37023
39	0.24188	0.34140	0.34376	0.37794
40	0.20500	0.28915	0.24818	0.26822
41	0.20994	0.31260	0.26424	0.30019
42	0.23304	0.33920	0.29087	0.32523
43	0.26729	0.37542	0.34586	0.37988
44	0.24905	0.34852	0.34741	0.38035
45	0.23716	0.32899	0.33703	0.36713
46	0.22361	0.30123	0.34512	0.37919
47	0.22675	0.29510	0.30010	0.32202
48	0.21813	0.29762	0.28721	0.32452
49	0.23450	0.31947	0.27221	0.29118
50	0.24295	0.33355	0.29500	0.32360

Appendix 5. ISFU, ISFC, DSFU, and DSFC at the 1.0 m level for the open-canopy PP Woodland Transect.

POSITION (m)	ISFU	ISFC	DSFU	DSFC
0	0.36721	0.47648	0.36915	0.37556
1	0.38769	0.50298	0.40207	0.40706
2	0.39212	0.50775	0.40220	0.40089
3	0.35690	0.46588	0.35660	0.34200
4	0.36852	0.48334	0.37861	0.36182
5	0.39637	0.51895	0.43488	0.42086
6	0.40503	0.53302	0.45726	0.45093
7	0.42286	0.55375	0.50534	0.50613
8	0.43534	0.57074	0.51786	0.51805
9	0.43502	0.57102	0.55013	0.55984
10	0.43680	0.57477	0.57159	0.58547
11	0.42285	0.55087	0.56233	0.57512
12	0.42490	0.55465	0.56159	0.56401
13	0.43496	0.56500	0.57924	0.58393
14	0.44093	0.56716	0.57944	0.57764
15	0.42456	0.54866	0.55199	0.54792
16	0.41138	0.53421	0.54356	0.55075
17	0.42243	0.54478	0.55336	0.55759
18	0.42912	0.55287	0.56446	0.56710
19	0.38025	0.49935	0.50885	0.51284
20	0.39384	0.51268	0.53560	0.53905
21	0.39717	0.51764	0.54129	0.54333
22	0.39922	0.52225	0.54969	0.55013
23	0.40847	0.53059	0.55877	0.55743
24	0.42041	0.53999	0.56704	0.56750
25	0.41979	0.53904	0.57439	0.57277
26	0.41806	0.53919	0.58844	0.58452
27	0.41532	0.53520	0.58371	0.58419
28	0.42811	0.54529	0.58065	0.58819
29	0.43246	0.55013	0.60069	0.60884
30	0.43202	0.55207	0.59867	0.61516
31	0.43840	0.56693	0.61603	0.63990
32	0.45750	0.59394	0.65681	0.68403
33	0.47381	0.61775	0.66121	0.69146
34	0.43184	0.58832	0.59789	0.65058
35	0.44372	0.60665	0.61272	0.66452
36	0.45125	0.61773	0.62294	0.67937
37	0.45868	0.62937	0.61524	0.67396
38	0.45751	0.62815	0.60848	0.67098
39	0.45870	0.62742	0.60774	0.66923
40	0.46497	0.63110	0.60646	0.66941
41	0.42892	0.59347	0.57439	0.64306
42	0.41865	0.57419	0.56795	0.63754
43	0.40808	0.55049	0.55736	0.62827
44	0.40100	0.53505	0.55994	0.62859
45	0.39222	0.51675	0.55785	0.61996
46	0.37593	0.47842	0.53994	0.59564
47	0.35911	0.45183	0.52675	0.56904
48	0.35996	0.45837	0.49539	0.53449
49	0.39366	0.51323	0.51816	0.56287
50	0.43117	0.57401	0.53920	0.59378

Appendix 6. ISFU, ISFC, DSFU, and DSFC at the 1.0 m level for closed-canopy PP Woodland Transect.

POSITION (m)	ISFU	ISFC	DSFU	DSFC
0	0.28618	0.38291	0.37579	0.39330
1	0.27608	0.37402	0.38294	0.40915
2	0.26605	0.35981	0.36719	0.39096
3	0.25417	0.35268	0.30115	0.32108
4	0.27012	0.37479	0.31563	0.33161
5	0.30280	0.41777	0.35157	0.37218
6	0.30512	0.42143	0.34479	0.36590
7	0.28384	0.38957	0.31137	0.33182
8	0.29792	0.41011	0.31600	0.33562
9	0.29287	0.40950	0.30498	0.33062
10	0.31862	0.44416	0.34555	0.37923
11	0.33085	0.46144	0.37402	0.40908
12	0.31026	0.43449	0.35113	0.38057
13	0.29274	0.41231	0.33294	0.36246
14	0.28887	0.40614	0.37306	0.41970
15	0.29486	0.41004	0.41071	0.46489
16	0.29861	0.41480	0.43264	0.48823
17	0.26966	0.37491	0.36042	0.40409
18	0.26477	0.36434	0.34577	0.38222
19	0.26875	0.37408	0.35805	0.39502
20	0.27419	0.37382	0.34179	0.37745
21	0.26993	0.37842	0.36657	0.40629
22	0.27881	0.38646	0.38342	0.42572
23	0.26233	0.36273	0.35300	0.39155
24	0.27445	0.38046	0.36043	0.39470
25	0.28772	0.39572	0.33248	0.36435
26	0.30653	0.42011	0.37376	0.40986
27	0.30476	0.41399	0.35563	0.38617
28	0.31390	0.42914	0.36737	0.40312
29	0.31953	0.44016	0.40872	0.44134
30	0.32577	0.44954	0.41863	0.45248
31	0.29520	0.41013	0.38620	0.41227
32	0.29329	0.40704	0.39509	0.42974
33	0.28757	0.39332	0.37096	0.40954
34	0.25459	0.34852	0.33069	0.36279
35	0.23627	0.32235	0.29732	0.32677
36	0.24052	0.32868	0.31920	0.34279
37	0.23938	0.33547	0.32010	0.34509
38	0.25867	0.36785	0.32715	0.36509
39	0.24785	0.34621	0.34446	0.37848
40	0.25996	0.36660	0.36075	0.40239
41	0.28458	0.40265	0.32314	0.36221
42	0.28063	0.39268	0.32712	0.36522
43	0.26292	0.36657	0.30551	0.33695
44	0.28918	0.39837	0.37490	0.40651
45	0.28726	0.39263	0.38947	0.42173
46	0.27389	0.37222	0.39336	0.42853
47	0.26764	0.36437	0.38292	0.41548
48	0.24935	0.34280	0.35587	0.39598
49	0.25951	0.35060	0.34329	0.37852
50	0.27144	0.37626	0.33425	0.37253

Appendix 7. Photosynthetically active radiation (PAR) and percent sunflecks for the PJ Woodland Transect.

POSITION(m)	PAR	SUNFLECK	POSITION (m)	PAR	SUNFLECK
0	702	63.7	51	587	49.3
1	552	47.8	52	454	35.2
2	395	29.5	53	236	15.2
3	498	45.1	54	975	90.7
4	230	16.3	55	545	46.1
5	246	18.9	56	413	31.7
6	139	14.6	57	204	17.4
7	616	59.7	58	617	52.5
8	263	19.9	59	217	25.2
9	390	31.6	60	175	19.2
10	230	18.1	61	269	28.7
11	116	13.2	62	321	27.0
12	244	16.3	63	252	18.9
13	485	42.6	64	968	83.7
14	625	49.3	65	1175	100.0
15	426	26.3	66	1167	100.0
16	794	64.4	67	911	77.4
17	1158	100	68	812	71.3
18	1169	100	69	593	73.4
19	1173	100	70	127	97.3
20	1170	100	71	146	50.1
21	1150	100	72	189	33.7
22	1151	100	73	334	27.3
23	1034	91.8	74	328	39.3
24	141	51.9	75	655	50.3
25	135	32.7	76	500	40.7
26	123	20.2	77	590	42.6
27		69	6.6	78	254
28	208	32.2	79	186	11.9
29	657	56.4	80	102	12.6
30	908	77.7	81	431	42.7
31	1014	89	82	928	73.7
32	294	48.2	83	1185	99.4
33	165	43.7	84	1202	100.0
34	291	23.4	85	1198	100.0
35	347	32.7	86	1182	100.0
36	1062	92.1	87	1195	100.0
37	1155	100	88	800	62.5
38	1146	100	89	126	21.5
39	1051	90.4	90	131	22.9
40	1125	99.3	91	154	19.9
41	575	49.7	92	104	8.2
42	182	16	93	173	22.3
43	121	12.4	94	547	38.9
44	129	13.1	95	162	28.4
45	167	16.3	96	415	33.2
46	202	16.7	97	154	17.7
47	431	31.5	98	277	20.5
48	556	45.2	99	165	26.2
49	487	37.7	100	587	47.3
50	343	42.3	101	1153	100
			102	1176	100

14.1

Appendix 8. Photosynthetically active radiation (PAR) and percent sunflecks for a) open-canopy and b) closed-canopy PP Woodland Transects.

	a) open-canopy		b) closed-canopy	
POSITION	PAR	SUNFLECK	PAR	SUNFLECK
0	264	66.6	172	37.1
1	134	61.6	245	53.8
2	56	74.7	422	50.4
3	75	56.4	688	87.4
4	80	66.9	761	100.0
5	145	44.9	763	100.0
6	81	41.7	755	100.0
7	59	62.2	759	100.0
8	59	67.7	769	100.0
9	75	89.3	762	100.0
10	75	71.6	767	100.0
11	103	52.3	767	100.0
12	234	48.0	691	88.8
13	219	55.3	753	97.5
14	160	24.8	650	81.0
15	257	58.4	596	74.6
16	87	69.3	466	70.8
17	64	69.2	347	78.8
18	85	33.1	236	32.8
19	62	53.2	160	60.2
20	146	27.6	237	54.9
21	287	46.1	175	61.7
22	276	44.5	278	56.9
23	222	25.2	167	81.3
24	91	34.9	182	64.8
25	85	24.2	237	59.8
26	97	40.5	233	68.5
27	70	58.1	203	76.7
28	217	25.2	157	60.5
29	334	42.1	119	97.9
30	122	31.3	130	67.3
31	129	28.2	473	90.6
32	104	51.5	499	92.7
33	227	29.1	188	34.9
34	229	64.5	128	53.8
35	265	41.3	124	62.1
36	228	51.0	192	57.4
37	87	66.5	187	49.6
38	67	50.9	173	63.7
39	47	91.0	158	60.2
40	158	60.3	165	53.6
41	130	30.3	161	66.8
42	159	38.0	139	98.5
43	128	34.6	148	72.2
44	143	35.5	140	61.2
45	151	37.2	164	88.6
46	71	68.5	188	66.0
47	76	60.4	129	89.7
48	80	41.6	154	81.2
49	81	31.4	162	38.2
50	55	60.4	341	38.1

Appendix 9. Soil moisture for PJ Woodland Transect measured with TDR.

LOCATION	POSITION(m)	% MOISTURE	LOCATION	POSITION(m)	% MOISTURE
1401.0	0	40.35	1406.3	52	34.93
1401.1	1	39.67	1406.4	53	31.32
1401.2	2	38.81	1406.5	54	34.73
1401.3	3	40.39	1406.6	55	35.19
1401.4	4	39.39	1406.7	56	33.96
1401.5	5	38.12	1406.8	57	31.48
1401.6	6	42.09	1406.9	58	34.39
1401.7	7	41.00	1406.10	59	36.15
1401.8	8	38.28	1406.11	60	34.6
1401.9	9	37.33	1407.0	61	35.38
1402.0	10	37.31	1407.1	62	36.04
1402.1	11	33.85	1407.2	63	31.36
1402.2	12	34.52	1407.3	64	33.23
1402.3	13	31.31	1407.4	65	29.03
1402.4	14	36.15	1407.5	66	24.51
1402.5	15	37.1	1407.6	67	29.82
1402.6	16	29.23	1407.7	68	27.12
1402.7	17	34.7	1407.8	69	28.18
1402.8	18	31.23	1408.0	70	36.39
1402.9	19	32.02	1408.1	71	32.22
1403.0	20	35.72	1408.2	72	32.63
1403.1	21	31.5	1408.3	73	31.09
1403.2	22	27.79	1408.4	74	31.91
1403.3	23	34.68	1408.5	75	31.68
1403.4	24	31.07	1408.6	76	35.25
1403.5	25	36.69	1408.7	77	31.16
1403.6	26	35.45	1408.8	78	32.38
1403.7	27	34.43	1408.9	79	28.48
1403.8	28	34.82	1408.10	80	28.16
1403.9	29	34.09	1408.11	81	26.28
1404.0	30	37.52	1409.0	82	34.74
1404.1	31	37.08	1409.1	83	30.26
1404.2	32	37.22	1409.2	84	29.45
1404.3	33	32.65	1409.3	85	22.31
1404.4	34	34.74	1409.4	86	31.09
1404.5	35	33.51	1409.5	87	28.21
1404.6	36	34.97	1409.6	88	23.13
1404.7	37	32.59	1409.7	89	29.37
1404.8	38	33.77	1409.8	90	27.48
1404.9	39	30.88	1409.9	91	28.88
1405.0	40	22.2	1409.10	92	31.12
1405.1	41	21.18	1410.0	93	35.02
1405.2	42	24.25	1410.1	94	31.67
1405.3	43	31.56	1410.2	95	32.52
1405.4	44	36.09	1410.3	96	34.36
1405.5	45	20.53	1410.4	97	35.73
1405.6	46	27.85	1410.5	98	33.49
1405.7	47	33.05	1410.6	99	16.22
1405.8	48	34.63	1410.7	100	24.47
1406.0	49	38.23	1410.8	101	33.16
1406.1	50	33.04	1411.0	102	34.59
1406.2	51	28.6			

Appendix 10. Soil moisture in a) open-canopy and b) closed canopy PP Woodland Transect measured with TDR.

	a) OPEN CANOPY	b) CLOSED CANOPY
POSITION(m)	%MOISTURE	%MOISTURE
0	42.8	29.91
1	35.91	29.69
2	33.91	27.71
3	36.36	29.48
4	33.4	28.78
5	38.33	33.66
6	35.65	31.95
7	34.5	30.26
8	37.83	25.77
9	36.25	19.8
10	35.7	32.31
11	35.08	31.51
12	35.39	31.86
13	36.63	31.19
14	36.54	29.12
15	34.93	31.36
16	33.6	30.55
17	32.42	30.7
18	34.45	32.21
19	33.93	27.02
20	35.23	32.03
21	33.0	28.59
22	33.18	26.41
23	32.01	28.64
24	32.67	28.79
25	35.08	33.71
26	30.57	34.09
27	31.53	32.27
28	29.27	33.23
29	27.05	30.77
30	31.21	34.56
31	30.31	29.64
32	29.94	32.55
33	29.92	29.8
34	30.75	34.13
35	33.72	35.72
36	31.51	33.43
37	31.33	34.89
38	31.04	27.92
39	29.6	35.14
40	31.72	34.33
41	30.86	34.39
42	29.26	34.74
43	23.57	34.16
44	27.65	34.7
45	28.0	33.11
46	24.3	32.24
47	26.19	15.45
48	27.96	31.4
49	31.45	34.93
50	33.48	35.59

Appendix 11. ISFU, ISFC, DSFU, and DSFC at the 1.75 m level for the lower elevation Tsierge PJ Woodland Site.

LOCATION	ISFU	ISFC	DSFU	DSFC
1	0.641660	0.790810	0.659180	0.693550
2	0.699830	0.875490	0.857000	0.876840
3	0.737010	0.912060	0.915700	0.932050
4	0.448540	0.552330	0.372030	0.337900
5	0.649910	0.777560	0.588760	0.608060
6	0.496960	0.567980	0.402590	0.413980
7	0.389060	0.410950	0.465830	0.462670
8	0.680970	0.842380	0.740260	0.794890
9	0.703830	0.866600	0.781290	0.828380
10	0.750570	0.883320	0.970020	0.961730
11	0.361590	0.367650	0.434850	0.402440
12	0.531790	0.660270	0.484960	0.517750
13	0.807460	0.942930	0.963570	0.958850
14	0.770020	0.912710	0.869650	0.896820
15	0.820680	0.951880	0.963320	0.958630
16	0.801860	0.934710	0.900020	0.915490
17	0.697590	0.814180	0.969120	0.961470
18	0.773230	0.905840	0.959750	0.956380
19	0.806010	0.945680	0.937700	0.937560
20	0.774430	0.927080	0.953030	0.953840
21	0.769810	0.920890	0.906370	0.923830
22	0.818070	0.952230	0.949420	0.946900
23	0.816170	0.952630	0.945400	0.946640
24	0.801880	0.927740	0.887660	0.891730
25	0.693670	0.790160	0.606680	0.593360
26	0.806360	0.942200	0.953380	0.951440
27	0.763220	0.912600	0.951920	0.952920
28	0.295430	0.311040	0.207960	0.191690
29	0.303740	0.324110	0.258660	0.250760
30	0.184170	0.164900	0.190320	0.163840
31	0.330950	0.364950	0.341830	0.322200
32	0.390980	0.421410	0.238380	0.242110
33	0.352610	0.341820	0.355040	0.307180
34	0.430210	0.521590	0.774890	0.822140
35	0.357640	0.362380	0.379550	0.345590

Appendix 12. ISFU, ISFC, DSFU, and DSFC at the protective barrier inclined plots analyzed incident on a horizontal plane. LOCATION is an x,y coordinate given in meters relative to an origin in the north corner, facing 138.95° (nearly southeast). Plots 1-5, repectively have inclinations 0% (0°), 5% (2.86°), 10% (5.71°), 15% (8.53°), and 25% (14.04°), with and aspect of 138.95° (nearly southeast).

PLOT	LOCATION	ISFU	ISFC	DSFU	DSFC
1	0,0	0.857450	0.973230	0.970790	0.962010
1	0,0	0.857400	0.971300	0.967430	0.960790
1	0,5	0.867360	0.975410	0.971580	0.962130
1	0,10	0.855980	0.964840	0.959490	0.954570
1	1,10	0.847800	0.960070	0.972880	0.962480
1	1,5	0.863490	0.972650	0.980360	0.976480
1	1,0	0.856790	0.972320	0.968920	0.961320
1	0,2.5	0.880870	0.979780	0.971440	0.962130
1	0,7.5	0.875790	0.975510	0.984900	0.980900
1	1,2.5	0.881660	0.979750	0.971670	0.964290
1	1,7.5	0.863990	0.971890	0.983070	0.978640
2	0,0	0.872000	0.976700	0.969560	0.964460
2	0,5	0.869020	0.974470	0.981870	0.979850
2	0,10	0.828090	0.943410	0.929290	0.934260
2	2,0	0.874800	0.974590	0.975230	0.977290
2	2,5	0.859810	0.971130	0.975310	0.972840
2	2,10	0.814400	0.935810	0.893820	0.911830
2	4,0	0.860780	0.967530	0.966000	0.972550
2	4,5	0.867140	0.971880	0.975030	0.976010
2	4,10	0.818390	0.940530	0.903170	0.921900
2	0,2.5	0.874040	0.979350	0.971270	0.961990
2	2,2.5	0.885140	0.979270	0.967890	0.960660
2	4,2.5	0.871210	0.975800	0.960820	0.957940
2	0,7.5	0.865400	0.969690	0.967640	0.962220
2	2,7.5	0.857140	0.965990	0.945540	0.949010
2	4,7.5	0.860870	0.966250	0.943120	0.947840
3	0,0	0.864890	0.960910	0.944770	0.958790
3	0,5	0.874480	0.974080	0.973090	0.971710
3	0,10	0.833390	0.953440	0.940020	0.946290
3	2,0	0.831330	0.935390	0.917890	0.928140
3	2,5	0.871910	0.974290	0.967960	0.960920
3	2,10	0.834290	0.955260	0.949010	0.950480
3	4,0	0.788570	0.880640	0.972080	0.969100
3	4,5	0.876370	0.975100	0.969570	0.961400
3	4.2,9.5	0.846590	0.955660	0.920030	0.929530
3	0,2.5	0.874290	0.975470	0.960980	0.957560
3	2,2.5	0.869460	0.970890	0.969760	0.961590
3	4,2.5	0.870530	0.967380	0.971340	0.962060
3	0,7.5	0.865230	0.969890	0.954730	0.954590
3	2,7.5	0.867260	0.971570	0.962860	0.958380
3	4,7.5	0.871060	0.971820	0.949320	0.950690
4	0,0	0.869310	0.963080	0.972600	0.962490
4	0,5	0.885450	0.979330	0.969560	0.961330
4	0,10	0.842940	0.959010	0.931920	0.938200
4	2,0	0.894100	0.979630	0.973280	0.962670
4	2,5	0.887500	0.980950	0.966900	0.960430
4	2,10	0.852240	0.965070	0.942170	0.946710
4	4,0	0.904590	0.984880	0.976430	0.967510
4	4,5	0.897320	0.982500	0.973760	0.967990

4	4,10	0.870670	0.972480	0.955900	0.954730
4	4,5	0.891580	0.983930	0.972200	0.964960
4	4,10	0.868570	0.973840	0.957870	0.955880
4	0,2.5	0.891550	0.980170	0.970890	0.961850
4	2,2.5	0.885470	0.981220	0.970330	0.961730
4	4,2.5	0.898040	0.985110	0.970710	0.961850
4	0,7.5	0.869860	0.974890	0.956790	0.955450
4	2,7.5	0.868980	0.975030	0.960040	0.957410
4	4,7.5	0.873040	0.977720	0.966160	0.960240
5	0,0	0.917440	0.991260	0.975470	0.965470
5	0,5	0.892410	0.985200	0.971390	0.962140
5	0,10	0.860090	0.973200	0.963630	0.958960
5	2,0	0.950810	0.995260	0.973910	0.962810
5	2,5	0.914350	0.989070	0.973040	0.962570
5	2,10	0.870300	0.975940	0.967370	0.960590
5	4,0	0.940930	0.994480	0.973880	0.962800
5	4,5	0.911360	0.989140	0.973000	0.962600
5	4,10	0.857050	0.966780	0.956080	0.949900
5	0,2.5	0.910710	0.988710	0.972500	0.962450
5	2,2.5	0.918870	0.991060	0.973480	0.962720
5	4,2.5	0.920060	0.990800	0.973340	0.962680
5	0,7.5	0.884920	0.981550	0.969280	0.961370
5	2,7.5	0.882620	0.981520	0.970330	0.961660
5	4,7.5	0.884890	0.982150	0.972100	0.962280

Appendix 13. ISFU, ISFC, DSFU, and DSFC at the protective barrier inclined plots analyzed incident on a plane parallel to the surface. LOCATION is an x,y coordinate given in meters relative to an origin in the north corner, facing 138.95° (nearly southeast). Plots 1-5, repectively have inclinations 0% (0°), 5% (2.86°), 10% (5.71°), 15% (8.53°), and 25% (14.04°), with and aspect of 138.95° (nearly southeast).

PLOT	LOCATION	ISFU	ISFC	DSFU	DSFC
1	0,0	0.857450	0.973230	0.970790	0.962010
1	0,0	0.857400	0.971300	0.967430	0.960790
1	0,5	0.867360	0.975410	0.971580	0.962130
1	0,10	0.855980	0.964840	0.959490	0.954570
1	1,10	0.847800	0.960070	0.972880	0.962480
1	1,5	0.863490	0.972650	0.980360	0.976480
1	1,0	0.856790	0.972320	0.968920	0.961320
1	0,2.5	0.880870	0.979780	0.971440	0.962130
1	0,7.5	0.875790	0.975510	0.984900	0.980900
1	1,2.5	0.881660	0.979750	0.971670	0.964290
1	1,7.5	0.863990	0.971890	0.983070	0.978640
2	0,0	0.872000	0.979380	0.969560	0.965360
2	0,5	0.869020	0.976720	0.981870	0.980440
2	0,10	0.828090	0.940840	0.929290	0.933000
2	2,0	0.874800	0.978280	0.975230	0.978000
2	2,5	0.859810	0.973350	0.975310	0.973600
2	2,10	0.814400	0.931580	0.893820	0.908640
2	4,0	0.860780	0.971910	0.966000	0.973410
2	4,5	0.867140	0.974520	0.975030	0.976600
2	4,10	0.818390	0.937530	0.903170	0.919430
2	0,2.5	0.874040	0.979690	0.971270	0.962870
2	2,2.5	0.885140	0.980540	0.967890	0.961590
2	4,2.5	0.871210	0.977130	0.960820	0.958720
2	0,7.5	0.865400	0.967800	0.967640	0.962450
2	2,7.5	0.857140	0.963810	0.945540	0.948290
2	4,7.5	0.860870	0.963890	0.943120	0.946910
3	0,0	0.864890	0.970650	0.944770	0.963660
3	0,5	0.874480	0.976580	0.973090	0.972600
3	0,10	0.833390	0.948560	0.940020	0.944610
3	2,0	0.831330	0.946480	0.917890	0.935730
3	2,5	0.871910	0.975860	0.967960	0.961870
3	2,10	0.834290	0.949200	0.949010	0.949770
3	4,0	0.788570	0.902240	0.972080	0.971150
3	4,5	0.876370	0.975990	0.969570	0.962570
3	4.2,9.5	0.846590	0.945910	0.920030	0.926220
3	0,2.5	0.874290	0.975680	0.960980	0.959460
3	2,2.5	0.869460	0.973160	0.969760	0.962690
3	4,2.5	0.870530	0.970970	0.971340	0.963310
3	0,7.5	0.865230	0.964090	0.954730	0.954140
3	2,7.5	0.867260	0.966530	0.962860	0.958810
3	4,7.5	0.871060	0.965360	0.949320	0.949710
4	0,0	0.869310	0.973980	0.972600	0.964790
4	0,5	0.885450	0.980570	0.969560	0.963040
4	0,10	0.842940	0.947010	0.931920	0.934380
4	2,0	0.894100	0.984730	0.973280	0.964950
4	2,5	0.887500	0.979130	0.966900	0.961620
4	2,10	0.852240	0.955490	0.942170	0.944150
4	4,0	0.904590	0.987970	0.976430	0.969460
4	4,5	0.897320	0.986230	0.973760	0.969800

4	4,10	0.870670	0.966040	0.955900	0.954850
4	4,5	0.891580	0.982890	0.972200	0.966730
4	4,10	0.868570	0.967270	0.957870	0.956330
4	0,2.5	0.891550	0.979070	0.970890	0.963550
4	2,2.5	0.885470	0.978220	0.970330	0.963380
4	4,2.5	0.898040	0.980040	0.970710	0.963490
4	0,7.5	0.869860	0.969190	0.956790	0.955060
4	2,7.5	0.868980	0.970580	0.960040	0.957580
4	4,7.5	0.873040	0.976200	0.966160	0.961840
5	0,0	0.917440	0.982800	0.975470	0.968780
5	0,5	0.892410	0.974030	0.971390	0.965250
5	0,10	0.860090	0.959440	0.963630	0.960750
5	2,0	0.950810	0.996280	0.973910	0.966430
5	2,5	0.914350	0.987270	0.973040	0.966000
5	2,10	0.870300	0.966730	0.967370	0.962740
5	4,0	0.940930	0.992820	0.973880	0.966410
5	4,5	0.911360	0.984570	0.973000	0.966120
5	4,10	0.857050	0.945710	0.956080	0.950540
5	0,2.5	0.910710	0.981050	0.972500	0.965530
5	2,2.5	0.918870	0.988010	0.973480	0.966280
5	4,2.5	0.920060	0.990340	0.973340	0.966370
5	0,7.5	0.884920	0.974020	0.969280	0.964130
5	2,7.5	0.882620	0.973340	0.970330	0.964480
5	4,7.5	0.884890	0.975280	0.972100	0.965710

Appendix 14. Theoretical direct monthly solar radiation for the protective barrier inclined plots (values in Joules/m^2), based on effect of slope alone.

MONTH	PLOT1	PLOT2	PLOT3	PLOT4	PLOT5
JAN	138645015	146898298	154746835	162141574	175429841
FEB	193740216	202260459	210237514	217624428	230510610
MAR	331908489	341119429	349439836	356827935	368749307
APR	440109932	446504169	451760833	455866804	460715717
MAY	539081072	542172428	543905684	544299986	541327559
JUN	554244426	555335363	555045550	553410426	546434777
JUL	557600444	559660915	560325100	559621367	554411360
AUG	490812033	496119674	500172257	502968608	504947298
SEP	366345618	374597030	381879750	388161501	397711245
OCT	251516804	261111667	270012253	278168119	292131903
NOV	144797593	153022616	160827866	168164939	181298755
DEC	117635421	125339678	132695307	139655661	152253739

Appendix 15. ISFU, ISFC, DSFU, and DSFC calculated from hemispherical photograph taken in 1994 for a series of TDR study sites in PJ woodland at LANL Technical Area 51.

LOCATION	HEIGHT	ISFU	ISFC	DSFU	DSFC	PHOTO#
1	1.0	0.22501	0.33002	0.31188	0.34933	1
2	1.0	0.42589	0.61299	0.62081	0.68978	2
3	1.0	0.42528	0.56532	0.5774	0.62531	3
4	1.0	0.57295	0.76962	0.81871	0.85242	4
5	1.0	0.2585	0.26793	0.23931	0.19795	5
6	1.0	0.56732	0.76549	0.67909	0.74022	6
7	1.0	0.3646	0.48762	0.37648	0.41052	7
8	1.0	0.15879	0.16505	0.21321	0.19142	8
1	0.3	0.17869	0.24219	0.19976	0.21584	10
2	0.3	0.37839	0.53636	0.4721	0.53467	11
3	0.3	0.3713	0.49376	0.50941	0.54731	12
4	0.3	0.51832	0.72888	0.76132	0.82388	13
5	0.3	0.21885	0.24935	0.23834	0.20992	14
6	0.3	0.50243	0.70272	0.5869	0.64716	15
7	0.3	0.29556	0.40519	0.27333	0.31052	16
8	0.3	0.18599	0.18783	0.29015	0.24657	17

Appendix 15. ISFU, ISFC, DSFU, and DSFC calculated from hemispherical photograph taken in 1994 for for the PP woodland hydrology study site at LANL Technical Area 6.

LOCATION	ISFU	ISFC	DSFU	DSFC	REF#
NAT-1	0.39356	0.56082	0.64751	0.72883	21
NAT-2	0.37779	0.51003	0.65719	0.73346	22
NAT-3	0.38391	0.511	0.64824	0.71511	23
NAT-4	0.43762	0.59129	0.65932	0.73377	24
NAT-5	0.42749	0.58526	0.58756	0.66211	25
NAT-6	0.3817	0.50729	0.42737	0.44099	26
NAT-7	0.44027	0.5781	0.62022	0.62717	27
NAT-8	0.41023	0.53309	0.56917	0.56522	28
NAT-9	0.39861	0.52161	0.50484	0.50178	29
NAT-10	0.4094	0.5368	0.47377	0.45912	30
NAT-11	0.40294	0.54026	0.49931	0.49079	31
NAT-12	0.40195	0.55733	0.49093	0.52711	32
NAT-13	0.3663	0.50269	0.46666	0.53498	33
NAT-14	0.36278	0.52746	0.46942	0.54631	34
NAT-15	0.18125	0.27062	0.27058	0.31811	35
NAT-16	0.2033	0.29155	0.19639	0.22356	36
NAT-17	0.15981	0.23494	0.11712	0.13027	37
SMP-10	0.33928	0.47244	0.47008	0.52107	38
SMP-11	0.36403	0.52051	0.41896	0.49574	39
SMP-4	0.37933	0.55003	0.48896	0.56247	40
SMP-14	0.15132	0.16844	0.06314	0.05137	41
SMP-18	0.24633	0.33306	0.10093	0.10037	42
SMP-23	0.29118	0.41051	0.21877	0.24847	43
SMP-27	0.23653	0.33122	0.24849	0.29301	44
SMP-28	0.23766	0.30107	0.1979	0.19561	45
SMP-26	0.34417	0.51691	0.47521	0.56286	46
SMP-24	0.35408	0.52038	0.50361	0.59209	47
SMP-22	0.27597	0.34607	0.38279	0.40394	48
SMP-16B	0.36686	0.51367	0.42541	0.48399	49
SMP-16	0.40069	0.5701	0.52204	0.59491	50
FLAG-50	0.41962	0.59887	0.65062	0.7294	51
FLAG-48	0.39751	0.55751	0.56827	0.63968	52
FLAG-46	0.43805	0.58722	0.58826	0.63776	53
FLAG-44	0.45511	0.60558	0.5692	0.6013	54
FLAG-42	0.42926	0.57924	0.60531	0.65783	55
SMP-6	0.43771	0.58753	0.6007	0.63849	56

DISCLAIMER

title page:

LA-XXXX-M
Manual

UC-XXXX
Issued: XXXX

Modelling Topographic Influences on Solar Radiation: a Manual for the SOLARFLUX Model

Paul M. Rich
William A. Hetrick
Shawn C. Saving

Department of Systematics & Ecology, Environmental Studies Program, and Kansas Biological Survey
University of Kansas
Lawrence, KS 66045
telephone: (913)864-7769
FAX: (913)864-7789
e-mail: prich@oz.kbs.ukans.edu

draft -- November 23, 1994

Los Alamos National Laboratory
Los Alamos, New Mexico 87545

cover:

LA-XXXX-M
Manual

Modelling Topographic Influences on Solar Radiation: a Manual for the SOLARFLUX Model

(4 panel color graphic)

Los Alamos
Los Alamos National Laboratory is operated by the University of California for the United States Department of Energy under contract W-7405-ENG-36.

front overleaf page:

This work was supported by the Center for Conservation Biology at Stanford University, the Kansas Applied Remote Sensing Program, the Kansas Biological Survey, the Kansas Center for Computer Aided Software Engineering, Los Alamos National Environmental Restoration Program, NASA grant NAG5-2358, National Science Foundation grant BSR90-02326, and the University of Kansas Research Development and General Research Funds.

Cover: *These four maps of daily incoming solar radiation demonstrate that SOLARFLUX can be used to model solar radiation for topographic surfaces at different spatial scales, ranging from landscape scales to local levels. The upper-left map shows clear-sky direct solar radiation on the equinox for the University of California Big Creek Reserve, the upper-right map shows clear-sky direct solar radiation on the equinox for a pinyon-juniper woodland stand at Los Alamos National Environmental Research Park, the lower-left map shows clear-sky direct solar radiation on the summer solstice for a series of experimental plots that test the influence of slope on waste site design, and the lower-right map shows spatial variability of solar radiation on the summer solstice for a simulated treefall gap. See Chapter III for further details.*

An Affirmative Action/Equal Opportunity Employer

page following title page:

SOFTWARE COPYRIGHT

CONTENTS

PREFACE

SOLARFLUX is a public domain computer program developed in my research laboratory for modelling effects of topography on incoming solar radiation. The conception of SOLARFLUX has roots that go back more than a decade, to the early 1980s when I first began grappling with concepts of how to model the complexities of solar radiation as it influences the ecology of tropical rainforests. Since that time, my thinking about geometric models of solar radiation has encompassed a wide range of systems, both natural and human made, and a wide range of temporal and spatial scales. For me, the development of SOLARFLUX is part of a natural progression from a focus on geometric models of solar radiation for point locations to a focus on geometric solar radiation models that integrate over areas. These areas may range in scale from meters to thousands of kilometers -- at local, landscape, or regional scales.

In a certain sense, I started by looking at the world upside down, from the perspective of a tree growing in the understory of a mature tropical rainforest. In the rainforest, light is a limiting resource, and the geometry of openings in the forest canopy determines how much light is available for growth by plants growing in the understory. From 1982 to 1989 I worked on developing CANOPY, a program for digital image analysis of hemispherical (fisheye) canopy photography. In essence, CANOPY can be used to quantify the pattern of sky obstruction and openings as seen from a given location looking upward, and to calculate the level of radiation that would penetrate to the location from unobstructed sky directions. The pattern of canopy openings, or gap fractions, can also be used to model the architecture of the canopy above, including such ecologically important characteristics as leaf area index and leaf angle distribution. CANOPY was written as a general program that could be used to analyze hemispherical imagery at any latitude, and not just in forest ecosystems. CANOPY can be used equally well to calculate the influence of mountains, buildings, or trees on incoming solar radiation. But CANOPY is limited to the perspective of looking upward from a given location. CANOPY and SOLARFLUX literally view the world from opposite directions: CANOPY looks upward from a point location, while SOLARFLUX looks downward on a topographic surface.

SOLARFLUX is not as different from CANOPY as it might appear upon first inspection. True, SOLARFLUX uses a different source of input than CANOPY -- SOLARFLUX starts with a topographic surface, generally specified as an array of elevation values, while CANOPY starts with a hemispherical image that is turned into an array of sky directions that are then classified as either obstructed or open. And true, the outputs are different in presentation -- SOLARFLUX produces a map of solar radiation values for a topographic surface, while CANOPY produces tables of solar radiation indices for a given location. But, in both input and output, the two programs are actually quite similar, and in some aspects identical. Both start with a representation of geometry that influences incoming solar radiation. And both end with calculations of how this geometry influences solar radiation. In fact, the core calculating algorithm of SOLARFLUX is the same as the algorithm used by CANOPY. SOLARFLUX progressively calculates the influence of sky obstruction and surface orientation for each location on a topographic surface. This is comparable to acquiring and analyzing an array of hemispherical photographs corresponding to each location on the surface. Thus, SOLARFLUX is a tool that integrates over space and time based upon relatively readily available information, namely specification of a topographic surface.

SOLARFLUX was my conception. But its realization is the result of efforts by many people, including various student assistants in my research laboratory and several key collaborators. In particular, I hired William Hetrick, a talented computer engineering undergraduate student at the University of Kansas, as a research assistant to develop the software code of SOLARFLUX. He did what I no longer have time for in my capacity as an assistant professor -- he spent long hours writing and debugging the computer code in SOLARFLUX. In the spirit of academic endeavor, the program development became more than a job in which

William Hetrick turned my ideas into well written code, but rather he contributed substantial ideas concerning design and implementation. In addition, Shawn Saving, Jue Wang, and Xiofei Tang, graduate research assistants in my laboratory at the University of Kansas, contributed substantially to testing of SOLARFLUX. Throughout the project, Stuart Weiss of the Stanford Center for Conservation Biology, offered constructive criticism, encouragement, and unending enthusiasm. As a kindred spirit, he offered insights into profound ecological and evolutionary implications of topographic modification of solar radiation. In the course of the project, I began collaboration with Ralph Dubayah of the University of Maryland Department of Geography, who has independently developed a topographic solar radiation model for application in remote sensing. Together, we have been working to produce a synthesis of the state of knowledge of such geometrically based solar radiation models. Our collaboration has contributed greatly to increasing both the depth and breadth of my understanding of the subject.

This manual serves as a technical reference to the program SOLARFLUX. More than that, it serves to show directions for developing more sophisticated and complete geometric models of solar radiation.

Paul M. Rich, 15 August 1994
Department of Systematics & Ecology, Environmental Studies Program, and Kansas Biological Survey
University of Kansas

MODELLING TOPOGRAPHIC INFLUENCES ON SOLAR RADIATION: A MANUAL FOR THE SOLARFLUX MODEL

by

Paul M. Rich, William A. Hetrick, and Shawn C. Saving

ABSTRACT

SOLARFLUX is a GIS-based (ARC/INFO, GRID) computer program that models incoming solar radiation based on surface orientation (slope and aspect), solar angle (azimuth and zenith) as it shifts over time, shadows caused by topographic features, and atmospheric conditions. A convenient user interface allows specification of program parameters including latitude, time interval for simulation, file name of a topographic surface, atmospheric conditions (transmittivity), and file names for output. The user specifies a topographic surface as an array of elevation values (GRID). SOLARFLUX generates five basic types of output: 1) total direct radiation, 2) duration of direct sunlight, 3) total diffuse radiation; 4) skyview factor, and 5) hemispherical viewsheds of sky obstruction for specified surface locations. This manual serves as the comprehensive guide to SOLARFLUX. Included are discussions on modelling insolation on complex surfaces, our theoretical approach, program setup and operation, and a set of applications illustrating characteristics of topographic insolation modelling.

CHAPTER I. INTRODUCTION

OVERVIEW

Motivation: Modelling Influences of Topography on Incoming Solar Radiation

The effects of solar radiation are pervasive. Solar radiation is the primary source of energy that drives earth system processes, such as weather patterns and rates of primary production by green plants. Topography is a major factor that determines the amount of solar radiation reaching any particular location at the Earth's surface. These topographic influences result from variability in elevation, surface orientation (slope and aspect), and shadows caused by topographic features. Models of the spatial and temporal patterns of incoming solar radiation (insolation), as influenced by topography, are of interest to a diverse community of scientists, engineers, planners, and resource managers. While the physical behavior of solar radiation is well understood (Gates 1980, Lunde 1980, Monteith and Unsworth 1990), because of intensive calculation requirements, it has not previously been practical to model incoming solar radiation for complex topographic surfaces. Appropriate solar radiation models must account for changes in solar angle with time, atmospheric effects, and topographic influences of elevation, surface orientation, and shadows. The detailed geometric analyses necessary to account for these topographic influences are only now becoming practical due to advances in both computer hardware and software technology (Dozier 1980, 1989, Brown 1992, Dubayah 1992, Dubayah et al. 1990, Hetrick et al. 1993a, 1993b, Dubayah and Rich 1995). Herein, we describe our approach to develop software, based on a geographical information system (GIS) platform, that takes advantage of new generation computers to model insolation on complex topographic surfaces.

Purpose and Organization of this Manual

This manual serves two basic purposes. First, it serves as a comprehensive guide to the program SOLARFLUX, a GIS-based solar radiation program. Second, it serves to showcase a series of SOLARFLUX applications at a variety of spatial scales. This manual is not meant to provide a comprehensive treatment of the theory and design of SOLARFLUX, since that has been published elsewhere. A detailed treatment concerning the theoretical basis of topographic solar radiation models is provided in Dubayah and Rich (1995), while Hetrick et al. (1993a, 1993b) provides background concerning the theory and conceptual basis for the SOLARFLUX model.

This chapter provides a general introduction and overview of topographic solar radiation modelling, background concerning solar radiation models and their applications, and introduction to the program SOLARFLUX. Chapter II presents a series of applications using SOLARFLUX to calculate incoming solar radiation for topographic at various spatial scales; and Chapter III details the operation of SOLARFLUX, including software setup, input and output, and program operation

BACKGROUND

Solar Radiation Models

Incoming solar radiation is variable at all temporal and spatial scales, but this variation is generally understandable and subject to quantitative modeling. Temporal variation in global insolation is a function of time of year and cloud cover, and drives seasonal cycles (Lieth 1973). Because insolation is poorly sampled in weather station networks, models have been developed to estimate insolation based on first principles (Gates 1980, Lunde 1980, Monteith and Unsworth 1990, Dubayah and Rich 1995), and many approaches incorporate standard weather data (Nicks and Harp 1980, Bristow and Campbell 1984, 1985, Becker and Weingarten 1991). Spatial and temporal variation in site-specific insolation at both local and landscape levels is predictable from basic geometric principles, and is a major cause of climatic differentiation across local topography (Geiger 1965, Rich and Weiss 1991, Galo et al. 1992, Dubayah 1992, Saving et al. 1993, Dubayah and Rich 1995). Insolation is a function of latitude, day of year, time of day, slope and aspect of the receiving surface, and horizon obstruction. Numerous algorithms and computer programs exist for geometric insolation calculations (*e.g.* Swift and Knoerr 1973, Lunde 1980, Nunez 1980, Revfeim 1982, Dozier and Frew 1990). Integration of spatio-temporal insolation models into a GIS-based model provides powerful analytical tools for numerous disciplines, from ecology and hydrology to architecture and urban planning.

Applications

Spatially based insolation models offer powerful analytical capabilities of value to numerous disciplines. Topographic effects on insolation and its effect on ecology has been the subject of literally hundreds of studies (see review in Hetrick et al. 1993a). In ecology, solar radiation models can be applied at individual, community, ecosystem, and landscape levels. For example, local light conditions influence growth of individual plants (Pearcy 1983); heterogeneity of microclimate influences distribution of different species in a community (Weiss *et al.* 1988, 1991, Weiss and Murphy 1990, Rich and Weiss 1991, Rich *et al.* 1992); solar radiation limits ecosystem productivity and influences energy and water balances (Lin *et al.* 1992); and quantifying solar radiation flux is essential for evaluating climate fluctuations at the landscape level (Running 1984, Running *et al.* 1987, Pacala and Hurtt 1993, Schimel 1993). In remote sensing, coupling insolation models with vegetation canopy reflectance models (Goel 1988, Hall et al. 1991, Schaaf and Strahler 1993) and landscape topographic patterns (Dubayah *et al.* 1989, 1990, Dubayah 1992) can enhance the interpretation of reflectance measurements.

Insolation models can also be used in architecture, design, and urban planning to simulate various design and management options. For example, different building sites can be evaluated on simulated landscapes. Similarly, changes in landscape features (e.g. addition or removal of trees or structures) can be evaluated. Because simulation of incident radiation on complex surfaces is scale independent, except at very local scales where penumbral effects become important (Smith et al. 1989), spatially based insolation models have broad applications in both theoretical and applied problems at many scales.

The Program SOLARFLUX

SOLARFLUX is a GIS-based program for modelling incoming solar radiation based on surface orientation, solar angle, shadowing due to topographic features, and atmospheric attenuation. Surface topography is defined in a raster-based array (grid) of elevation data. Global location of the surface (longitude and latitude) and time interval for calculation are specified by the user. The result is a grid of insolation values for each surface location during the specified time interval. SOLARFLUX calculates five basic types of output: 1) total direct radiation, 2) duration of direct sunlight, 3) total diffuse radiation, 4) skyview factor (proportion of unobscured sky), and 5) hemispherical viewsheds of sky obstruction for specified surface locations. Our approach is basically geometrical in nature and can incorporate either empirical or theoretical distributions of incoming solar radiation.

FUNDAMENTAL PRINCIPLES

Incoming Solar Radiation

Solar radiation refers to electromagnetic radiation originating in thermonuclear reactions on the sun. Because of the large distances involved, and the relatively small size of the Earth as compared with the sun, only a very small fraction of the energy emitted reaches the Earth. Solar radiation is transmitted directly to the Earth through a virtual vacuum. The amount of solar radiation reaching the Earth is relatively constant, and can be described a single value of 1353 W/m^2, known as the solar constant S_o adjusted by a factor to account for the elliptical orbit of the Earth about the sun. The gases and particles of the Earth's atmosphere modifies incoming solar radiation by processes of scattering, absorption, and reradiation. Solar radiation is further modified at the Earth's surface by topography and local surface characteristics. For any given location at the Earth's surface, the incoming solar radiation, or insolation, consists of three components: 1) direct radiation, which is transmitted unimpeded along the path between the sun and the Earth; 2) diffuse radiation, which results from atmospheric scattering from any sky direction; and 3) reflected radiation, which consists of direct and diffuse radiation that is reflected off surrounding terrain features (Figure 1). Insolation is calculated by integrating direct, diffuse, and reflected radiation components over a specified time interval.

Topographic Effects:

Topography has two important effects on the insolation at a given location: 1) surface orientation determines the angle of incidence of direct, diffuse, and reflected radiation; 2) sky obstruction by surrounding topography limits the directions from which direct and diffuse radiation can originate. In the case of direct radiation, sky obstruction by topographic features along the path of the sun leads to shadows and times when no direct radiation reaches the location. Sky obstruction in any sky direction will limit the amount of diffuse solar radiation reaching a given location.

The hemispherical viewshed algorithm (Rich et al. 1994) warrants further description, because it is at the heart of SOLARFLUX's skyview factor and diffuse calculations and has

broad applicability for efficient geometric modelling. The algorithm, originally developed by Rich (1989, 1990) for analysis of hemispherical photography, can be generalized in the following way. First, the angular distribution of sky obstruction is specified in a hemispherical coordinate system, in which the hemisphere of sky directions is projected on a plane. Second, the sky is divided into a discrete number of sectors, corresponding to reasonably small ranges of zenith and azimuth angles, and the angular area of unobstructed sky corresponding to each sky sector is determined. Third, for each sky sector the proportion of unobstructed sky is multiplied by the corresponding irradiance for that entire sky sector, and by a factor that provides a cosine weighting appropriate for the angle of incidence between the sky sector and the surface of interest. Finally, the resulting radiance values of all sky sectors, which now account for sky obstruction and angle of incidence, are summed to obtain total incident radiation for the location of interest. By using precalculated lookup tables of direct and diffuse irradiance values corresponding to each sky direction, calculations can be made very rapidly.

Calculation of Topographic Influences on Insolation

Topographic models must account for the effects of surface orientation and sky obstruction by surrounding topographic features. Two different, but related approaches can be used to account for topographic effects on solar radiation. The first approach, applicable for direct radiation calculations, involves calculating shadow patterns, using ray tracing techniques, across a topographic surface at a series of discrete time steps and then calculating the angle of incidence of direct radiation reaching each surface location that is not in shadow for each time step. This is the approach currently used for direct insolation calculations by SOLARFLUX (Hetrick et al. 1993a, 1993b). The second approach, applicable for either direct or diffuse calculations, involves calculating hemispherical viewsheds for each surface location, wherein the geometry of sky obstruction is determined by ray tracing techniques (Rich et al. 1994). This hemispherical viewshed approach can then be used to integrate values of direct and diffuse insolation originating from non-obscured sky directions.

CAPABILITIES OF SOLARFLUX

Total direct radiation, the intercepted direct beam solar energy, is calculated for each position on the surface using standard calculating formulae to determine solar angle (zenith and azimuth) and atmospheric attenuation. Atmospheric attenuation is based on a transmittivity value τ, the proportion of radiation that passes unimpeded through the atmosphere in a vertical direction, and the length of atmosphere traversed in non-vertical directions. Larger zenith angles lead to lower incident direct radiation due to atmospheric attenuation. Elevation effects are accounted for on surfaces with high relief by calculating changes in transmittivity as a function of elevation. The effect of surface orientation is accounted for by using a cosine correction based on the angle of incidence, i.e., the angle between the solar angle and the axis normal to the surface. For each time interval, shadow patterns are determined using the *hillshade* function in ARC/INFO, which assigns values of zero to locations shaded by topographic features (i.e., no direct radiation received during that time interval). The *hillshade* function can be disabled by the user, which makes it possible to evaluate the importance of shadows.

Duration of direct sunlight, the total time during which a surface position receives direct beam radiation, is calculated by summing time intervals when surface locations are not shaded.

Skyview factor, the ratio of diffuse sky irradiance relative to that on an unobstructed horizontal surface, is calculated for each surface location. The current implementation of SOLARFLUX assumes an isotropic distribution of diffuse irradiance throughout the hemisphere of sky directions sky direction (see Dozier and Frew 1990). However, the hemispherical

viewshed algorithm used in SOLARFLUX can accommodate either isotropic or anisotropic irradiance distributions (Rich et al. 1994).

Total diffuse radiation, the intercepted solar energy that is scattered by the atmosphere, is currently calculated based on an isotropic model, i.e., all sky directions contribute equally to diffuse radiation. This is accomplished by multiplying the skyview factor by a coefficient that converts to units of diffuse radiation flux.

Hemispherical viewsheds of sky obstructions are calculated by storing the elevation angles calculated when determining skyview factors. These angles can be used to generate hemispherical views upward from a particular surface location and used as input to programs for analysis of hemispherical imagery, for example the analysis program CANOPY (Rich 1989, 1990). CANOPY can calculate a variety of insolation indices, including direct and diffuse site factors (the proportion of direct and diffuse radiation reaching a location, relative to an unobstructed sky) and the duration and timing of direct radiation.

MODEL REFINEMENT AND ENHANCEMENT

It is our intention that the SOLARFLUX model will serve as a prototype for more comprehensive and efficient geometric models of solar radiation. In terms of efficiency, perhaps the greatest advances will be made by implementing optimized subsampling and interpolation techniques that serve in place of the current brute-force method that must perform calculations for every surface location. Three basic extensions of SOLARFLUX are desirable. First, improved atmospheric transmittivity and diffuse submodels, tailored to describe conditions as they change with time and space, could be implemented as user-specifiable mathematical expressions or lookup tables. Second, the ability to account for sky anisotropy could be implemented based on a hemispherical viewshed algorithm (Rich et al. 1994). Third, a reflectance submodel, which calculates how surrounding topography affects reflected insolation, could be implemented using viewsheds of terrain (Dubayah and Rich 1995, Rich et al. 1994). All of these enhancements could permit incorporation of either theoretical or empirically derived parameter values (Rich et al. 1993b).

CONCLUSION

Computer technology has advanced to a level where it is now feasible to model insolation for complex topographic surfaces. SOLARFLUX is a GIS-based model for calculating insolation for topographic surfaces based on first principles, in particular taking into account effects of surface orientation and sky obstruction due to topographic features. The GIS approach offers scale independent simulations and facilitates coupling insolation analysis with other earth system models. SOLARFLUX serves as a useful tool for modelling solar radiation at various spatial scales, and as a prototype for more comprehensive geometric models of solar radiation.

CHAPTER II: APPLICATIONS

APPLICATION OF SOLARFLUX AT VARIOUS SPATIAL SCALES

The following are five case studies in which SOLARFLUX is used to model insolation in markedly different systems. Each case study illustrates principles, problems, actual findings, and important implications. The topographic surfaces used for input span scales from tens of kilometers to fractions of a meter -- from the landscape level, in which insolation for an entire mountain range is modelled; to the stand level, in which insolation at the surface of a plant canopy is modelled; to the local level, in which insolation for a treefall gap is modelled.

LANDSCAPE LEVEL MODELLING

Case Study 1: Insolation for the Spring Mountains, Nevada

At the landscape level, topographic effects on insolation can define the range of microclimates that serve as the physical determinants of habitat for biological organisms (Weiss et al. 1988, Rich and Weiss 1991, Rich *et al.* 1992). In an initial application, we are using insolation calculations to examine the distribution of biophysical determinants of habitat as they influence the distribution and abundance of butterflies in the Spring Range, Nevada, as part of the Nevada Biodiversity Research and Conservation Initiative (Austin and Austin 1980, Saving et a. 1994, Weiss et al. 1994). An elevation grid was derived from USGS 1:250,000-scale DEM data, at a cell size of 94 m (Saving and Weiss 1994) (Figure 2A,B). Potential clear-sky insolation was then calculated using SOLARFLUX at 30-minute intervals under clear-sky conditions (transmittance 0.6) for three days: the vernal equinox, the summer solstice, and winter solstice (Julian days 81, 172, 355, respectively) (Figure 2C,D,E).

Case Study 2: Insolation for Big Creek Reserve, California

In a second application, we are using insolation as a primary driver for a microclimate habitat model that can be used to predict the distribution of vegetation for the University of California Big Creek Reserve (Saving et al. 1993). Big Creek, situated in the rugged Santa Lucia Mountains of the central California coast, includes elevations ranging from sea level to 1200 m (4000 ft) with an average slope of 30 degrees (Norris 1985, Saving et al. 1993). Because of its topographic diversity, Big Creek comprises a broad range of microclimates, which in turn leads to a high diversity of plant communities, ranging from mesic redwood forest to xeric coastal scrub (Bickford and Rich 1979).

From a vector topographic contour coverage derived by scanning the USGS 1:24,000-scale quad sheets (Figure 3A), we constructed an interpolated surface model using a triangulated irregular network (TIN). An elevation grid was then created from the TIN (Figure 3B). Next SOLARFLUX was used to calculate skyview factors for each location on the surface. Then SOLARFLUX was used to calculate daily direct insolation for Big Creek at 5-minute intervals under clear-sky conditions (transmittance 0.6) for three days: the vernal equinox, the summer solstice, and winter solstice (Julian days 81, 172, 355, respectively). Calculations of skyview factor show the lowest values in the valley bottoms and the highest values on the ridges (Figure 3C). Daily insolation at Big Creek is intermediate at the equinox, highest at the summer solstice, and lowest at the winter solstice (Figure 3D,E,F). Spatial variation is greatest in the winter and lowest in the summer. In general, insolation is highest on ridge tops and south-facing slopes and lowest in canyon bottoms and on north-facing slopes.

These studies of insolation demonstrate that topography strongly determines microclimate conditions. In turn, plant distributions follow those microclimate gradients. South-facing slopes and ridge tops receive high insolation and thus have higher potential

evapotranspiration. Consequently, these regions are drier than north-facing slopes and canyon bottoms, which receive considerably less insolation. Inspection of the vegetation map for Big Creek (figure 3G) reveals that plant communities adapted to drier, hotter conditions, such as coastal scrub, are found in the localities where insolation is, on average, highest. Where insolation is low for at least part of the year, water availability is higher and communities such as mixed-hardwood predominate. Where insolation is lowest, pure redwood and redwood mixed-hardwood forests occur. Thus topographic heterogeneity leads to a distribution of biotic assemblages that can be predicted on the basis of the effects of insolation on microclimate.

Slope, aspect, and elevation are known by ecologists to have a significant influence on microclimate, however, the importance of sky obstruction by topographic features is less appreciated and was previously difficult to quantify. By calculating hemispherical viewsheds for any location on a topographic surface, it is possible to determine direction in which the sky is obscured (Figure 4). Sky obstruction by topographic features affects both direct and diffuse insolation components. In the case of diffuse insolation, sky obstruction in any sky direction can block insolation from that direction. In the case of direct insolation, sky obstruction along the path of the sun leads to shadows, wherein direct sunlight is blocked during certain times of day. The importance of this process, herein referred to as topographic shadowing, increases with surface complexity. For complex surfaces, topographic shadowing may be more important than surface orientation in limiting incoming solar radiation. As an example of the importance of topographic shadowing at a landscape scale, we simulated insolation with and without topographic shadowing for Big Creek Reserve (Figure 5A,B,C). An index of topographic shadowing can be calculated as the proportional decrease in solar radiation due to topographic shadowing, i.e., one minus the ratio of insolation calculations with and without topographic shadowing. This topographic shadowing index ranges from zero, with no shadow effect, to one, for a location that is completely in shadow. As would be expected, the topographic shadowing index, based on direct insolation calculations, is highest at the canyon bottoms and on north-facing slopes and lowest on the ridgetops and south-facing slopes (Figure 5D,E,F). Likewise, topographic shadowing is least pronounced at the summer solstice and most pronounced at the winter solstice.

STAND LEVEL MODELLING

Case Study 3: Insolation for Semiarid Woodlands at Los Alamos National Environmental Research Park

Study of insolation at the stand level is important because canopy architecture, here defined as the three-dimensional organization of aboveground plant parts, leads to heterogeneity in flux processes involving carbon, heat, and water. For example, in pinyon-juniper woodlands, variation in near-ground solar radiation flux, associated with clumped tree distributions, has a strong influence on water balance (Lin *et al.* 1992), which in turn affects ecological processes at all levels of organization (Martens and Rich in press). In a third application, we employ a novel approach whereby we examine insolation as it is modified by plant canopies. This work has been focused at a three-hectare pinyon-juniper woodland study site at the Los Alamos National Environmental Research Park (TA-51 West) (Rich et al. 1993b). In preliminary studies, our approach to modelling insolation has involved three basic steps: 1) mapping and automation of georeferenced locations, stem diameters, and heights of all pinyons and junipers in a three-hectare stand using GIS (ARC/INFO and GRID) (Figure 6A); 2) using GIS to construct a canopy digital elevation model (CDEM) based on the allometry of crown radius to stem diameter and the assumption that tree crown form can be approximated as the upper half of an ellipsoid (Figure 6B); and 3) simulation of intercepted solar radiation using SOLARFLUX (Figure 6C,D,E,F).

Skyview factors were highest on the tops of shrubs and trees and in the center of openings. Overall, the estimated daily insolation was highest at the summer solstice and lowest at the winter solstice. Heterogeneity of insolation was important during all times of year, but most pronounced on the winter solstice, when the south sides of clumps tended to receive the most insolation. For the relatively open, heterogeneous canopies of semiarid woodlands, interactions between canopy architecture and solar radiation lead to heterogeneous microclimates. There is strong differentiation between microsites on different sides of clumps; and sharp microclimate gradients extend from the center of clumps to the center of openings. Thus modelling the explicit geometry of the canopy architecture as it interacts with solar angle permits prediction of the distribution of microclimates as they shift during the day and through the seasons. The ecological implications are important at population, community, and ecosystems scales. We have proposed a "safe microsite model" of community dynamics in semiarid woodlands that would provide a synthesis of the known physiology, demography, water relations, productivity, and nutrient dynamics for pinyon-juniper woodlands (Martens and Rich in press). From the perspective of a seedling pinyon or juniper plant, establishment requires growth in a safe microsite, the distribution and extent of which vary in predictable spatial patterns with climatic fluctuations.

LOCAL LEVEL MODELLING

Case Study 4: Insolation for Inclined Plots, Waste Cover Design

In a fourth application, we are using SOLARFLUX to examine highly localized patterns of insolation as they affect energy and water balance of waste sites at Los Alamos National Laboratory. In particular, we have examined daily and seasonal patterns of incoming solar radiation on a series of protective barrier plots that range in slope from 0% to 25% while holding aspect constant (azimuth 139°, approximately southeast). Preliminary studies demonstrate that slope orientation (slope and aspect) can lead to significant differences in energy and water balance. Between-slope differences were more pronounced on the winter solstice (Figure 7A) than on the summer solstice (Figure 7B). Even more dramatic differences would be expected for slopes with different aspects.

Case Study 5: Insolation in Treefall Gaps

In a fifth application, we are using SOLARFLUX to examine highly localized patterns of insolation in forest canopy gaps. Spatial and temporal variation of solar radiation regimes within plant canopy gaps influences energy balance, microclimate, primary production, and water balance. We are conducting a systematic study of the effects of canopy gap geometry on insolation regimes. In particular, we are examining the effects of gap radius, canopy height, and latitude on insolation under clear sky conditions. We are examining insolation for a series of theoretical cylindrical and irregular shaped gaps across two orders of magnitude of gap radii (1-100 m) and canopy heights (also 1-100 m), and across latitudes ranging from 0° to 90°. First, we have represented gap geometry by constructing a series of digital elevation models using ARC/INFO GRID. Then, SOLARFLUX is being used used to simulate 1) incident direct insolation at five-minute intervals through the day, 2) duration of direct radiation, 3) skyview factor, 4) incident diffuse radiation, and 5) hemispherical viewsheds.

Skyview factors are distributed in a radially symmetrical pattern, with the highest values in the gap center and the lowest values at the gap edges (Figure 8A). Morning shade on east sides of gaps and afternoon shade on west sides of gaps result in pronounced east-west temporal variation of insolation within each day (Figure 8B). Seasonal shifts in solar angle result in pronounced north-south spatial variation of insolation across seasons for all latitudes (Figure 8C,D). For a fixed gap radius, increasing canopy height leads to decreased insolation and decreased spatial variability (Figure 8E,F). The temporal and spatial variation in canopy gaps defines distinct gradients of microclimate, available solar radiation, and water stress, which in turn can affect rates of primary productivity and influence growth and survivorship of plants that become established in a gap.

CHAPTER III: GUIDE TO OPERATION OF SOLARFLUX

SOFTWARE AND HARDWARE REQUIREMENTS

SOLARFLUX is based on an ARC/INFO and GRID GIS platform (Environmental Systems Research Institute, Inc., Redlands, CA), running under XWINDOWS on a UNIX workstation. SOLARFLUX has three functional modules: 1) a direct solar radiation module, 2) a diffuse/skyview factor module, and 3) a hemispherical viewshed module. The direct solar radiation module of SOLARFLUX was implemented as set of Arc Macro Languange (AML) programs within the GRID GIS environment, while the diffuse/skyview factor and hemispherical viewshed modules were written primarily in the "C" programming language. SOLARFLUX was developed and tested on a SUN SPARCstation running versions 6.1 and 7.0 of ARC/INFO and GRID. The basic functionality of SOLARFLUX requires ARC/INFO version 6.1 or 7.0; however, the hemispherical viewshed and skyview factor modules require the GRID commands *gridfloat* and *floatgrid* functions introduced in ARC/INFO 7.0. Because of the AML implementation, SOLARFLUX is expected to be nearly completely compatible across all computing platforms on which ARC/INFO will run. However, SOLARFLUX is computationally very intensive so a recommended minimum platform is a RISC-based processor workstation. Details of installation are provided in Appendix A.

PREPARING INPUT DATA -- ELEVATION GRIDS

Input Format

Elevation data for the surface to be analyzed must be in an ARC/INFO grid format. Due to the elevational compensation of the relative optical air mass, the current version of SOLARFLUX requires the cell size and elevation units in meters. When building the elevation grid, be sure to generate the data at a resolution appropriate for the question being asked.

Input Elevation GRID Preparation

Elevation grids can be constructed using a variety of sources: 1) USGS DEMs, 2) contour lines, and 3) other sources (e.g. stereo imagery and survey data).

Converting USGS DEMs to GRID: Standard USGS digital elevation model (DEM) data can be converted to an elevation grid using the ARC/INFO command *demlattice*.

Generating a GRID From Contour Lines: Topographic contour lines can be used to build a triangulated irregular network (TIN) model using *createtin*. When building a TIN model, the number of flat triangles should be minimized. To display flat triangles, use the *tinerrors* command in ARCPLOT (set the shadeset to colors.shd before using the command). Breaklines along ridge tops and streamless valleys may be useful for correcting errors in the TIN model. A point coverage of know elevations can also be used. With an adequate TIN model, a grid can be generated using the *tinlattice* command in ARC. The resolution of the grid should not be smaller than the proximal tolerance of the points, or nodes, in the TIN model. ARC/INFO 7.0 provides a new function *topogrid*, which converts topographic contour lines directly to grids.

PROGRAM OPERATION

Starting SOLARFLUX

SOLARFLUX runs within the GIS program GRID. GRID can be started directly from the system prompt using a command line argument:

unix% *arc grid*

The following GRID command will invoke the SOLARFLUX menu:

GRID: *solarflux*

Specifying Model Parameters

Menu Control: SOLARFLUX uses a form menu that provides a convenient interface for specifying model parameters. The user must supply the input surface grid name, the output grid names, day of analysis, start and end times, calculation time increment, global position (latitude and longitude), local time meridian, and atmospheric transmittivity.

Julian day: The day for the simulation must be specified in the form menu. The parameter can be entered as Julian day (e.g. 81) or in a month-day format (e.g. 3-22 for March 22). If the parameter is entered in the month-day format, the value is immediately converted to Julian day.

Start time, end time, and increment: Start and end times specify the period for which calculations of insolation are to be performed. The time increment specifies the step between each of the series of calculations that are performed between start and end times. Time parameters can be specified as decimal hours, comma delimited, or colon delimited (see example below). Morning or afternoon can be specified with *am* or *pm*. Time parameters may also be entered in solar time (i.e. military time, so *13:00* is *1:00* pm). For example, all of the following inputs represent the same time (*1:00 pm*): *1:00pm*, *1:00p*, *13:00*, *1,00p*, or *13.0*. All time parameters are converted to decimal hours and displayed on the input line. In our example, the displayed value would be *13.0*.

Latitude, longitude, and local time meridian: Latitude and longitude define an approximate global position of the surface. The lattitude and longitude coordinates should correspond to a location near the center of the surface being analyzed. The local time meridian is the longitude where the local time zone begins. Specification of longitude and local time meridian is only necessary for situations where it is important to keep track of the time zone. In cases where the user is only interested in solar time, a value of zero should be specified for both the longitude and local time meridian. The surface location parameters may be specified as decimal degrees or comma delimited degrees, minutes and seconds. As parameters are entered, they are converted and displayed as decimal degrees. For example, 10 deg, 5 min, 2 sec can be entered as *10,5,2* or *10.083888*. South and West parameters should be entered as negative numbers. Latitudes must have values between -90 and 90, whereas longitude and local time meridian must have values between -180 and 180.

Transmittivity: Surfaces at higher elevations experience greater transimittivity than surfaces at lower elevations due to the shorter attenuation path. SOLARFLUX compensates for elevational effects on transimittivity, so sea-level values should be used when specifying the transmittivity parameter.

Surface elevation grid: A display box lists all elevation grids in the current workspace. A grid file may be chosen from the list or specified explicitly by entering the grid file name in the space provided.

Output Options: Output options are chosen by clicking the SELECT mouse button on the small raised box near the option title. A check-mark will be displayed in the box if it has been selected. All output options must have a corresponding output grid file name. Three output options can be selected:

1) total direct with hillshade on: specifies output of direct insolation that includes the effects of topographic shadowing.

2) total direct with hillshade off: specifies output of direct insolation that is based only on surface orientation, i.e. topographic shadowing effects are not included.

3) duration of direct: specifies output of the duration of direct insolation in hours.

Save Parameters: By choosing the save parameters button with the mouse, the user can save the parameters defined in the menu to a file. The user is prompted for a file name, which should be named with a .sf extension.

Load Parameters: By choosing the load parameters button with the mouse, the user can load values stored in a parameter file. A pop-up menu lists all parameter files in the current workspace (indicated with a .sf file extension), and prompts the user for a file name. After the parameters file is loaded, the values are displayed in the menu.

Running SOLARFLUX

To begin running the SOLARFLUX program, click the Apply button with the mouse. While the program is running, a graphical display shows a hemispherical viewshed of the solar track for each incremental time of simulation.

Quitting SOLARFLUX

To quit the SOLARFLUX menu without running the program, click the Quit button.

Running SOLARFLUX In Batch Mode Using Parameter Files

A convenient use of parameter files, besides archiving the simulation parameters, is to run SOLARFLUX in a batch mode. Batch mode operation supplies SOLARFLUX with a list of parameter files, and the program is run for each configuration. Considering the time requirements for typical simulations, the batch mode can be used to run the program through a series of configurations over night, when computers are typically idle. To use the batch function, generate the parameter files with the SOLARFLUX menu by entering all necessary parameters and clicking the SELECT mouse button on the Save Parameters button. Quit the menu without running the program. Then run SOLARFLUX with a command line argument *file*, followed by a list of the parameter file names. For example, if *file1.sf*, *file2.sf* and *file3.sf* are the parameter files, the command at the GRID prompt would be entered as follows:

GRID: *solarflux file file1.sf file2.sf file3.sf*

Displaying Output Results

Output grid results can be displayed using standard GRID commands. The following is a summary of some of the useful commands for displaying output grids.

1) Describe the output grid to get the value range:

Grid: *describe <outputgridfile>*

2) Select an appropriate shadeset:

Grid: *shadeset <shadesetfile>*

For example, use *color.shd* as the *<shadesetfile>*.

3) Use a text editor to create an ASCII look-up table, the left column of which is a range of actual values in the grid, the right column the color value, and with the two columns separated by a ":".

4) Set the map extent of the grid:

Grid: *mapextent <outputgridfile>*

5) Use gridshade to display the grid file:

Grid: *gridshade <outputgridfile> # <lookuptablefile>*

6) The *cellvalue* command can be used to examine values of individual cells within the ouput grid:

Grid: *cellvalue <outputgridfile>* *

Calculating Skyview Factors

To run the skyview factor module, first the user must use ARC/INFO and GRID to prepare elevation, slope, and aspect floating point files. This can be accomplished by the following steps:

1) Create an elevation grid, in the same format as for the direct insolation SOLARFLUX module.

2) From the elevation grid, produce a slope grid:

Grid: *<slopegrid> = slope(<elevationgrid>)*

3) Produce an aspect grid from the elevation grid:

Grid: *<aspectgrid> = aspect(<elevationgrid>)*

4) Convert the elevation, slope, and aspect grids to floating point files (note: the *gridfloat* command requires ARC/INFO v.7.0 or higher):

Arc: *gridfloat <elevationgrid> <elevationfloatfile>*
Arc: *gridfloat <slopegrid> <slopefloatfile>*
Arc: *gridfloat <aspectgrid> <aspectfloatfile>*

5) Create an ASCII text file, for example *svf_batch*, containing the following batch process command:

svfactor <elevationfloatfile> <slopefloatfile> <aspectfloatfile> <outputfloatfile>

6) Run the skyview factor program by invoking the batch process at the UNIX prompt:

unix% *batch svf_batch*

Depending on the size of grid files and the computer used, the program can take considerable time to run. For example, a 160KB input grid file running on a 32M RAM SUN SPARCstation 2 requires about 7 hours, whereas a 2.1M grid file requires about 150 hours.

7) Convert the output floating point file to grid file:

Arc: *floatgrid <outputfloatfile> <outputgrid>*

Calculating Hemispherical Viewsheds

To run the hemispherical viewshed module, the user must specify the elevation, slope, and aspect files as floating point input files, along with X and Y grid locations. The following steps produce

1) Create the floating point input files following steps 1-4 in the ***Calculating Skyview Factor*** section (above).

2) Determine the X,Y position of interest on the input surface. The GRID *cellvalue* command can be used with the mouse to allow interactive examination of a given point's X,Y position:

Grid: *mapextent <elevationgridfile>* *
Grid: *image <elevationgridfile>*
Grid: *cellvalue <elevationgridfile>* *

3) Run the hemispherical viewshed module:

unix% *hemiview <elevationfloatfile> <slopefloatfile> <aspectfloatfile> <xgridlocation> <ygridlocation> <outputfile>*

4) The output file consists of an ASCII list of sky direction (azimuth angle, zenith) values that connect up to define a hemispherical viewshed.

Calculating Surface Area Effects

Surface area of the input topographic surface can be calculated as follows, using an AML program developed by Saving and Hetrick (1994):

Grid: *<surfaceareagrid> = sa(<elevationgrid>)*

The resulting surface area grid can be used to examine incoming solar radiation on a per cell basis, projected in the horizontal plane, as opposed to a flux measurement along the surface itself. This is accomplished by multiplying the surface area grid and the insolation grid of interest:

Grid: *<horizontalfluxgrid> = <surfaceareagrid> * <insolationgrid>*

IMPORTANT CONSIDERATIONS

Hard Disk Storage Requirements

SOLARFLUX creates several temporary grids while performing calculations. Adequate space must be available on the hard drive to accomodate the temporary files. After calculations are complete, SOLARFLUX automatically deletes all temporary files. The following methodology can be used to ensure that there is sufficient hard disk space to run SOLARFLUX.

1) Determine the size of the input elevation grid:

unix% *cd <workingdirectory>*
unix% *ls -l*

File sizes are displayed in bytes.

2) Calculate the disk space (D) required to run SOLARFLUX, based on the number of output options selected (O) and the size of the input elevation grid (I):

$$D = (3 + 2O)\, I$$

3) Determine whether enough disk space is available on the current file system or partition to store the temporary grids:

unix% *df .*

The available disk space will be displayed in kilobytes. If using SOLARIS 2.x, use the *-k* switch with this command to display the information in kilobytes:

solaris% *df -k .*

Note the period in these commands. This period will cause the *df* command to show the space available on the file system or partition where the coverage exists. Without the period, the command will show the space available on all file systems.

Trade-Offs: Input Grid Size, Calculation Period, and Calculation Interval

Insolation models are inherently calculation intensive. Therefore it is important to consider trade-offs between input elevation grid size, calculation period, and calculation time interval. In particular, simulations involving large grids, long time periods, or small calculation intervals will tend to be slower than smaller grids, shorter time periods, or larger calculation intervals. For example, using a SUN SPARCstation 2 simulations for an input elevation grid of 100 by 600 cells required from 4-6 computing hours to calculate a full day of direct insolation using 30 minute calculation increments, but 8-16 hours using 15 minute calculation increments. It is always important to scale insolation simulations appropriately for the problem being addressed.

ACKNOWLEDGEMENTS

We thank Fairley Barnes, David Breshears, Ralph Dubayah, Andrew Weiss, and Stuart Weiss for critical scientific discussion. This work was supported by the Center for Conservation Biology at Stanford University, the Kansas Applied Remote Sensing Program, the Kansas Biological Survey, the Kansas Center for Computer Aided Software Engineering, Los Alamos National Environmental Restoration Program, NASA grant NAG5-2358, National Science Foundation grant BSR90-02326, and the University of Kansas Research Development and General Research Funds.

LITERATURE CITED

Austin, G.T., and A.T. Austin. 1980 Butterflies of Clark County, Nevada. Journal of Research on the Lepidoptera 19:1-63.

Becker, P. and D.S. Weingarten. 1991. A comparison of several models for separating direct and diffuse components of solar radiation. Agricultural and Forest Meteorology 53: 347-353.

Bickford, C. and P.M. Rich. 1979. Vegetation and flora of the Landels-Hills Big Creek Reserve, Monterey County, California. USCS Environmental Field Program Publication No. 2.

Bristow, K.L. and G.S. Campbell. 1985. An equation for separating daily solar radiation into direct and diffuse components. Agricultural and Forest Meteorology 35: 123-131.

Brown, D.G. 1992. Topographical and biophysical modeling of vegetation patterns at alpine treeline. PhD dissertation, University of North Carolina at Chapel Hill.

Dozier, J. 1980. A clear-sky spectral solar radiation model for snow-covered mountainous terrain. Water Resources Research 16:709-718.

Dozier, J. and J. Frew. 1990. Rapid calculation of terrain parameters for radiation modeling from digital elevation data. IEEE Transactions on Geoscience and Remote Sensing 28:963-969.

Dubayah, R. 1992. Estimating net solar radiation using Landsat Thematic Mapper and digital elevation data. Water Resources Research 28:2469-2484.

Dubayah, R., J. Dozier, and F.W. Davis. 1989. The distribution of clear-sky radiation over varying terrain. Proceedings IGARSS '89. pp 2469-2484.

Dubayah, R., J. Dozier, and F.W. Davis. 1990. Topographic distribution of clear-sky radiation over the Konza Prairie., Kansas. Water Resources Research 26: 679-690.

Dubayah, R. and P.M. Rich. 1995. Topographic solar radiation models for GIS. International Journal of Geographic Information Systems. In Press.

Galo, A.T., P.M. Rich, and J.J. Ewel. 1992. Effects of forest edges on the solar radiation regime in a series of reconstructed tropical ecosystems. American Society for Photogrammetry and Remote Sensing Technical Papers, Albuquerque, NM. pp 98-108.

Gates, D.M. 1980. Biophysical Ecology. Springer-Verlang. New York.

Geiger, R.J. 1965. The Climate Near the Ground. Harvard University Press. Cambridge.

Goel, N.S. 1988. Models of vegetation canopy reflectance and their use in estimation of biophysical parameters from reflectance data. Remote Sensing Reviews 4: 1-212.

Gray, J.T. 1979. The vegetation of two California mountain slopes. Madroño 25:177-185.

Hall, F.G., D. Botkin, D.E. Strebel, K.D. Woods, and S.J. Goetz. 1991. Large-scale patterns of forest succession as determined by remote sensing. *Ecology*, 72:628-640.

Hetrick, W.A., P.M. Rich, F.J. Barnes, and S.B. Weiss. 1993. GIS-based solar radiation flux models. American Society for Photogrammetry and Remote Sensing Technical Papers, Vol 3, GIS, Photogrammetry, and Modeling. pp 132-143.

Lieth, H. 1973. Phenology and Seasonality Modeling. Ecological Studies 8. Springer Verlag. New York.

Lin, T., P.M. Rich, D.A. Heisler, and F.J. Barnes. 1992. Influences of canopy geometry on near-ground solar radiation and water balances of pinyon-juniper and ponderosa pine woodlands. American Society for Photogrammetry and Remote Sensing Technical Papers, Albuquerque, NM. pp 285-294.

Lunde, P.J. 1980. Solar Thermal Engineering. John Wiley and Sons: New York.

Monteith J.L. and M.H. Unsworth. 1990. Principles of Environmental Physics. Edward Arnold: London.

Nicks, A.D. and J.F. Harp. 1980. The stochastic generation of temperature and solar radiation data. Journal of Hydrology 48: 1-17.

Norris, R. 1985. Geology of the Landels-Hills Big Creek Reserve, Monterey County, California. UCSC Environmental Field Program Publication No. 16.

Nunez, M. 1980. The calculation of solar and net radiation in mountainous terrain. Journal of Biogeography 7: 173-186.

Pacala, S.W. and G.C. Hurtt. 1993. Terrestrial vegetation and climate change: integrating models and experiments. pp. 57-74 In: P.M. Kareiva, J.G. Kingsolver, R.B. Huey (eds). Biotic interaction and global change. Sinauer Associates Inc. Sunderland, MA.

Pearcy, R.W. 1983. The light environment and growth of C3 and C4 tree species in the understory of a Hawaiian forest. Oecologia 58: 19-25.

Revfeim, K.J.A. 1982. Estimating global radiation on sloping surfaces. New Zealand Journal of Agricultural Research 25: 281-283.

Rich, P.M. 1989. A manual for analysis of hemispherical canopy photography. Los Alamos National Laboratory Technical Report LA-11733-M, Los Alamos, NM.

Rich, P.M. 1990. Characterizing plant canopies with hemispherical photography. In: N.S. Goel and J.M. Norman (eds). Instrumentation for studying vegetation canopies for remote sensing in optical and thermal infrared regions. Remote Sensing Reviews 5:13-29.

Rich, P.M., S.B. Weiss, D.A. Debinski, and J.F. McLaughlin. 1992. Physiographic inventory of a tropical reserve. Proceedings of the Twelfth Annual ESRI User Conference. pp 197-208.

Rich, P.M., D.A. Clark, D.B. Clark, and S.F. Oberbauer. 1993a. Long-term study of solar radiation regimes in a tropical wet forest using quantum sensors and hemispherical photography. Agricultural and Forest Meteorology 65:107-127.

Rich, P.M., G.S. Hughes, and F.J. Barnes. 1993b. Using GIS to reconstruct canopy architecture and model ecological processes in pinyon-juniper woodlands. Thirteenth Annual ESRI User Conference, Volume 2. pp 435-445.

Rich, P.M., R. Dubayah, W.A. Hetrick, and S.C. Saving. 1994. Using viewshed models to calculate intercepted solar radiation: applications in ecology. American Society for Photogrammetry and Remote Sensing Technical Papers. pp 524-529.

Rich, P.M. and S.B. Weiss. 1991. Spatial models of microclimate and habitat suitability: lessons from threatened species. pp. 95-102 in Proceedings of the Eleventh Annual ESRI User's Conference. ESRI, Inc: Redlands.

Rich, P.M., S.B. Weiss, D.A. Debinski, and J.F. McLaughlin. 1992. Physiographic inventory of a tropical reserve. Proceedings of the Twelfth Annual ESRI User Conference, Palm Springs, CA. pp 197-208.

Roise, J.P. and D.R. Betters. 1981. An aspect transformation with regard to elevation for site productivity models. Forest Science 27: 483-486.

Running, S.W. 1984. Microclimate control of forest productivity: analysis by computer simulation of annual photosynthesis/transpiration balance in different environments. Agricultural and Forest Meteorology 32: 267-288.

Running, S.W., R.R. Nemani, and R.D. Hungerford. 1987. Extrapolation of synoptic meteorological data in mountainous terrain and its use for simulating forest evapotranspiration and photosynthesis. Canadian Journal of Forestry Research 17:472-483.

Saving, S.C., P.M. Rich, J.T. Smiley, and S.B. Weiss. 1993. GIS- based microclimate models for assessment of habitat quality in natural reserves. American Society for Photogrammetry and Remote Sensing Technical Papers, Vol 3, GIS, Photogrammetry, and Modeling. pp 319-330.

Saving, S.C. and W.A. Hetrick. 1994. Reference guide to TERRACLASS: a physiographic inventory methodology for ARC/INFO.

Saving, S.C. and A.D. Weiss. 1994. Importation protocols and GIS database development for the Spring Mountains, Nevada project. Center for Conservation Biology Open File Report. Stanford University.

Schaaf, C.B. and A.H. Strahler. 1993. Solar zenith angle effects on forest canopy hemispherical reflectances calculated with a geometric-optical bidirectional reflectance model. *IEEE Transactions on Geoscience and Remote Sensing* 31:921-927.

Schimel, D.S. 1993. Population and community processes in the response of terrestrial ecosystems to global change. pp. 45-54 In: P.M. Kareiva, J.G. Kingsolver, R.B. Huey (eds). Biotic interaction and global change. Sinauer Associates Inc. Sunderland, MA.

Smith, W.K., A.K. Knapp, and W.A. Reiners. 1989. Penumbral effects on sunlight penetration in plant communities. Ecology 70:1603-1609

Swift, L.W and K.R. Knoerr. 1973. Estimating solar radiation on mountain slopes. Agricultural Meteorology 12: 329-336.

Weiss, S.B. and D.D. Murphy. 1990. Thermal microenvironments and the restoration of rare butterfly habitat. pp. 50-60 in J. Berger (ed). Environmental Restoration. Island Press. Covelo.

Weiss, S.B., D.D. Murphy, and R.R. White. 1988. Sun, slope, and butterflies: topographic determinants of habitat quality for *Euphydryas editha*. Ecology 69: 1486-1496.

Weiss, S.B., P.M. Rich, D.D. Murphy, W.H. Calvert, and P.R. Ehrlich. 1991. Forest canopy structure at overwintering monarch butterfly sites: measurements with hemispherical photography. Conservation Biology 5: 165-175.

Weiss, A.D., S.B. Weiss, A.T. Galo, S.C. Saving, W.A. Hetrick, and P.M. Rich. 1994. Biodiversity studies of butterflies and plants in the Spring Mountains, southern Nevada. Fourteenth Annual ESRI User Conference.

APPENDIX A: INSTALLING SOLARFLUX

Installation using FTP

1) Set up and change to the installation directory (this example will show */solarflux* to represent the user-defined installation directory):

unix% *mkdir /solarflux*
unix% *cd /solarflux*

2) Use anonymous FTP via the internet to get copies of the documentation and program files:

unix%: *ftp glinda.kbs.ukans.edu*
or
unix%: *ftp 129.237.122.65*

User Name: *anonymous*
Password: [enter your e-mail address]
ftp> *cd solarflux*
ftp> *get README*
ftp> *bin*
ftp> *get solarflux.a4.tar.Z*
ftp> *quit*

1) Extract the program files:

unix%: *uncompress solarflux.a4.tar.Z*
unix%: *tar xvf solarflux.a4.tar.Z*

Installation from a UNIX-Formatted Floppy Disk

1) First log in as root or as a superuser:

login: *root*
password: *<superuser_password>*

or

unix% *su*
password: *<superuser_password>*

2) Set up the installation directory (this example will show */solarflux* to represent the user-defined installation directory):

unix% *mkdir /solarflux*

3) Create a mounting point for the floppy drive file system:

unix% *mkdir /fd*

4) Mount the floppy drive device:

unix% *mount /dev/device /fd*

For SUN systems, the *device* file is usually */dev/fd0*. Note that mount */pcfs* will not work for this installation because the pcfs mount looks for a DOS formatted disk. The installation disk is a UNIX formatted disk and must be mounted and accessed as a UNIX file system.

5) Copy the program files to the installation directory:

unix% *cp /fd/solarflux.a4.tar.Z /solarflux*

6) Untar the program files:

unix% *cd /solarflux*
unix% *tar xvf solarflux.a4.tar.Z*

Configuring SOLARFLUX

1) Edit *solarflux.aml*. One of the first lines of the program (after some beginning comments) is a variable declaration: *&sv sfpath /dorothy/sf_a4*. Change the value of the variable to the installation directory: *&sv sfpath /solarflux*. The following are some useful vi commands that can be used for editing the *solarflux.aml* file:

- **arrow keys** move the cursor.
- **x** deletes the character at the current cursor postion.
- **i** enters insert mode.
- **<ESC>** to exit insert mode.
- **:wq** saves and exits.
- **:q!** exits without saving.

2) Copy the edited *solarflux.aml* to the $ARCHOME/atools/grid directory:

unix% *cp solarflux.aml $ARCHOME/atools/grid*

Compiling Skyview Factor and Hemispherical Viewshed Programs

If you wish to run the SKYVIEW and VIEWSHED modules on a UNIX computer other than a SUN workstation, it will probably be necessary to compile the program before it can be run. "C" source code files and compilation instructions are included in the anonymous FTP directory or on the UNIX installation disk. Some compiler-specific changes in the source code may be necessary before the code can be compiled.

APPENDIX B: COMMUNICATION CONCERNING BUGS, PROBLEMS, SUGGESTIONS, AND APPLICATIONS

Please send communications concerning bugs encountered, problems, suggestions for improving SOLARFLUX, descriptions of applications, or other relevant matters to the SOLARFLUX internet e-mail address (sflux@glinda.kbs.ukans.edu).

FIGURE LEGENDS

Figure 1. Incoming solar radiation (insolation) at a location on a topographic surface consists of three components: 1) direct radiation, originating from the direction of the sun; 2) diffuse radiation, originating from any sky direction as the result of scattering by atmospheric gases and particles; and 3) reflected radiation from nearby terrain. Calculations of insolation must account for atmospheric attenuation, angle of incidence of all radiation components, and sky obstruction by surrounding topographic features.

Figure 2. At the regional landscape scale, studies of relations of biophysical determinants of habitat and biodiversity for the Spring Mountains involve A) constructing GIS coverages for topography and butterfly biodiversity sampling sites; B) use of the USGS 1:250,000 digital elevation model (DEM) for input to SOLARFLUX; and calculation of daily direct insolation for C) the summer solstice, D) the equinox, and E) the winter solstice.

Figure 3. At a more localized landscape scale, construction of microclimate habitat models for the University of California Big Creek Reserve start with A) topography from USGS 1:24,000 quad sheets; next a triangulated irregular network (TIN) model is used to produce B) an elevation grid for input to SOLARFLUX; then SOLARFLUX is used to calculate C) skyview factor; finally SOLARFLUX is used to calculate daily direct insolation for D) the summer solstice, E) the equinox, and F) the winter solstice. There is strong correspondence between topography, solar radiation, and G) the distribution of vegetation at Big Creek.

Figure 4. Hemispherical viewsheds, calculated for locations corresponding to the A) low, B) mid, and C) high elevation weather stations at Big Creek, show sky directions that are obscured by surrounding topographic features.

Figure 5. An index of topographic shadowing for Big Creek Reserve can be constructed by calculating daily direct insolation with shadow effects taken into account (see Figure 3) and daily direct insolation without shadow effects taken into account for A) the summer solstice, B) the equinox, and C) the winter solstice. The index, calculated as one minus the ratio of radiation values with topographic shadows and the values without topographic shadows, serves to show the proportional decrease in direct radiation due to shadows for D) the summer solstice, E) the equinox, and F) the winter solstice. Note that a topographic index value of 0 indicates no shadow effect and a value of 1 indicates a 100% reduction in direct insolation due to shadows. Gray areas signify undefined topographic indices, resulting for locations always in the shadow of their own slope.

Figure 6. At the stand scale, studies of influences of canopy surface topography in pinyon-juniper woodlands at Los Alamos National Environmental Research Park involve A) mapping all tree and shrub locations; B) construction of a canopy digital elevation model (CDEM) based on the height and crown radius of each tree and shrub, with the assumption that a hemiellipse approximates the outer envelope of the canopy surface; use of SOLARFLUX to calculate C) skyview factor; and use of SOLARFLUX to calculate of daily direct insolation for D) the summer solstice, E) the equinox, and F) the winter solstice.

Figure 7. At the local scale, daily direct insolation was calculated using SOLARFLUX for A) the summer solstice, and B) the winter solstice for a series of demonstration plots, being used to evaluate the influences of slope on water balance in waste sites. All plots are oriented toward a southeasterly aspect and slope varies from 0% to 25%.

Figure 8. SOLARFLUX calculations of spatial and temporal insolation variation for a series of simulated forest canopy gaps. A) Skyview factors are distributed in a radially symmetrical pattern. B) Instantaneous direct insolation depends upon time of day and time of year. Effects of latitude on spatial and temporal unsolation variation are shown in terms of C) daily direct radiation, and D) hours of direct radiation. Similarly, effects of relative gap size are shown by increasing canopy height, while holding gap size constant, in terms of E) daily direct radiation, and F) hours of direct radiation.

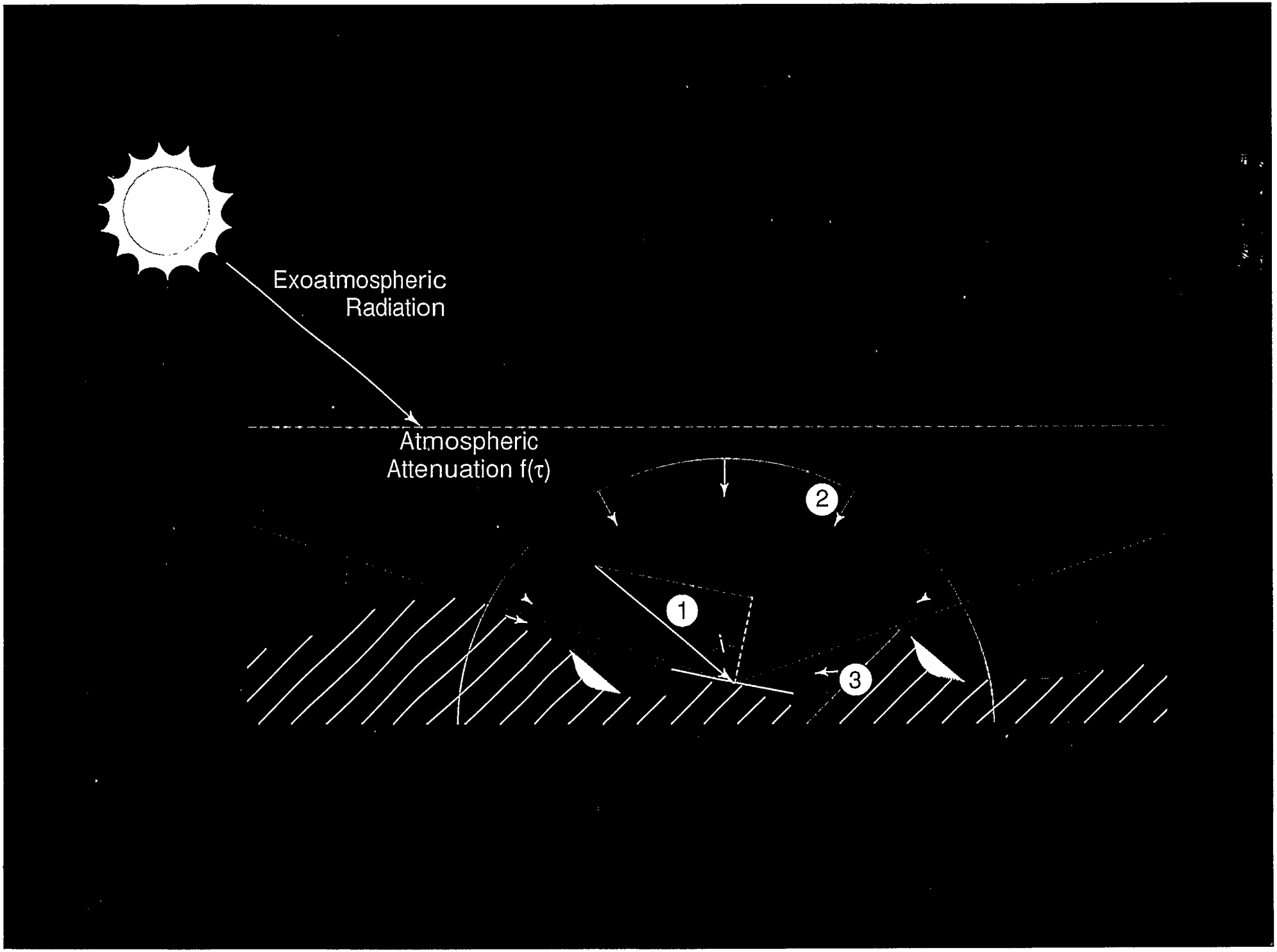
Exoatmospheric
Radiation
Atmospheric
Attenuation f(τ)
1
2
3

Fig. 2.

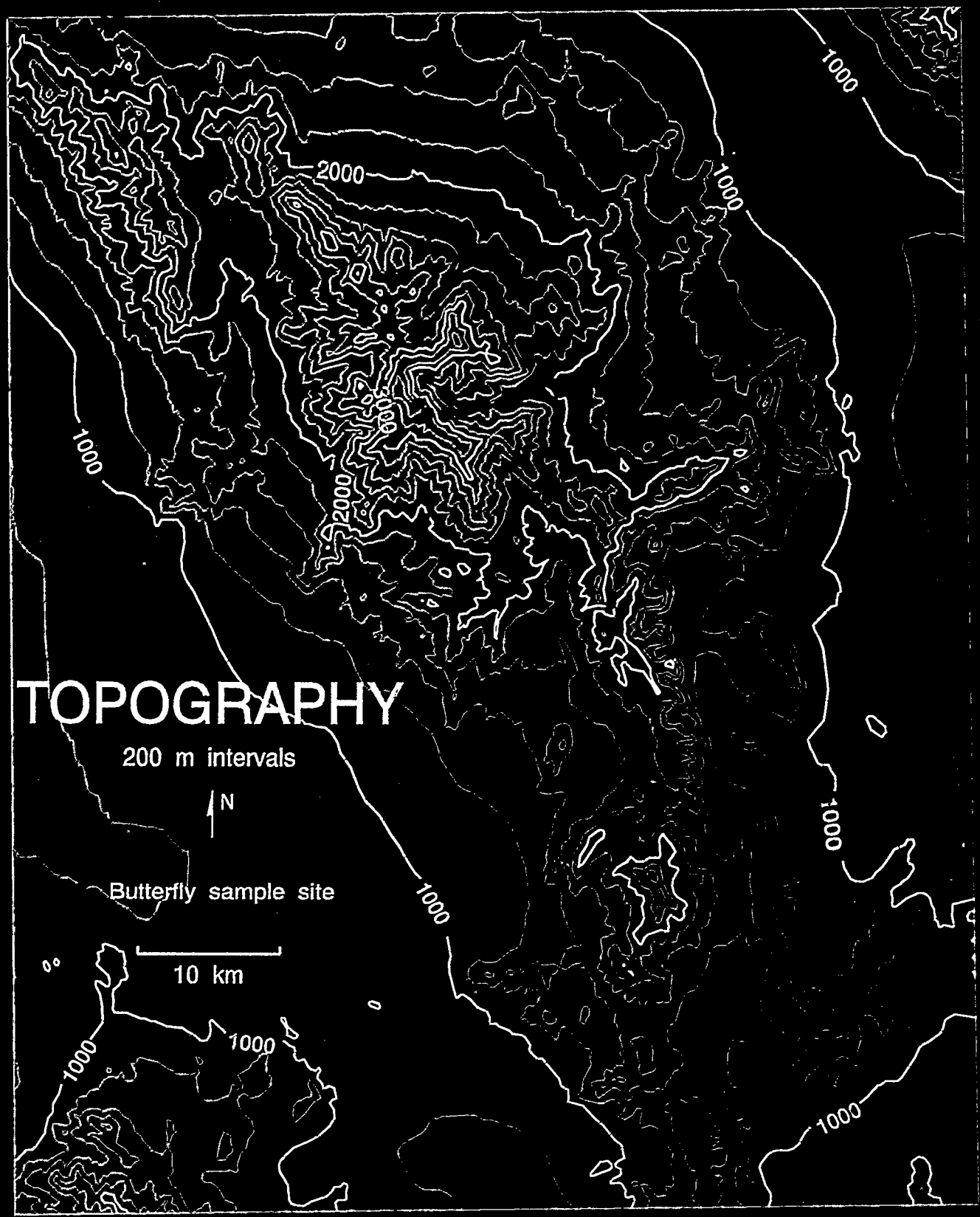
TOPOGRAPHY
200 m intervals
N
Butterfly sample site
10 km
2000
1000
1000
2000
1000
1000
1000
1000
1000

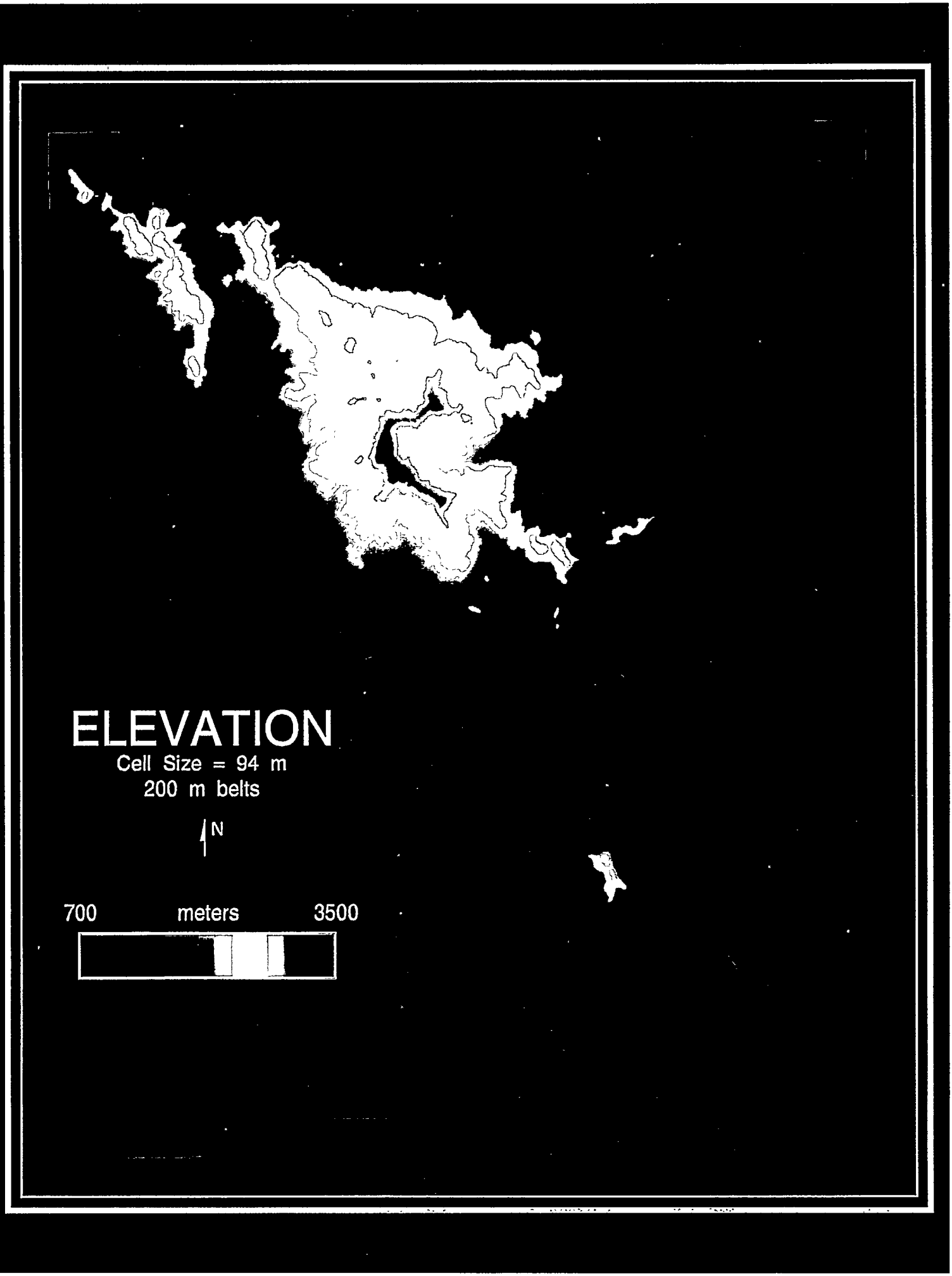
ELEVATION
Cell Size = 94 m
200 m belts
N
700
meters
3500

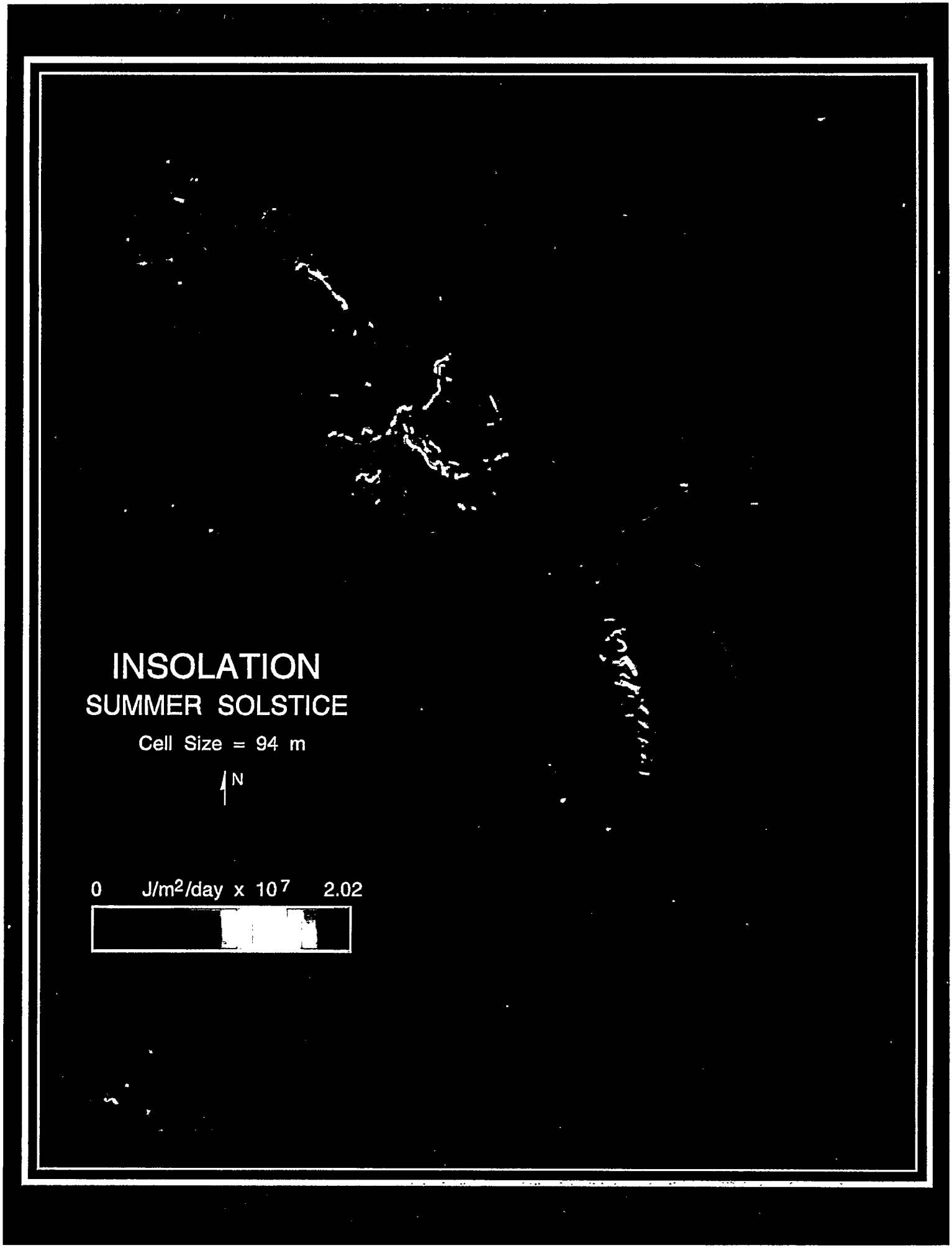
INSOLATION
SUMMER SOLSTICE
Cell Size = 94 m
N
0
J/m2/day x 107
2.02

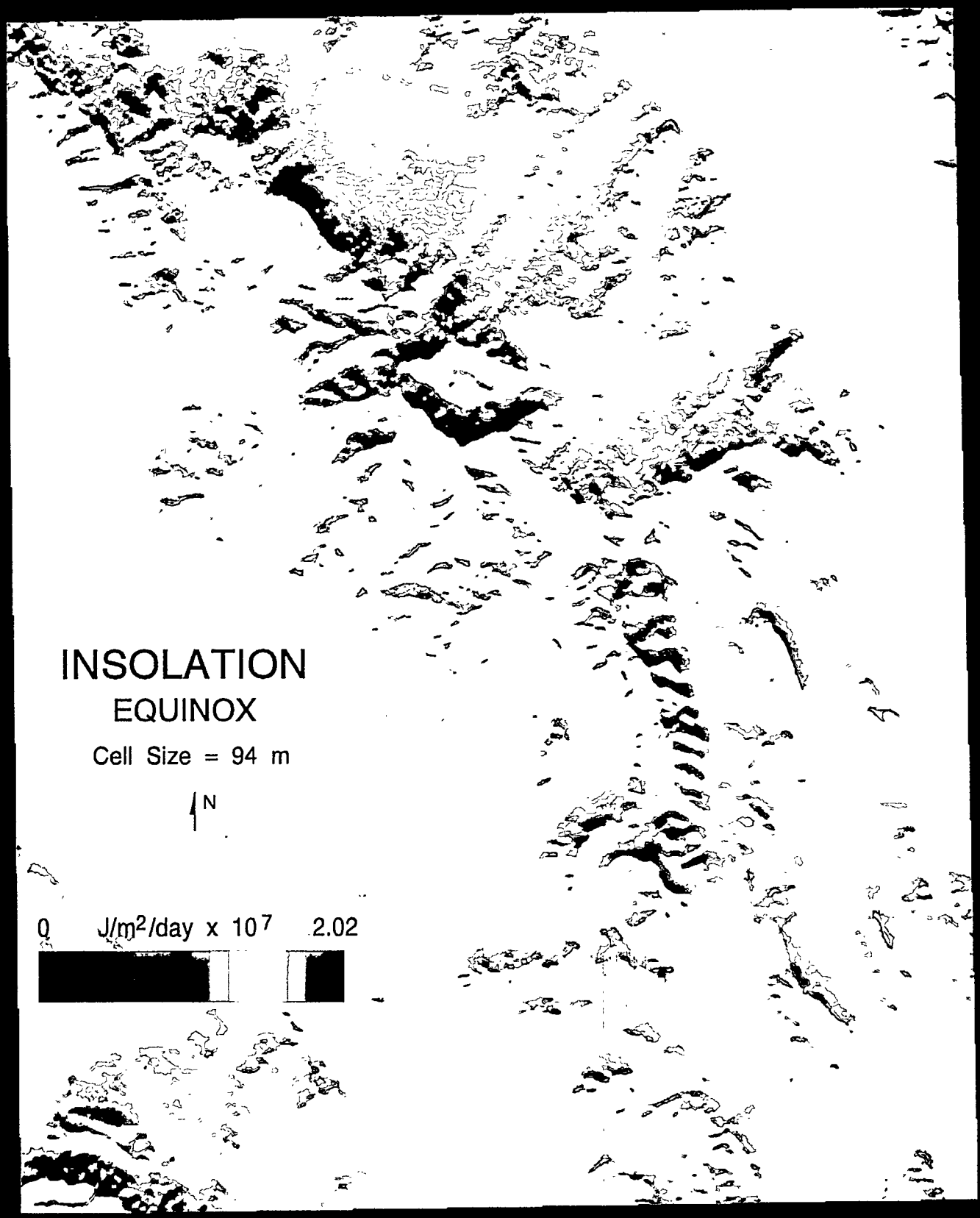
INSOLATION
EQUINOX
Cell Size = 94 m
N
0
J/m2/day x 10 7
2.02

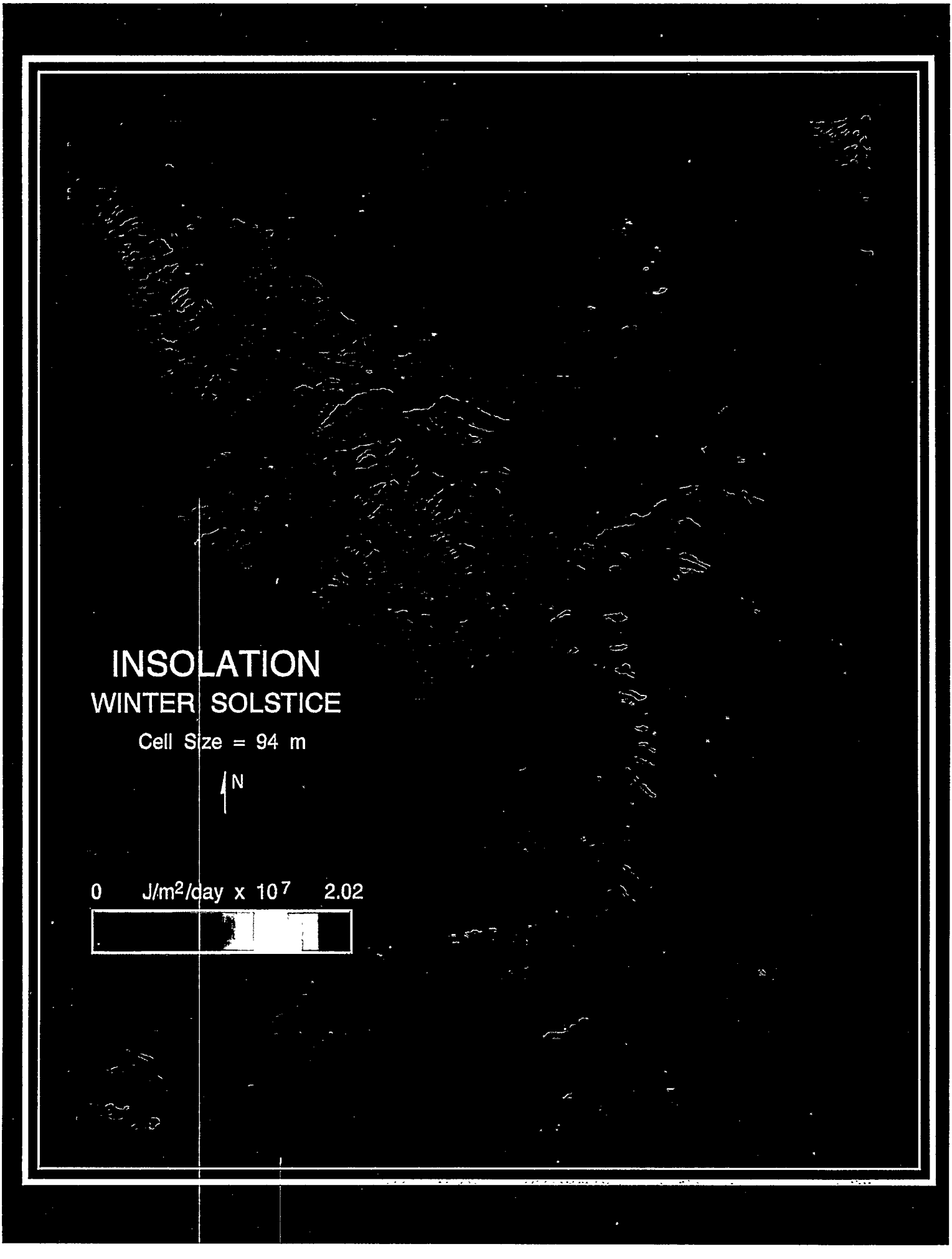
INSOLATION
WINTER SOLSTICE
Cell Size = 94 m
N
0
J/m2/day x 10 7
2.02

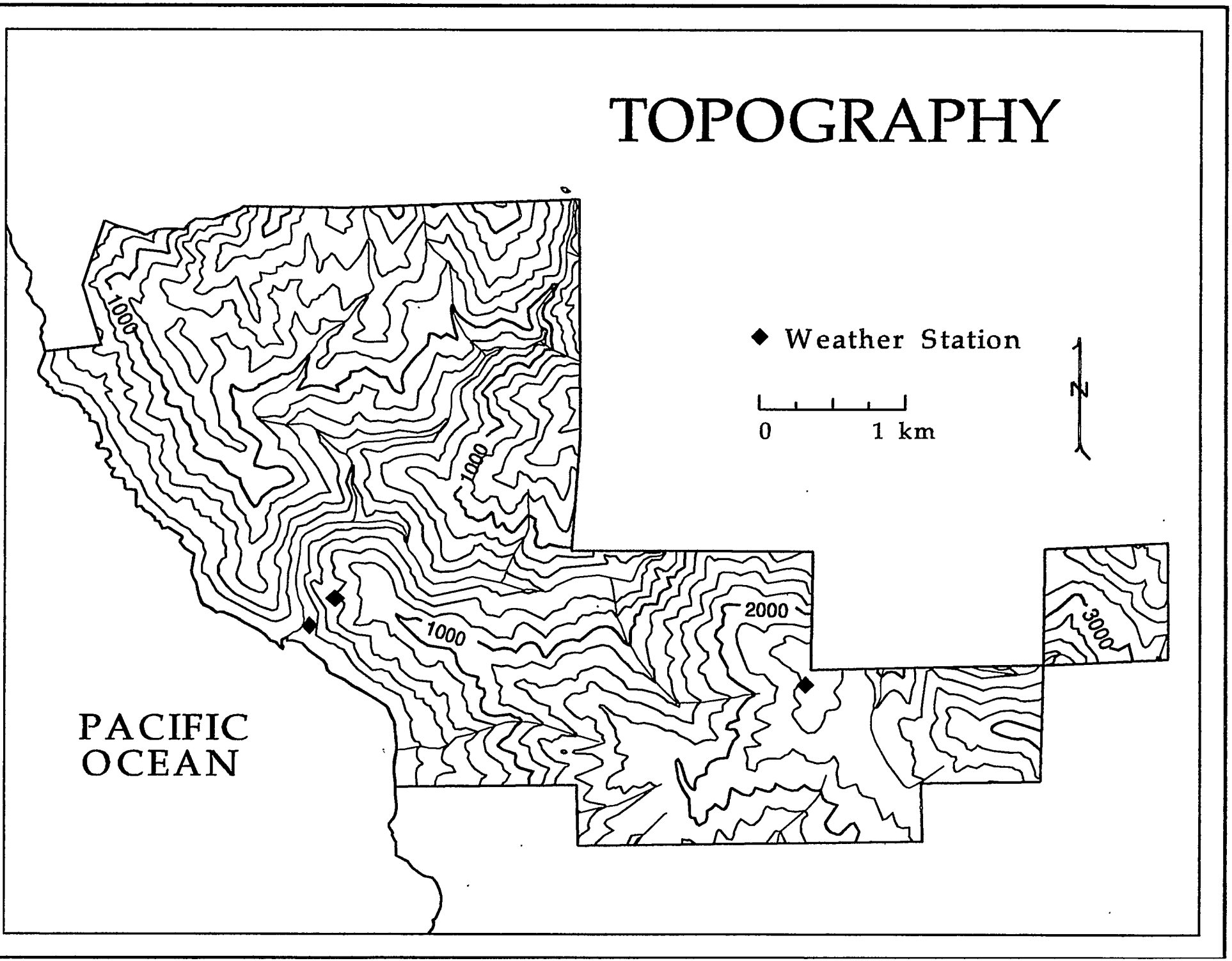
TOPOGRAPHY
Weather Station
0
1 km
N
1000
1000
1000
2000
3000
PACIFIC
OCEAN

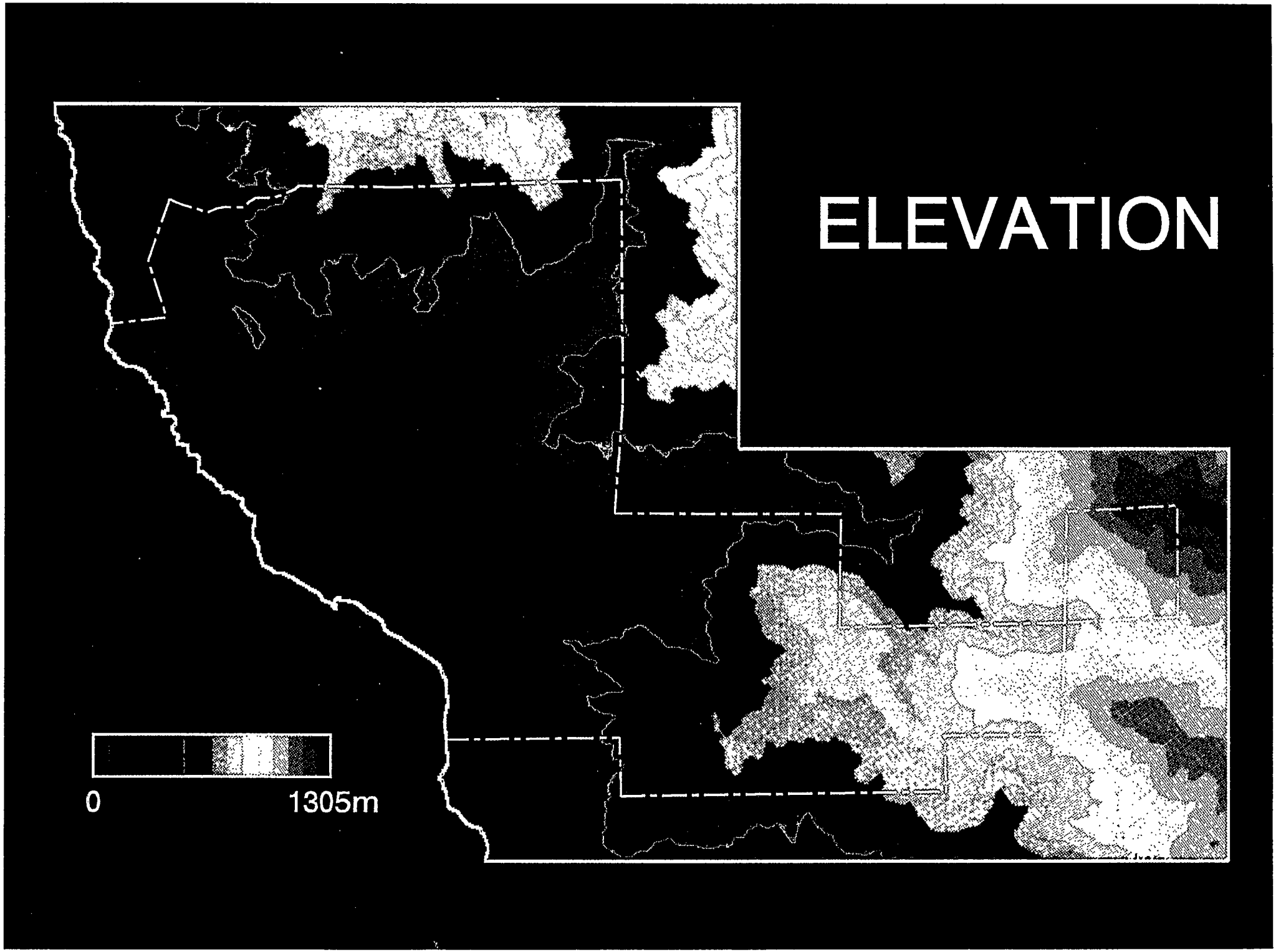
ELEVATION
0
1305m

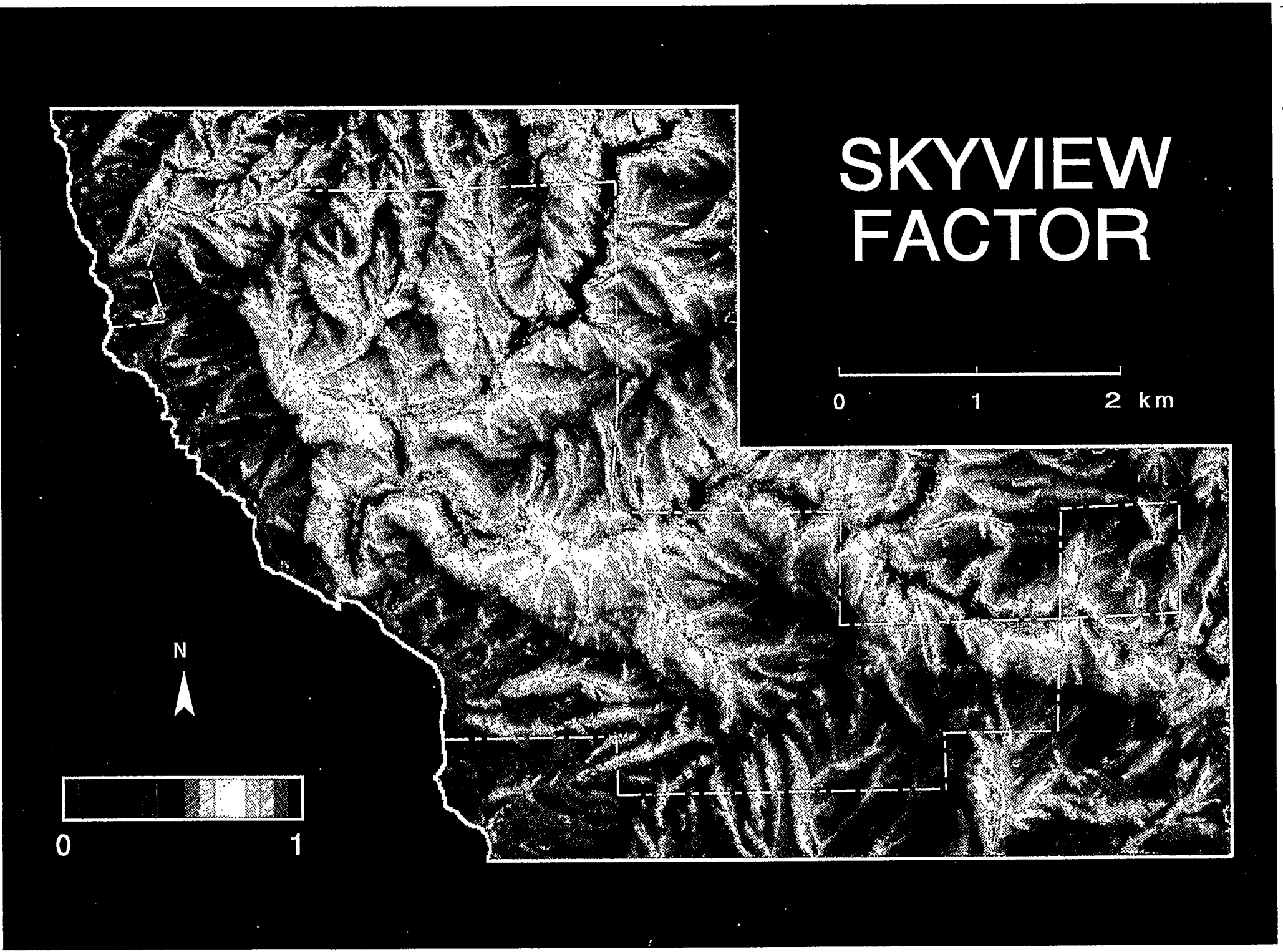
SKYVIEW
FACTOR
0
1
2 km
N
0
1

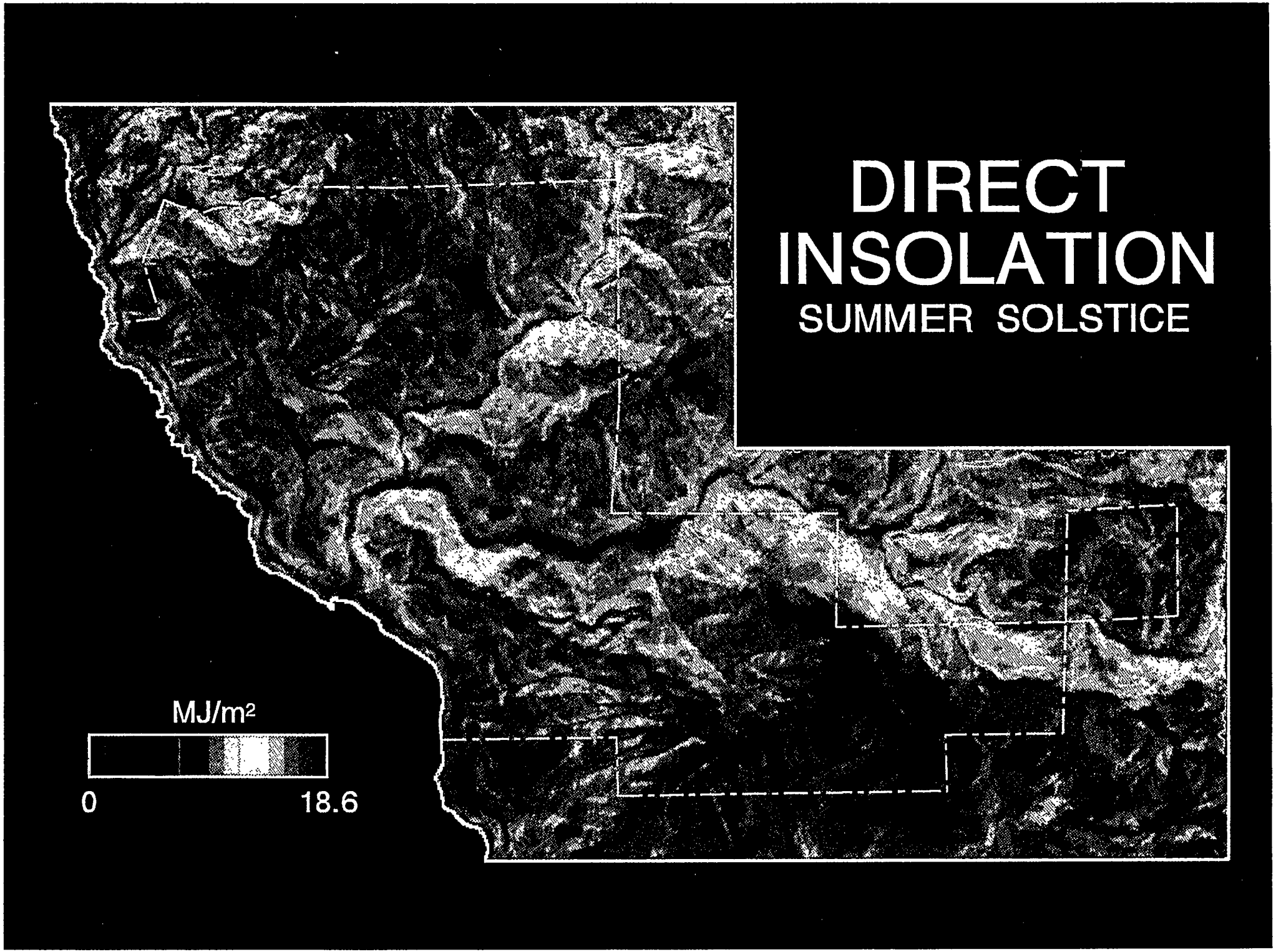
DIRECT
INSOLATION
SUMMER SOLSTICE
MJ/m2
0
18.6

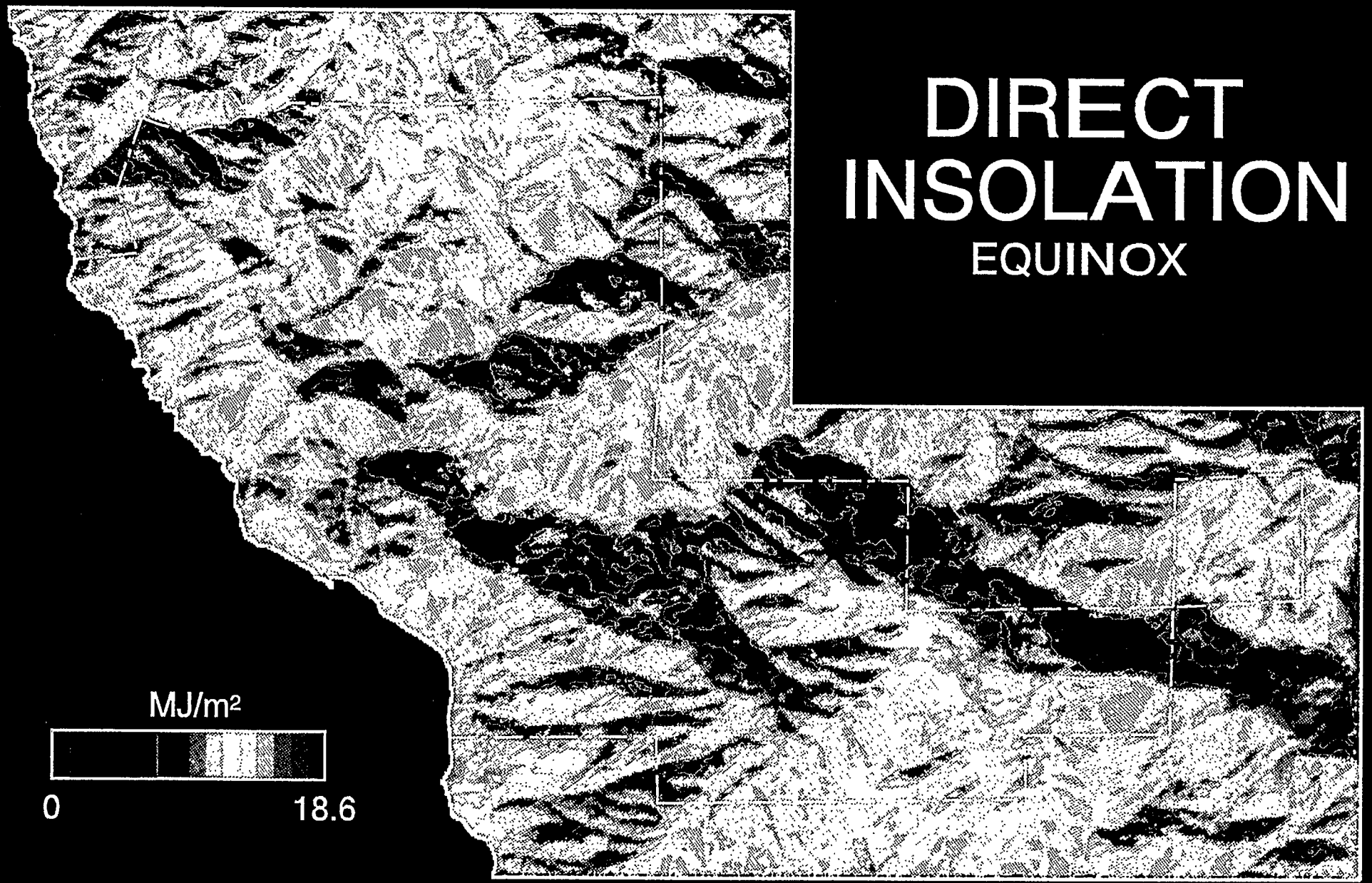
DIRECT
INSOLATION
EQUINOX
MJ/m2
0
18.6

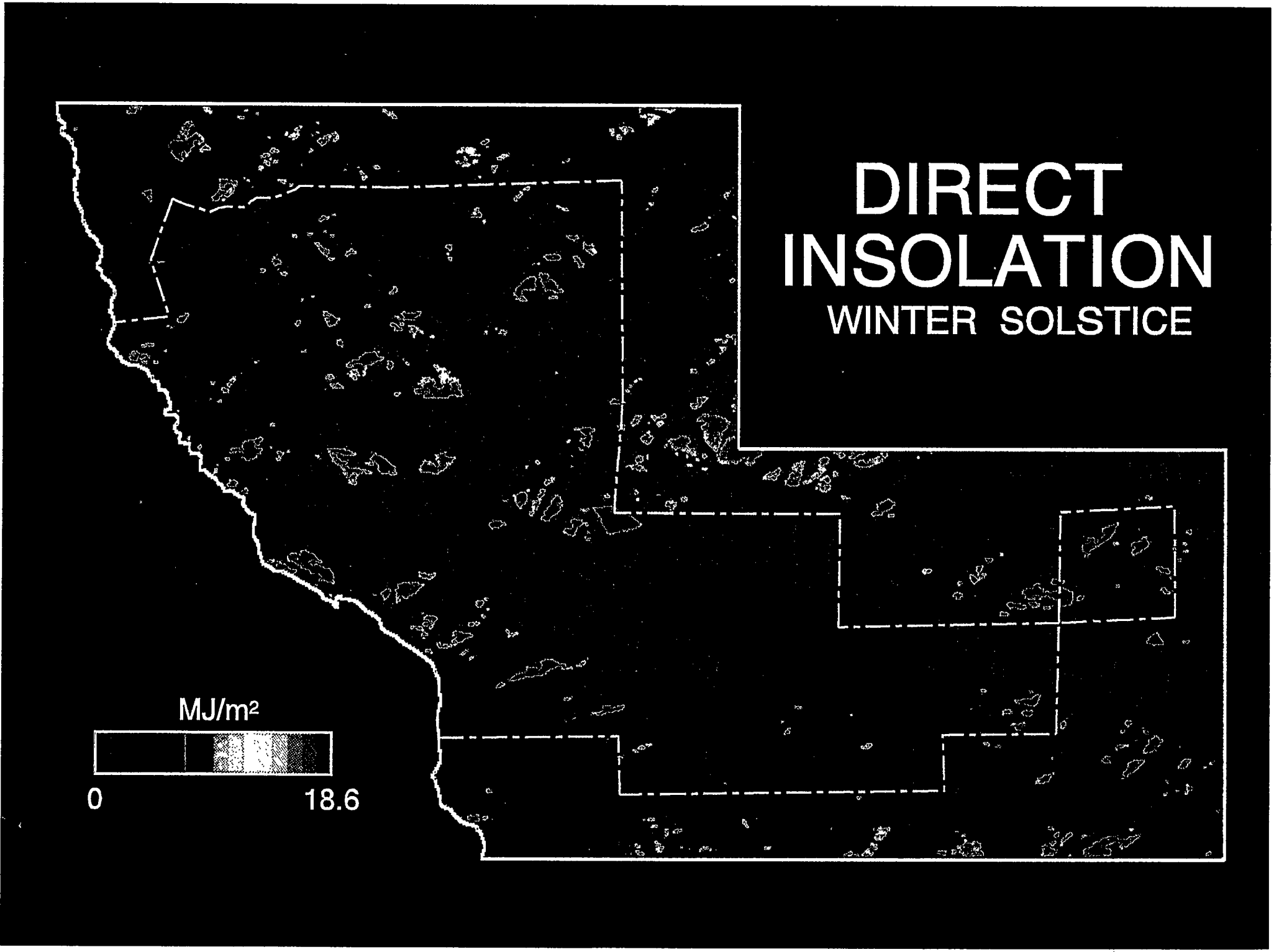
DIRECT
INSOLATION
WINTER SOLSTICE
MJ/m2
0
18.6

FIGURE 3G

VEGETATION

FIGURE 4A

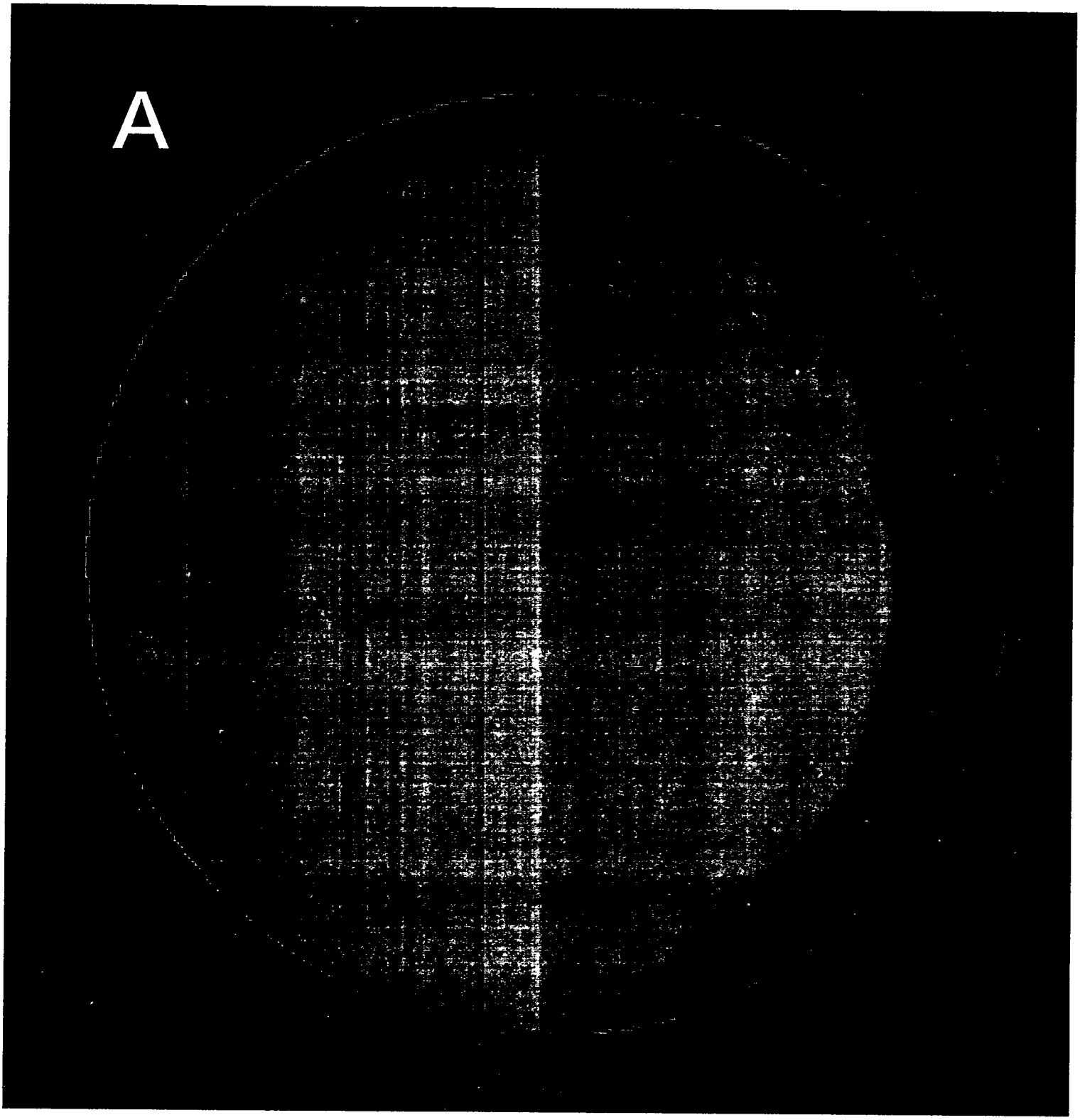

FIGURE 4E

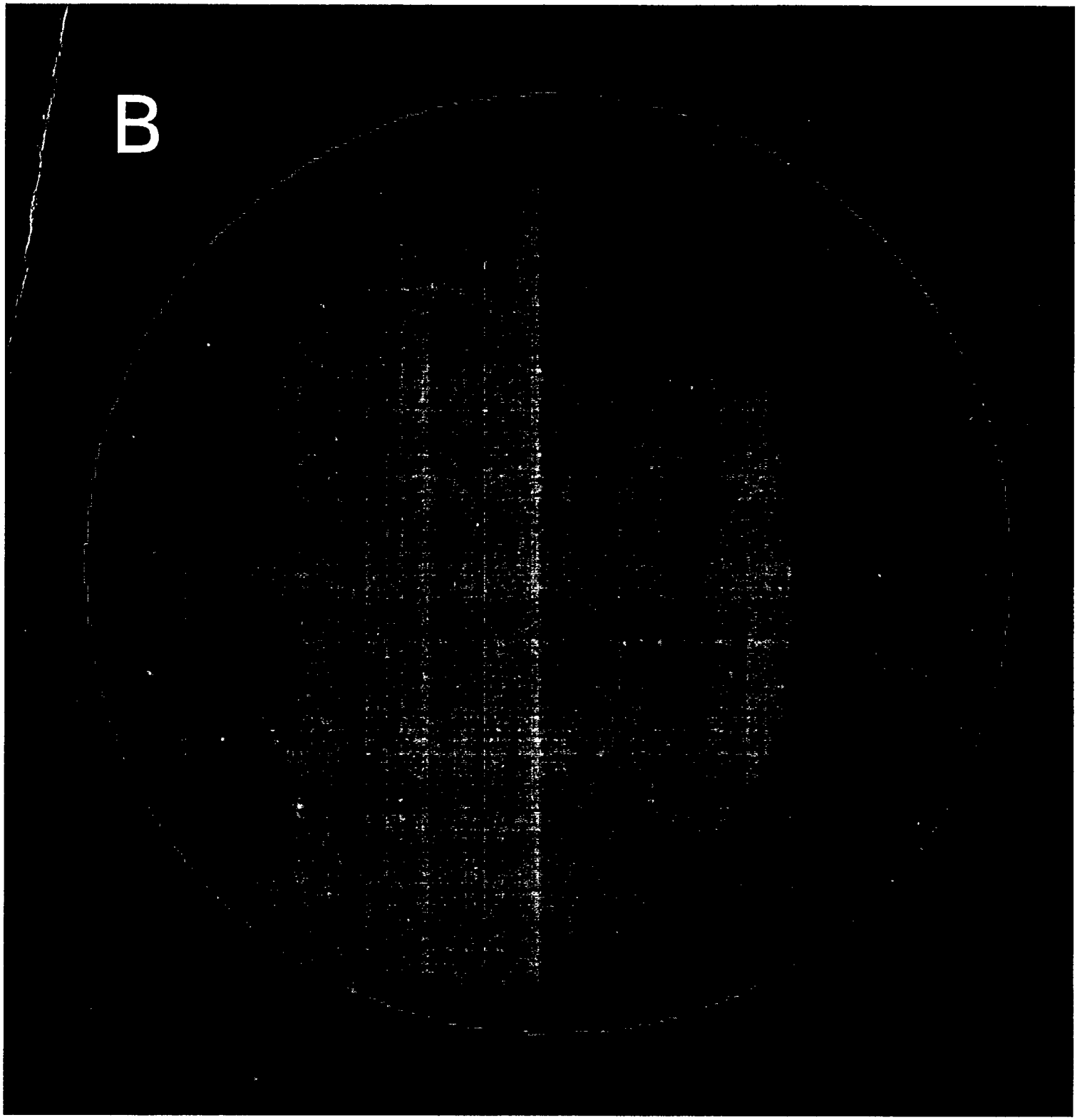

FIGURE 4C

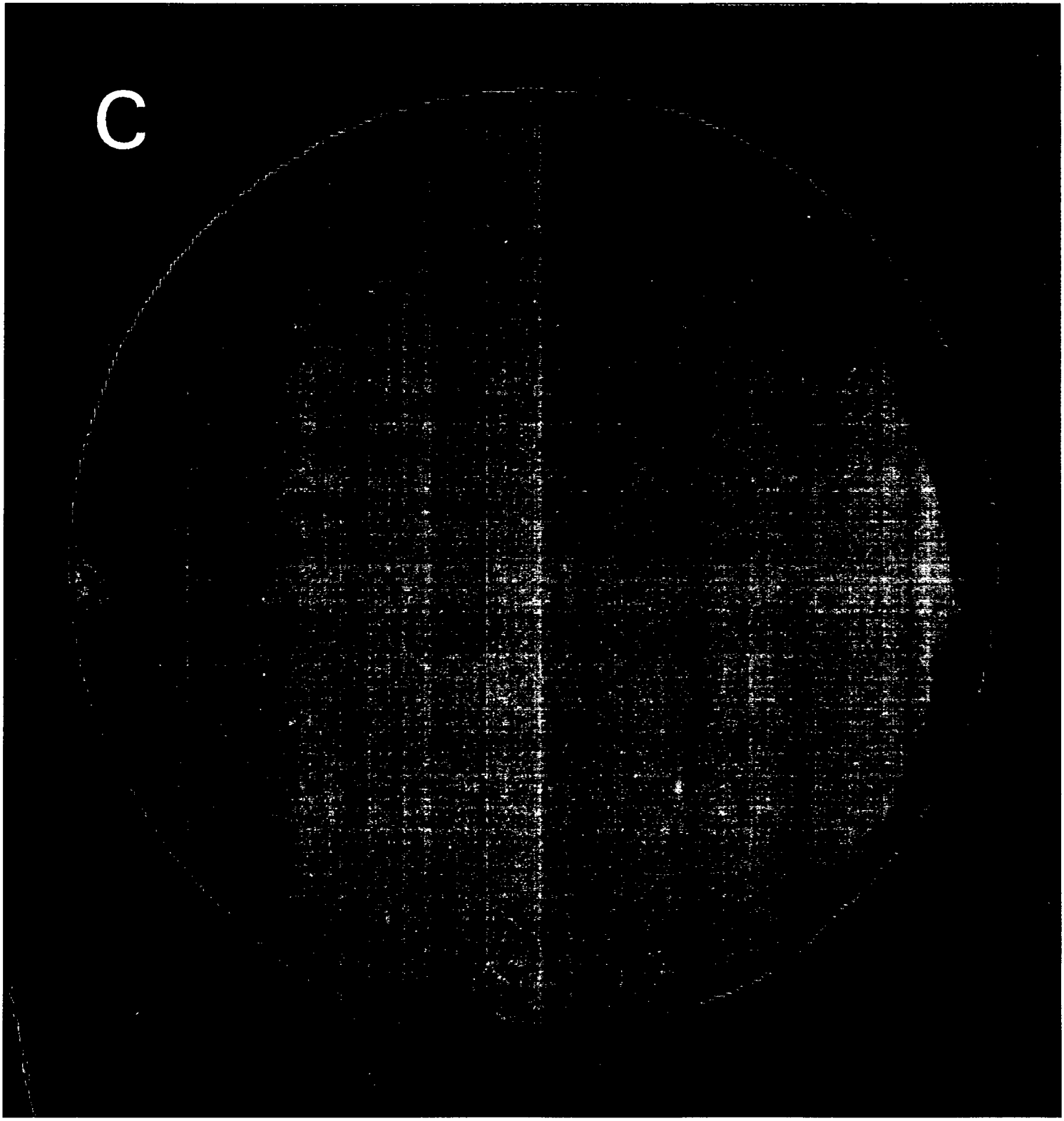


DIRECT
INSOLATION
WITHOUT SHADOWING
SUMMER SOLSTICE
0
1
2 km
N
0
19 MJ/m2

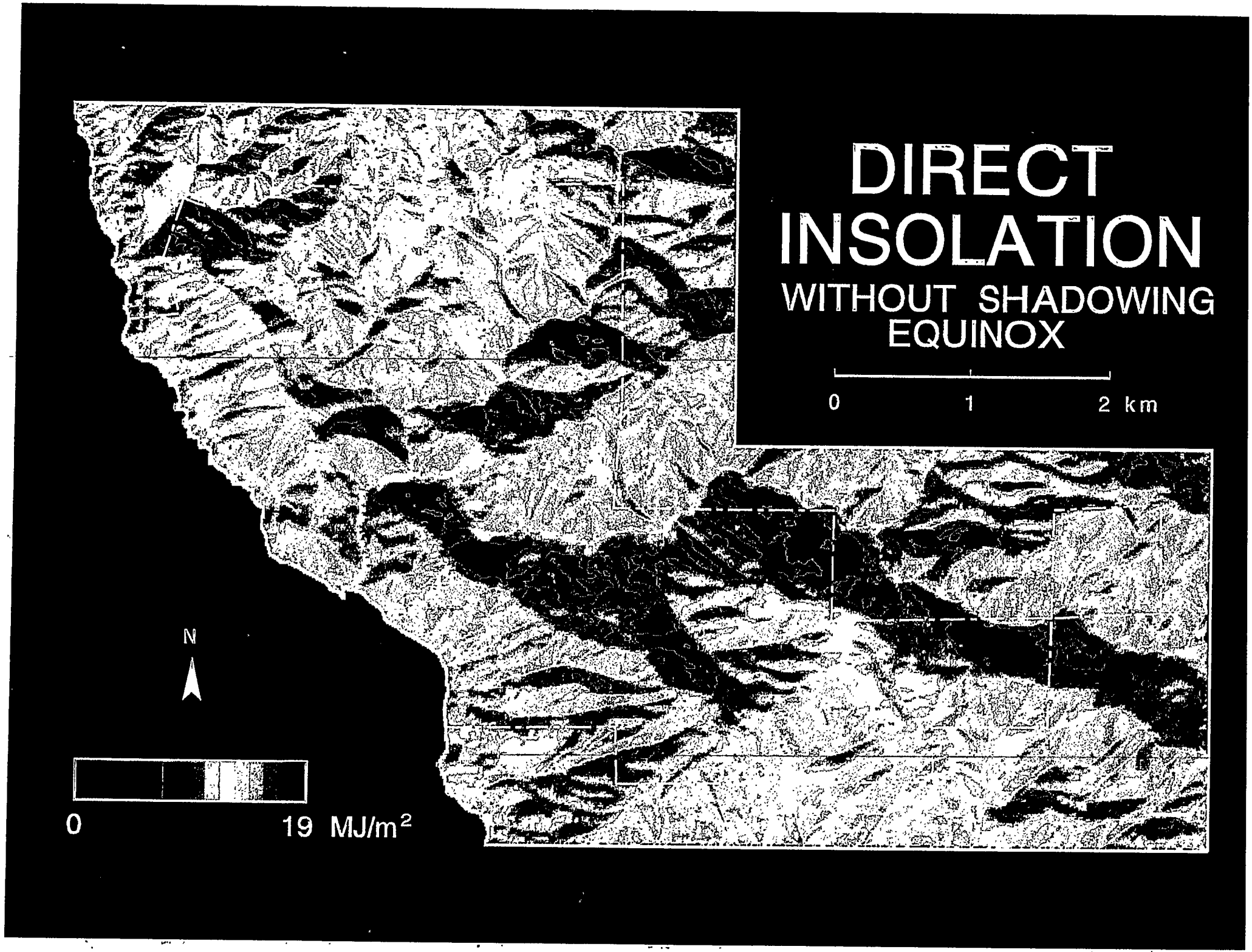
DIRECT
INSOLATION
WITHOUT SHADOWING
EQUINOX
0
1
2 km
N
0
19 MJ/m2

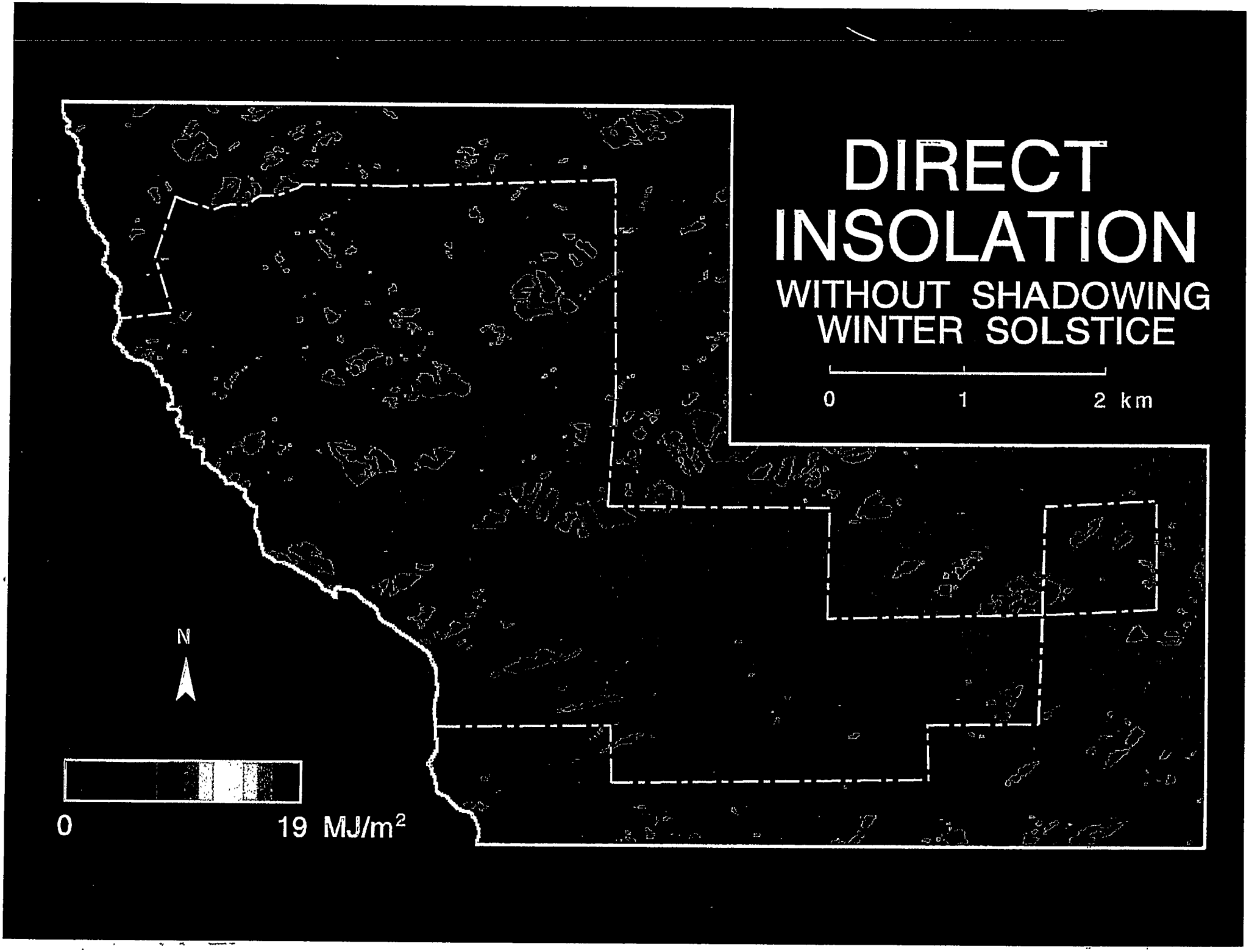
DIRECT
INSOLATION
WITHOUT SHADOWING
WINTER SOLSTICE
0
1
2 km
N
0
19 MJ/m²

FIGURE 5C

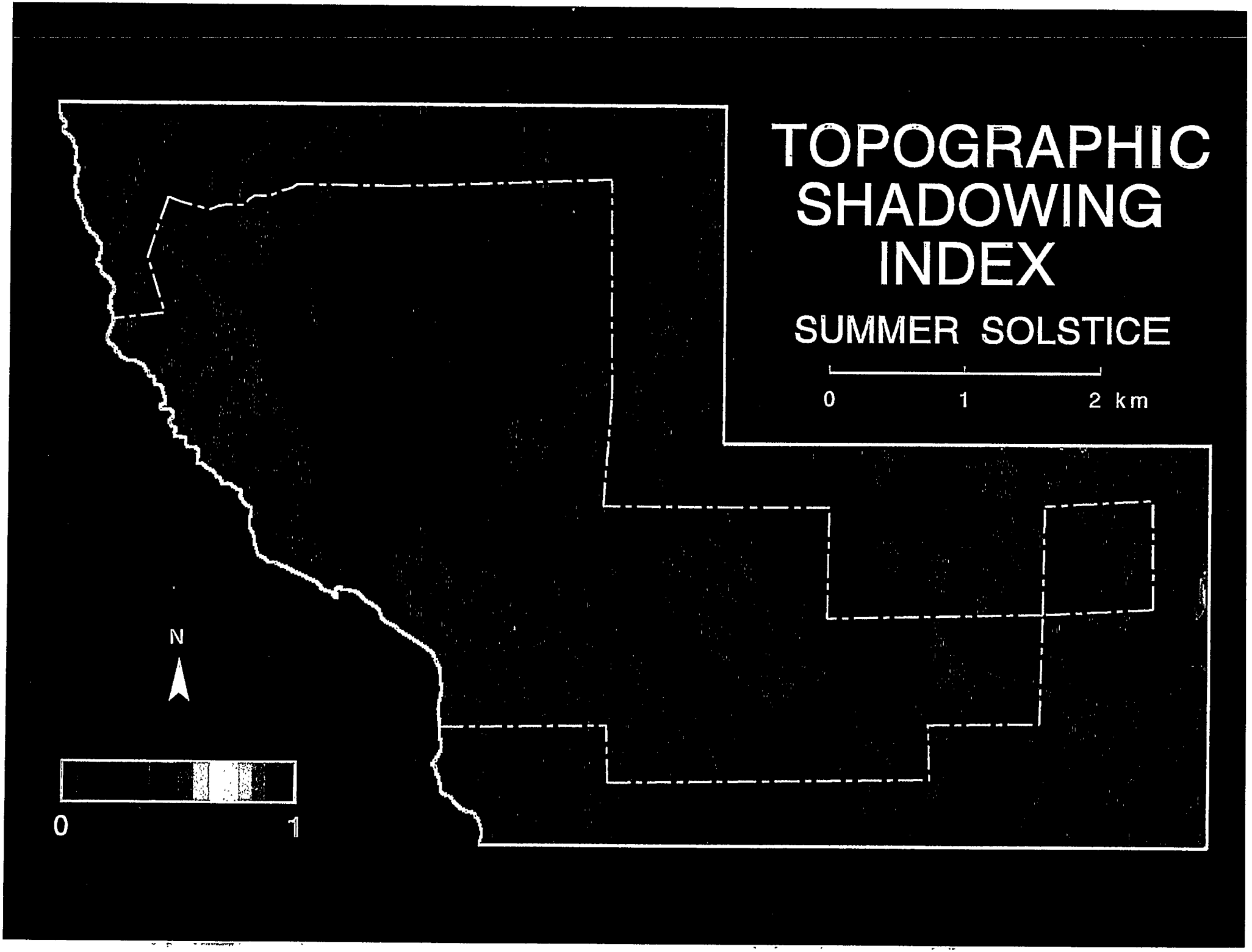
TOPOGRAPHIC
SHADOWING
INDEX
SUMMER SOLSTICE
0
1
2 km
N
0
1

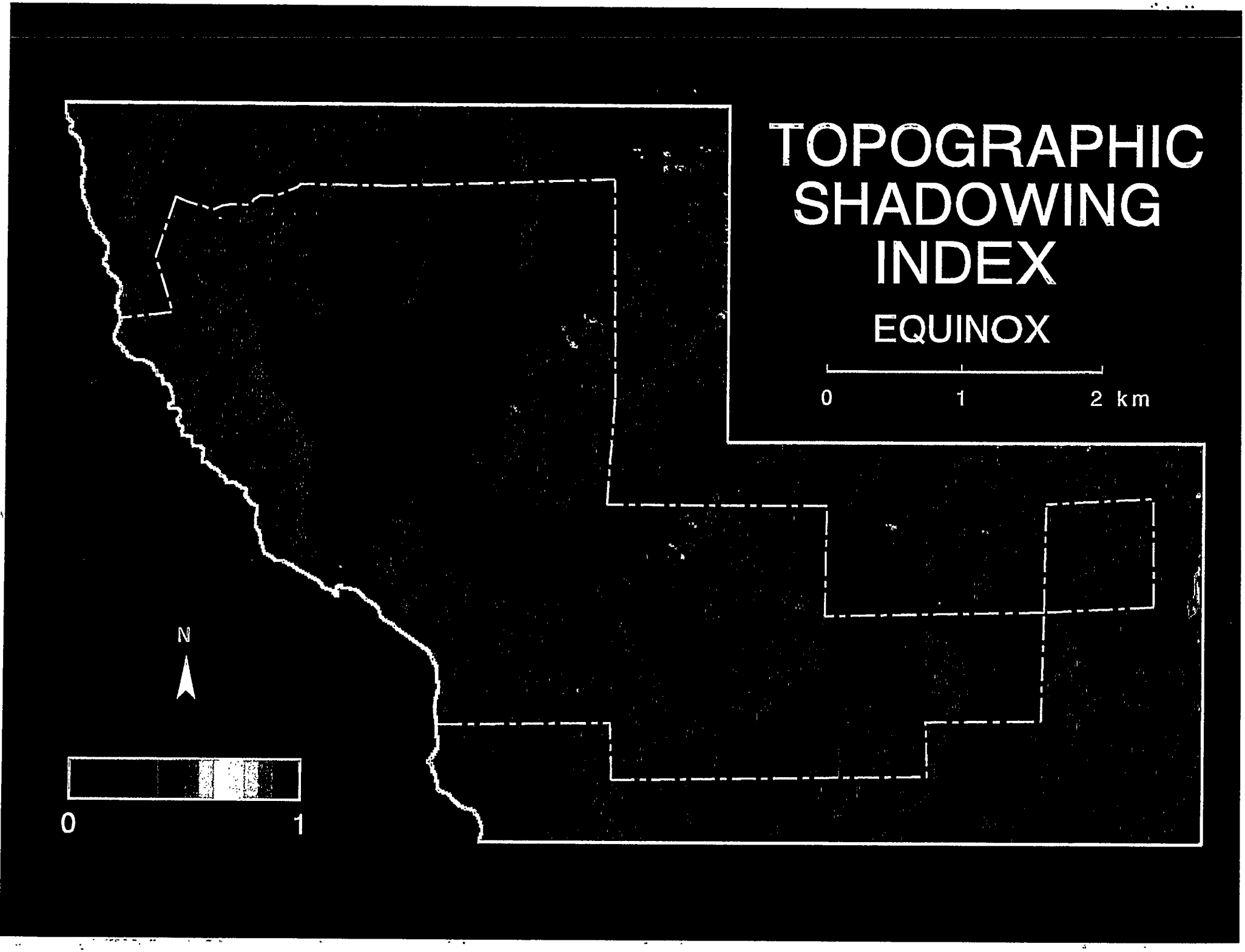
TOPOGRAPHIC
SHADOWING
INDEX
EQUINOX
0
1
2 km
N
0
1

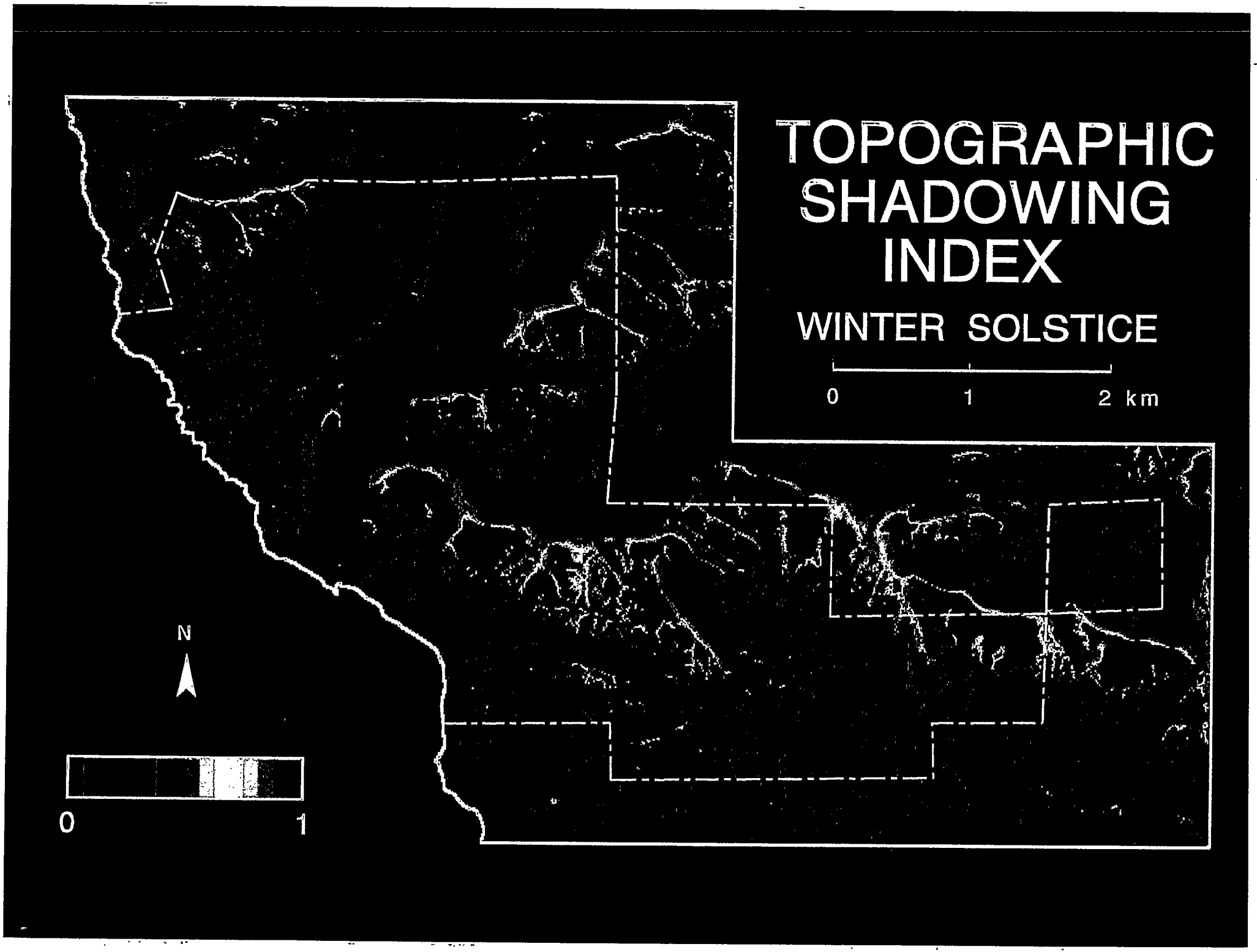
TOPOGRAPHIC SHADOWING INDEX
WINTER SOLSTICE
0
1
2 km
N
0
1

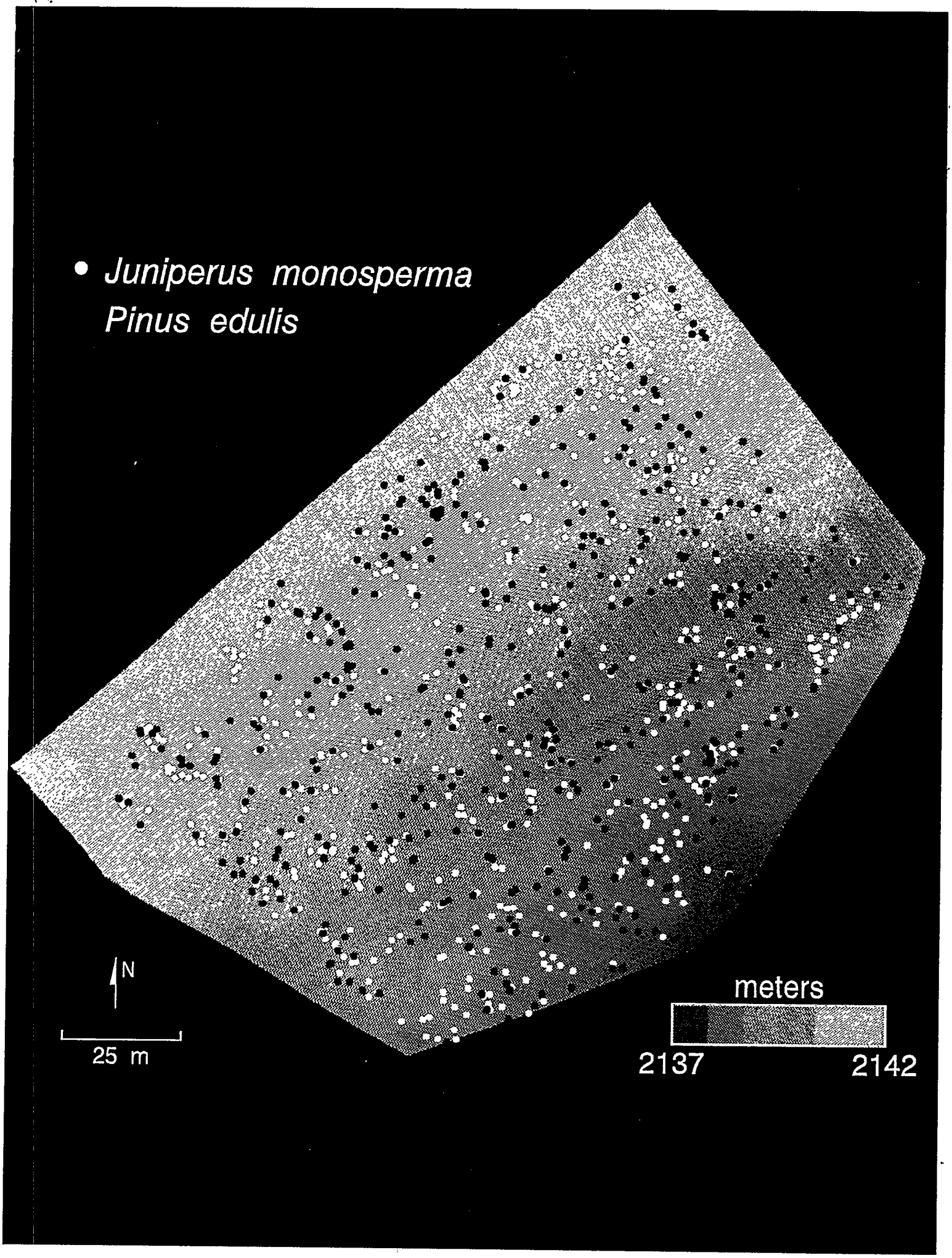
• Juniperus monosperma
Pinus edulis
N
25 m
meters
2137
2142

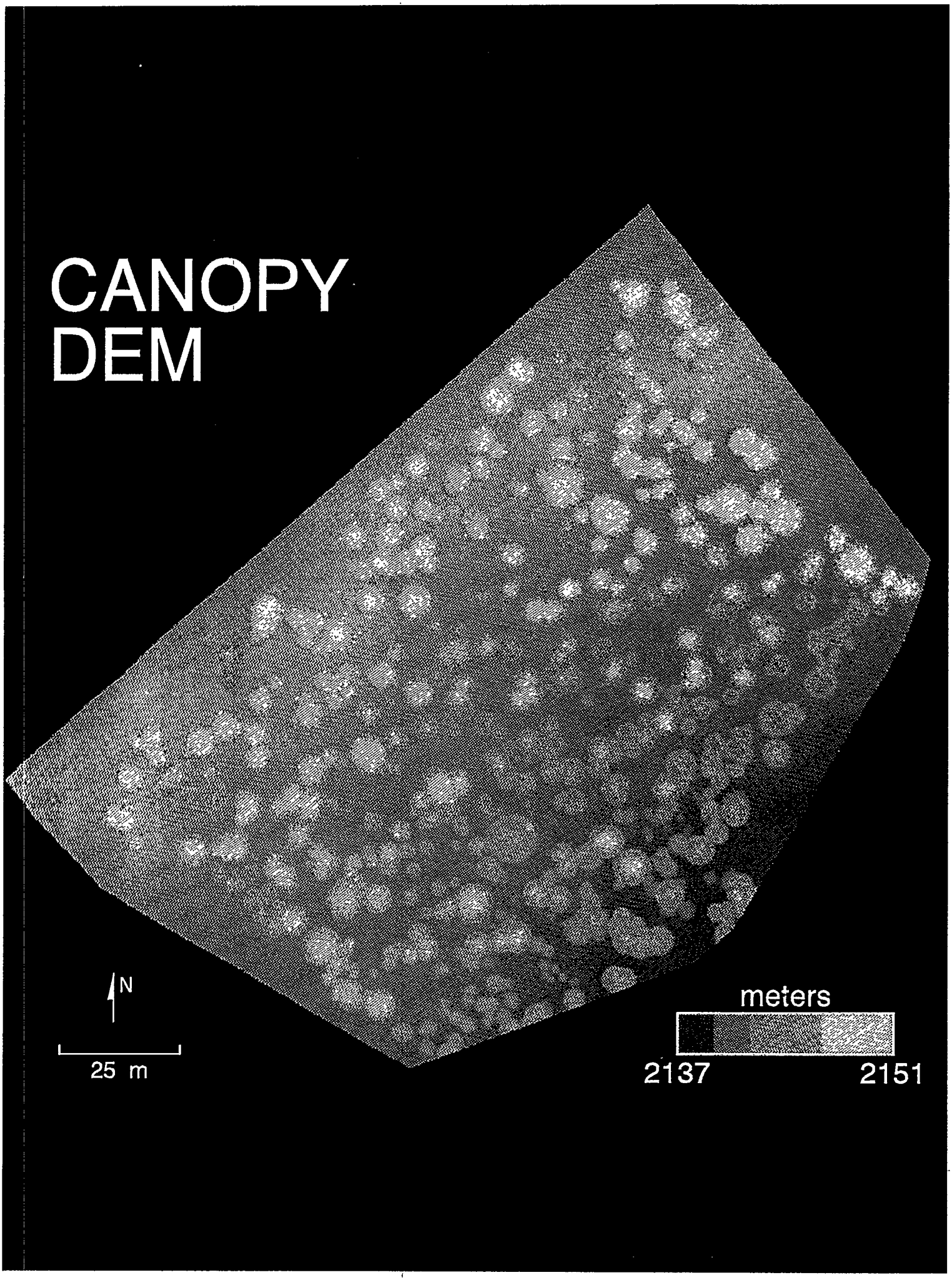
CANOPY
DEM
N
25 m
meters
2137
2151

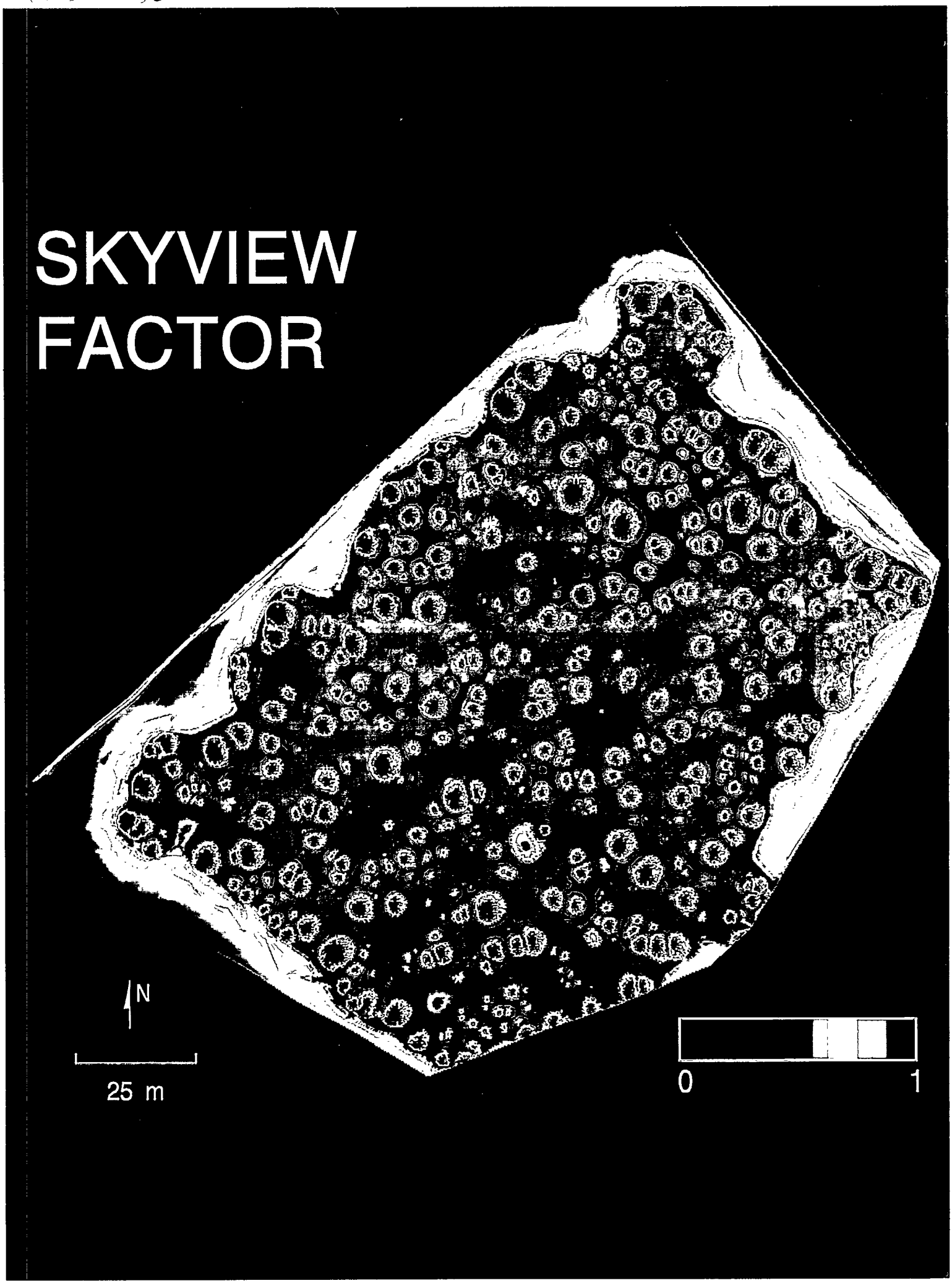
SKYVIEW
FACTOR
N
25 m
0
1

FIGURE 6D

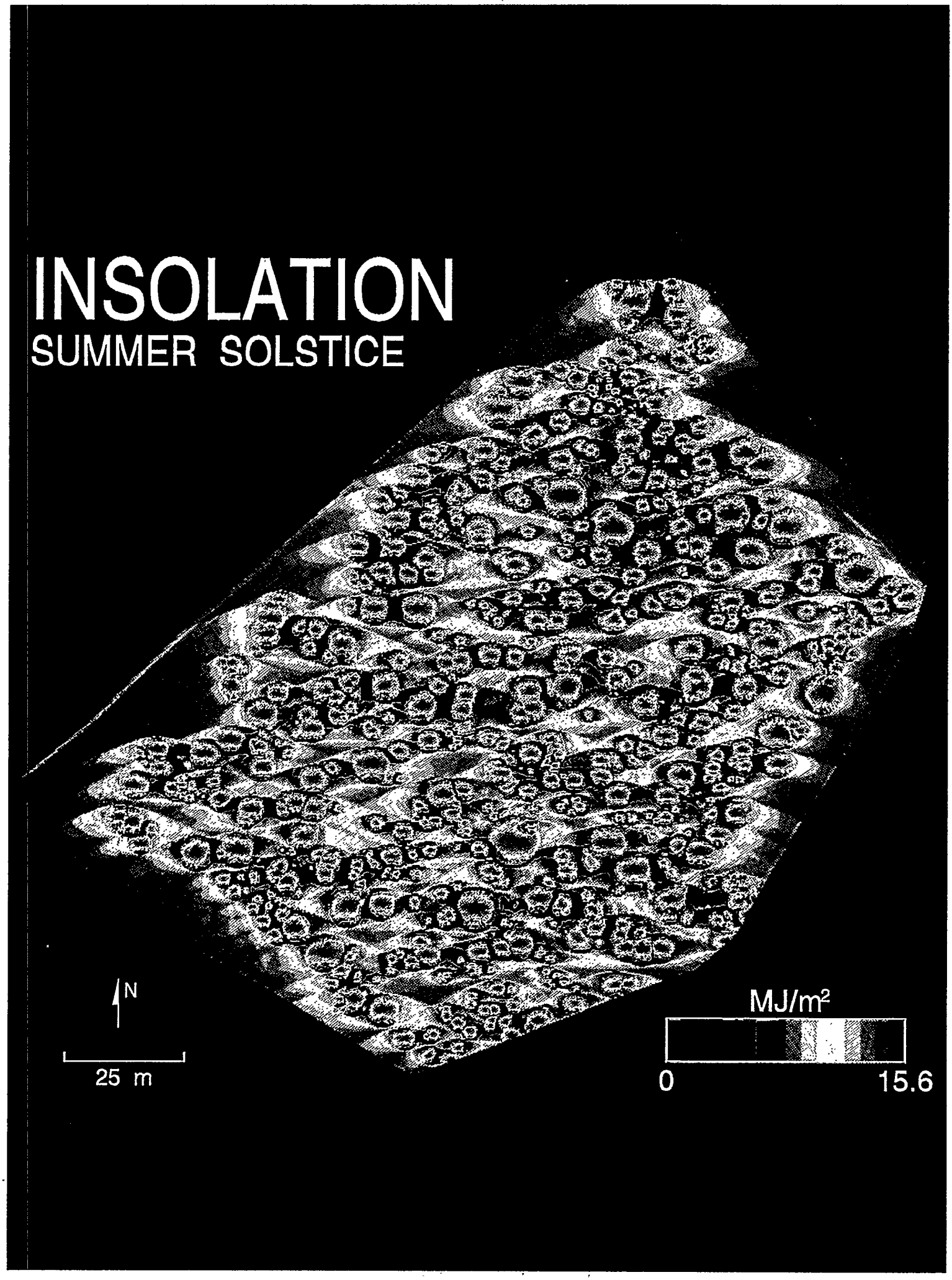

FIGURE 6E

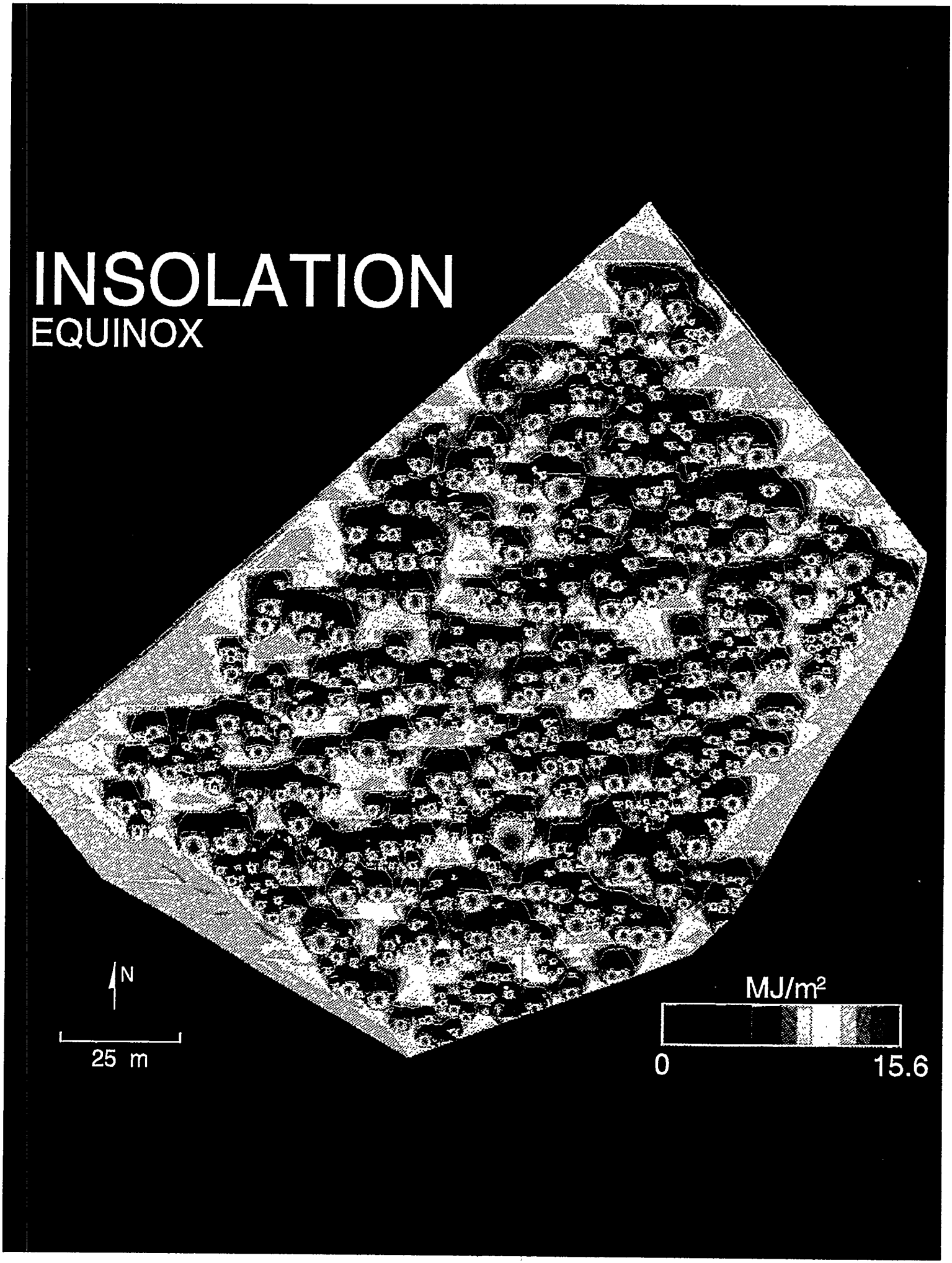

FIGURE 6F

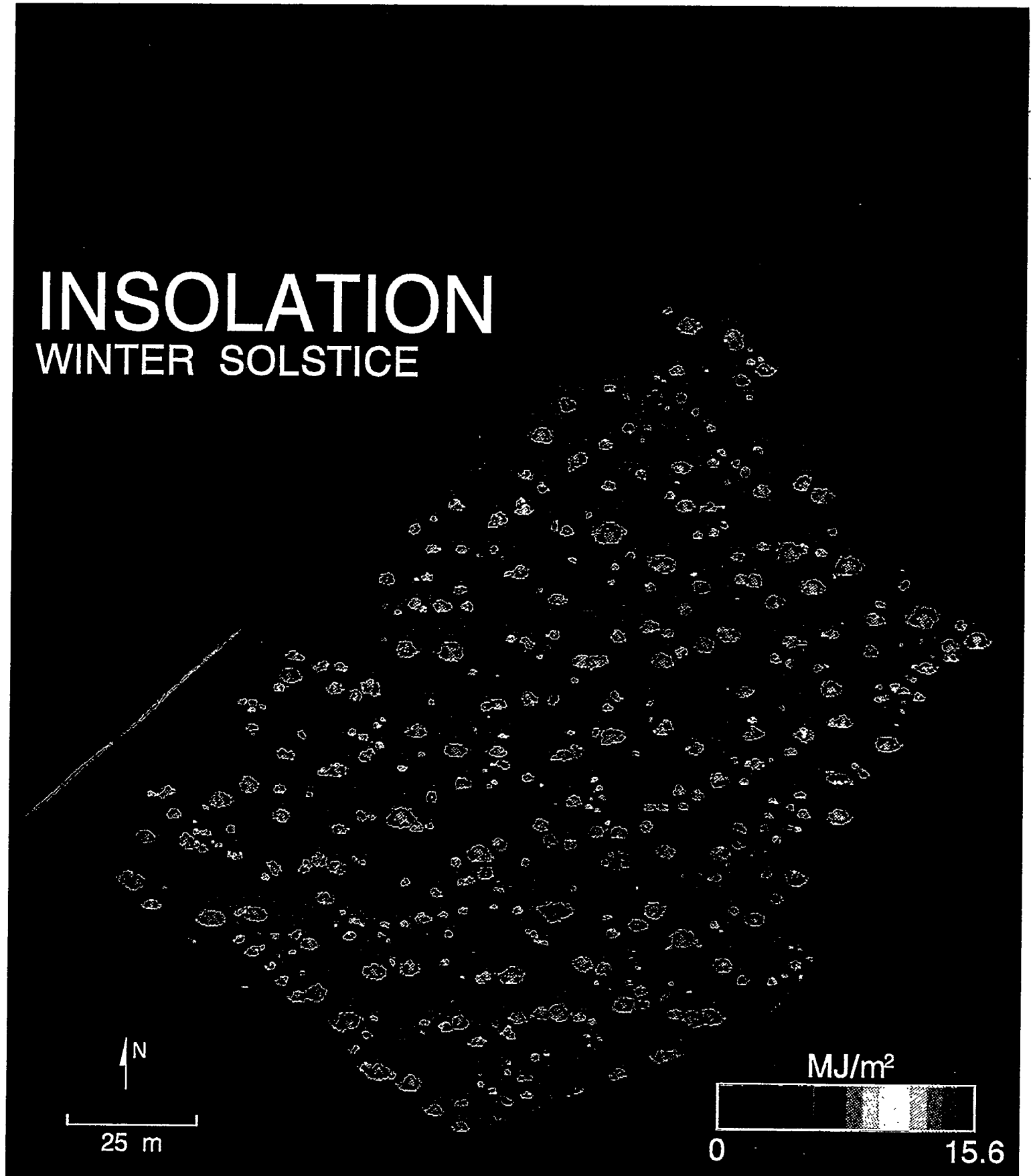

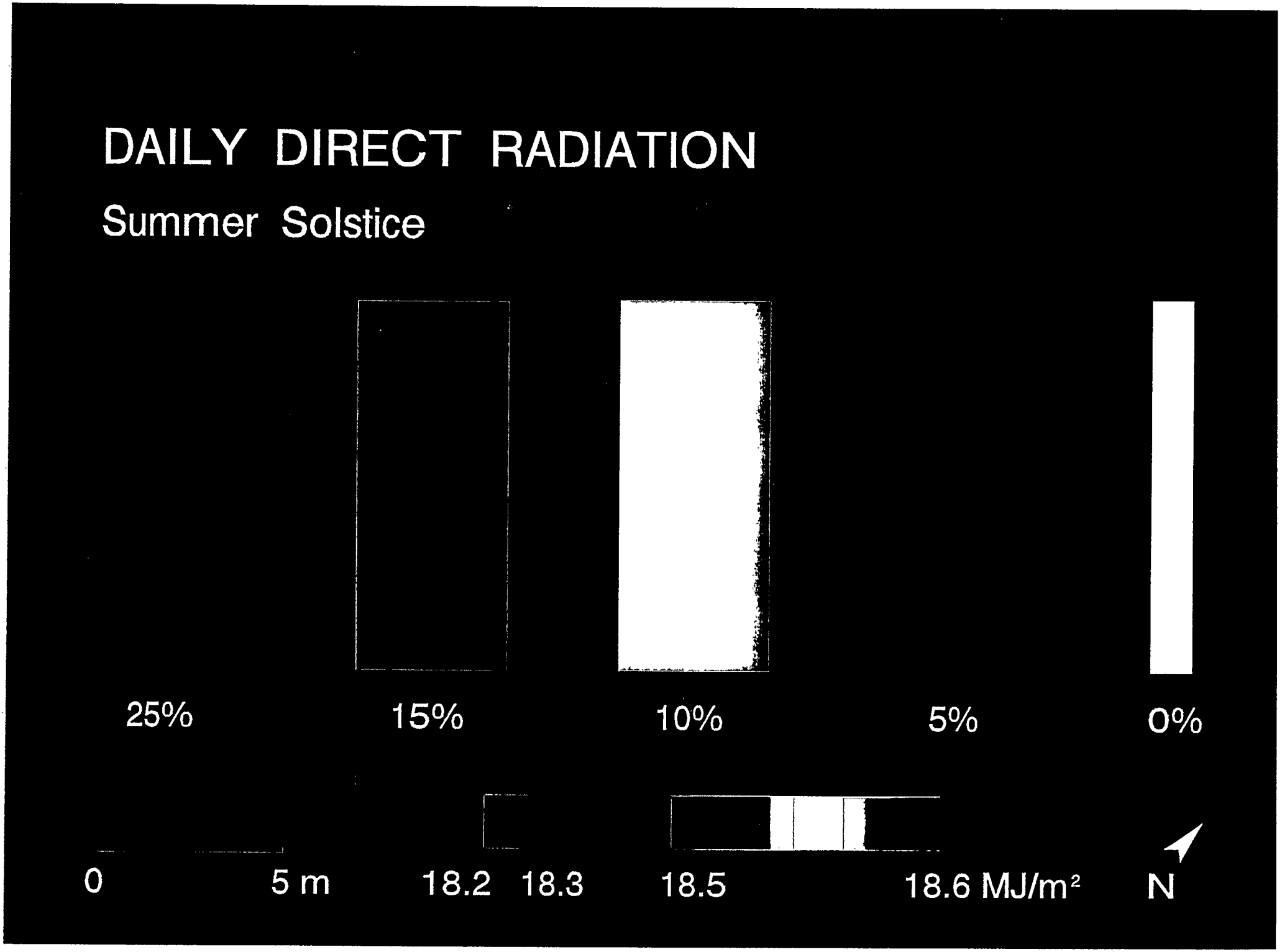
DAILY DIRECT RADIATION
Summer Solstice
25%
15%
10%
5%
0%
0
5 m
18.2
18.3
18.5
18.6 MJ/m²
N

FIGURE 7A

FIGURE 7D

DAILY DIRECT RADIATION

Winter Solstice

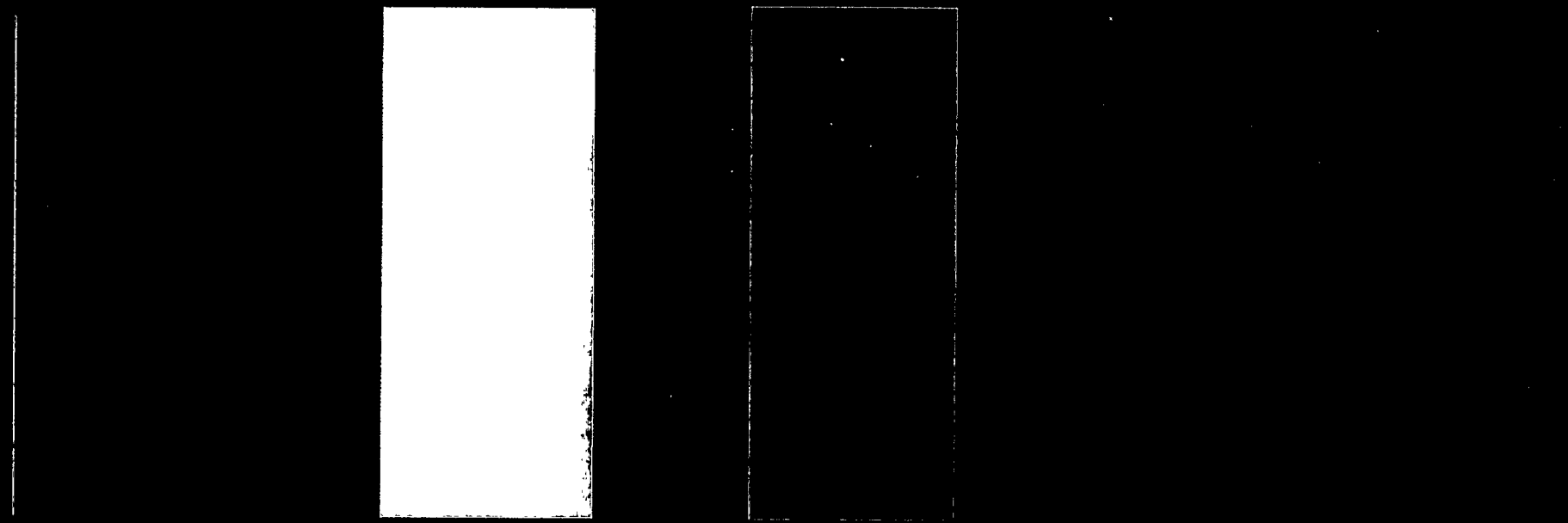

0 5 m

3.5 5.0 MJ/m²

N

FIGURE 8A

SKYVIEW FACTOR

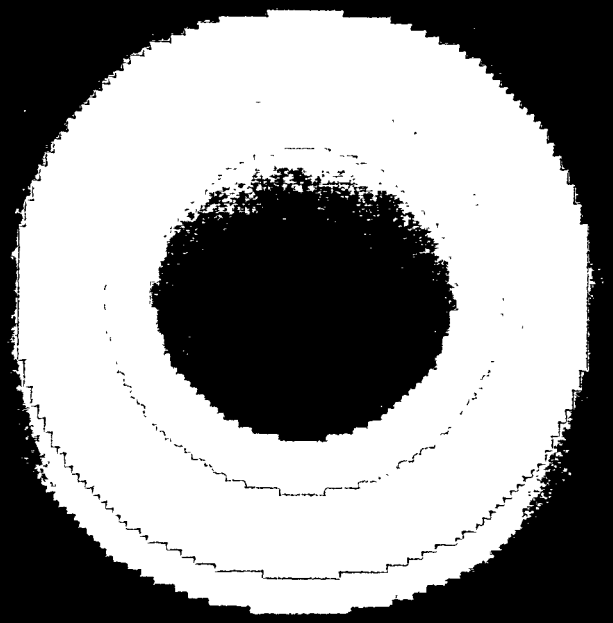

Radius = 10m
Height = 10m

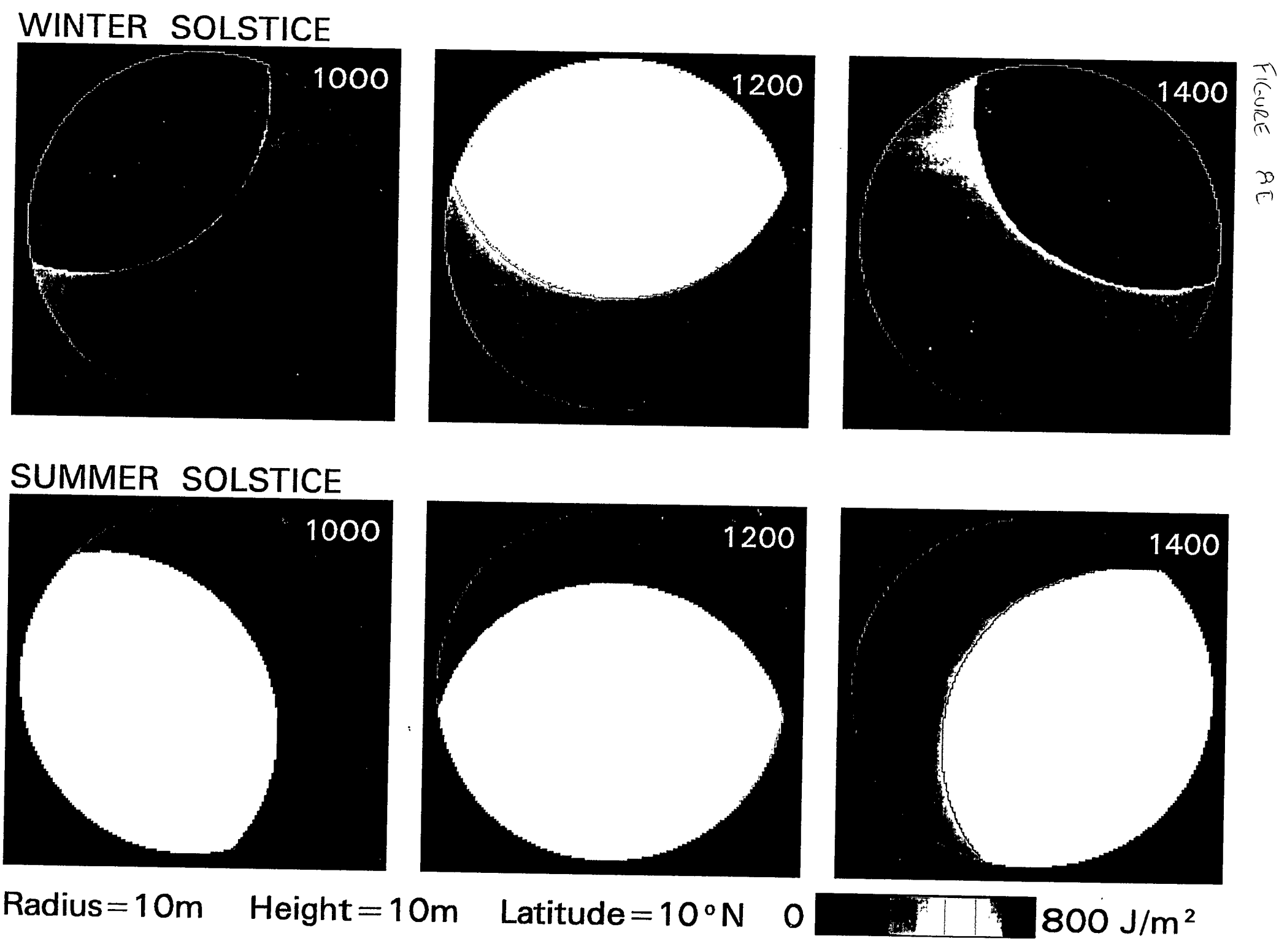
WINTER SOLSTICE
1000
1200
1400
SUMMER SOLSTICE
1000
1200
1400
Radius = 10m
Height = 10m
Latitude = 10°N
0
800 J/m²

FIGURE 8E

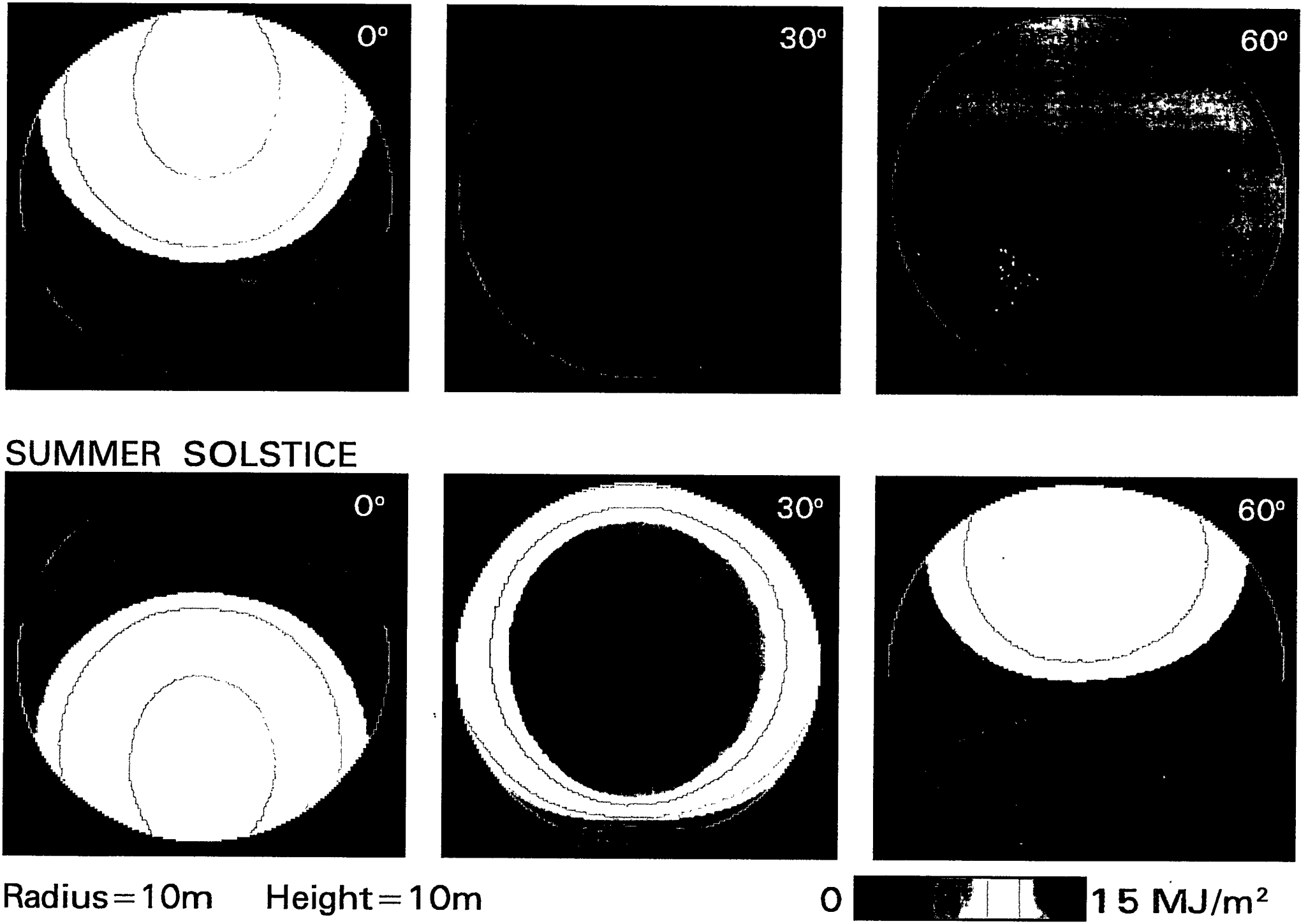
WINTER SOLSTICE
0°
30°
60°
SUMMER SOLSTICE
0°
30°
60°
Radius=10m
Height=10m
0
15 MJ/m²

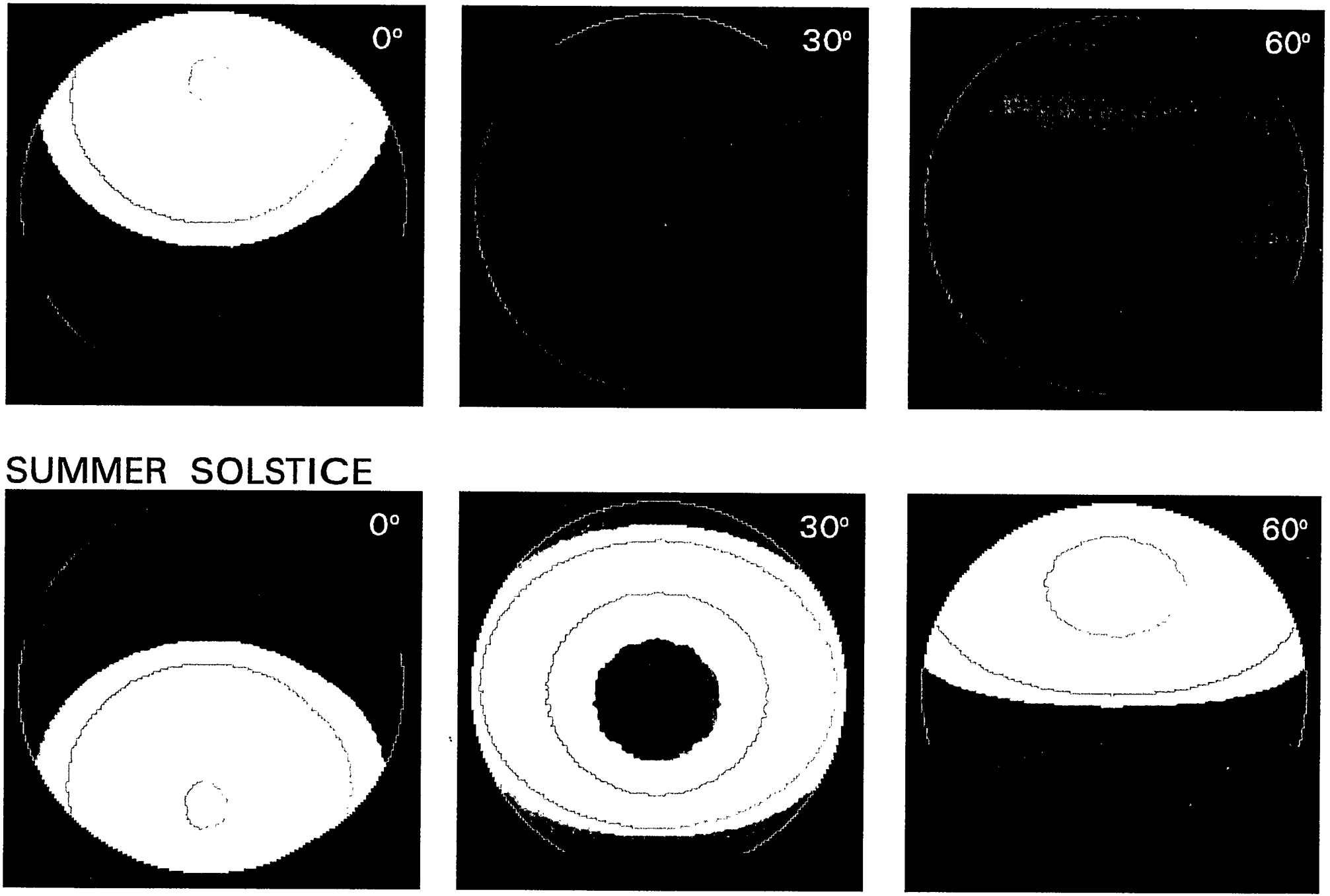
WINTER SOLSTICE
0°
30°
60°
SUMMER SOLSTICE
0°
30°
60°
Radius=10m
Height=10m
0
8hrs

FIGURE A1

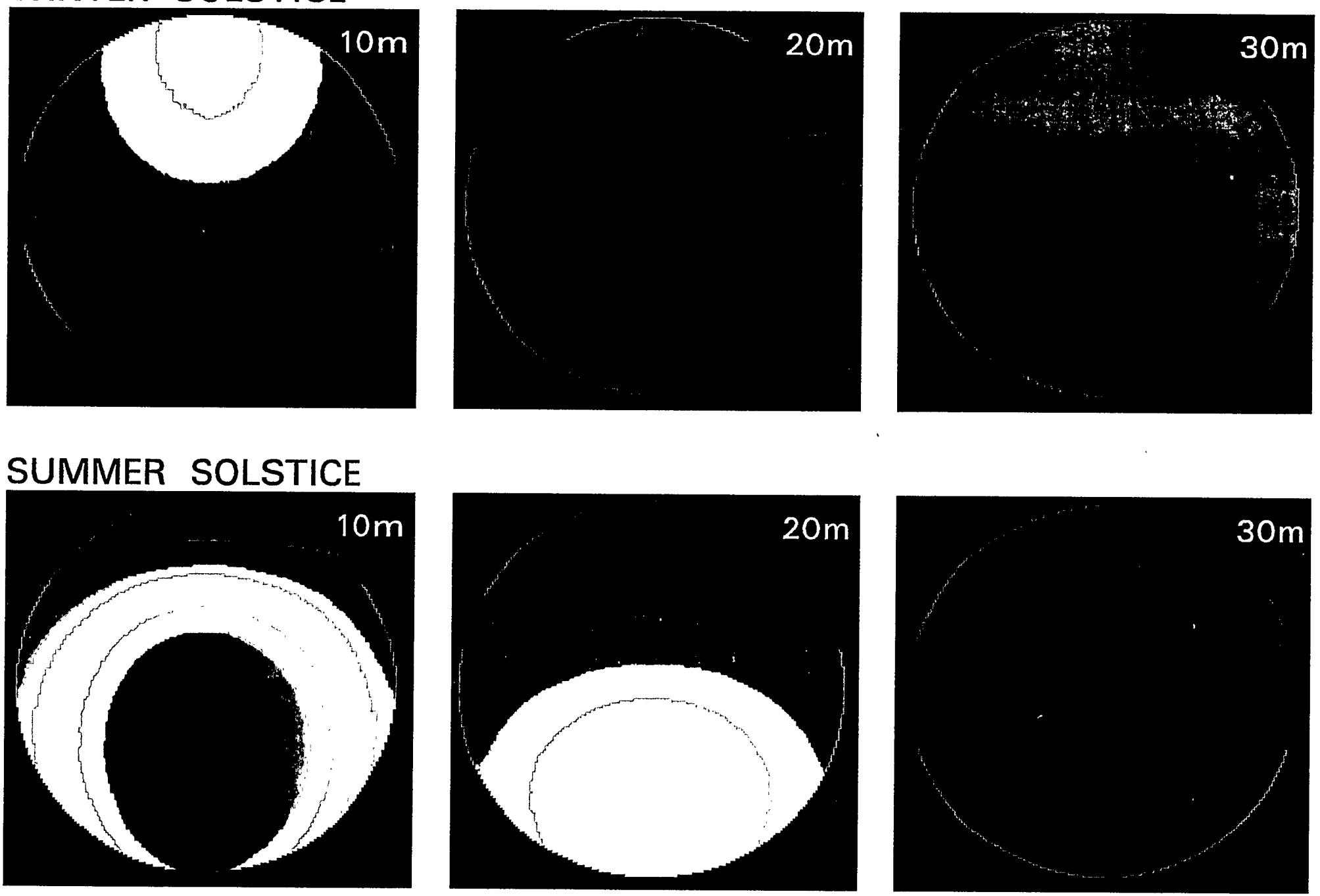
WINTER SOLSTICE
10m
20m
30m
SUMMER SOLSTICE
10m
20m
30m
Radius=10m
Latitude=10° N
0
15 MJ/m²

FIGURE 2E

WINTER SOLSTICE

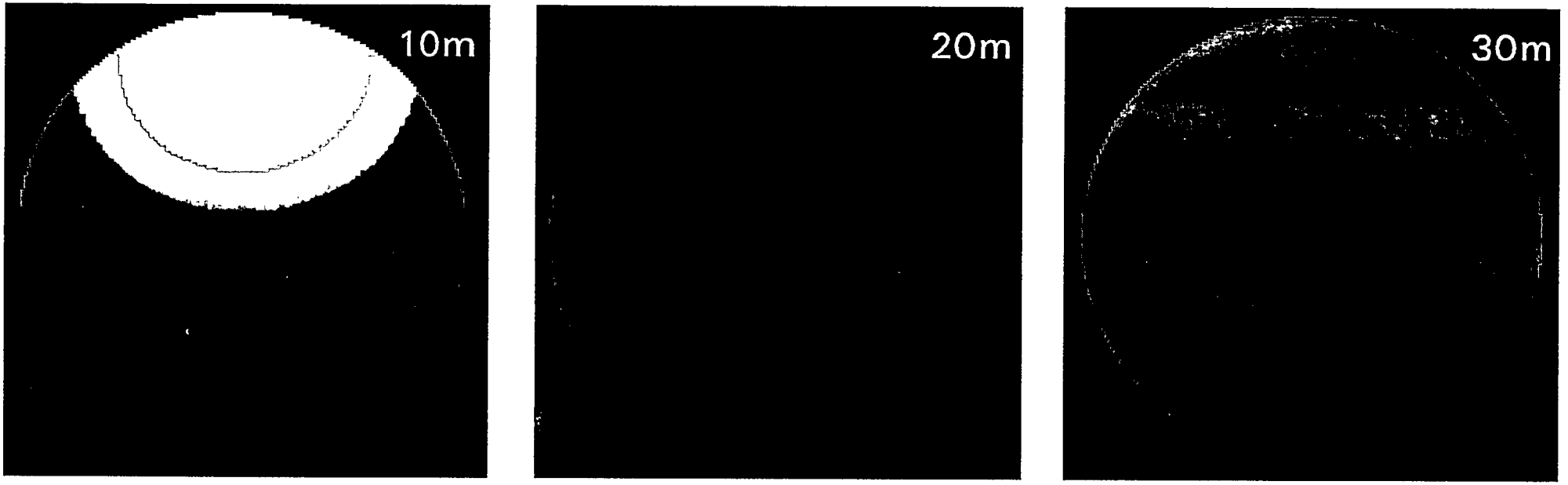

SUMMER SOLSTICE

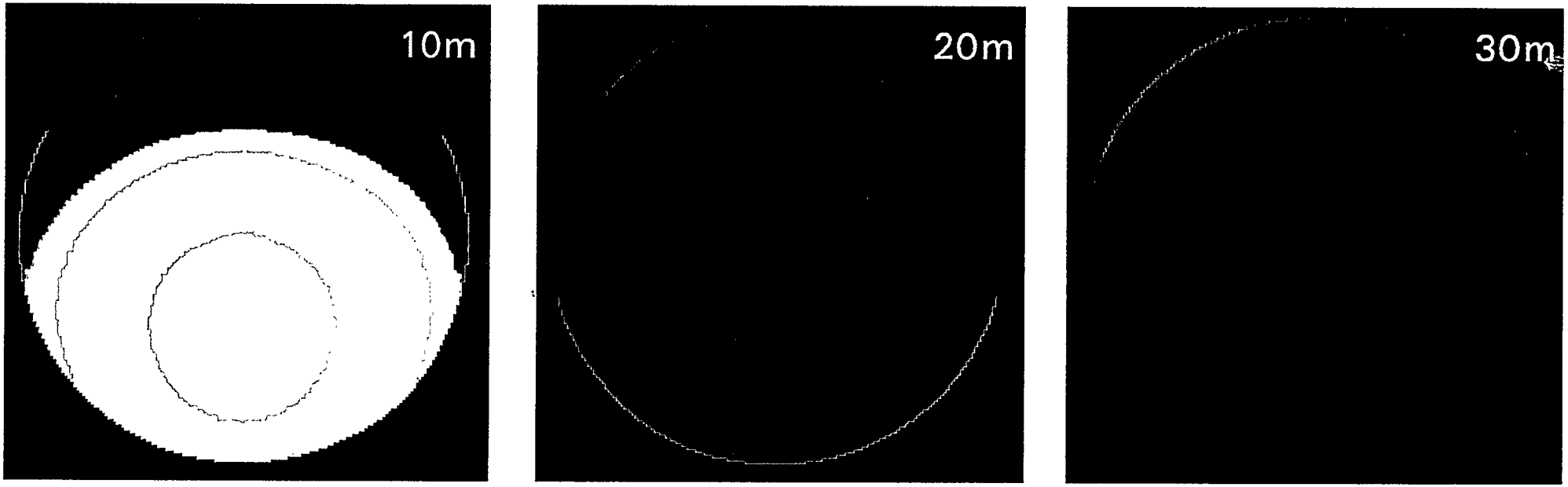

Radius = 10m Latitude = 10° N

0 8 hrs